PFC/JA-88-4

# Effect of Scattering Parameters on the Detection of the Alpha Particle Distribution Function for $CO_2$ Laser or Millimeter Incident Radiation

Vahala, L.*; Vahala, G.**; Sigmar, D.

Plasma Fusion Center
Massachusetts Institute of Technology
Cambridge, MA 02139
*Old Dominion University, Norfolk, VA 23508
**College of William and Mary,
Williamsburg, VA 23185

February 1988

Submitted to: Nuclear Fusion

This work was supported by the U. S. Department of Energy Contract No. DE-AC02-78ET51013. Reproduction, translation, publication, use and disposal, in whole or in part by or for the United States government is permitted.

# EFFECT OF SCATTERING PARAMETERS ON THE DETECTION OF THE ALPHA PARTICLE DISTRIBUTION FUNCTION FOR $CO_2$ LASER OR MILLIMETER INCIDENT RADIATION

LINDA VAHALA
Department of Electrical and Computer Engineering
Old Dominion University, Norfolk, VA 23508

GEORGE VAHALA
Department of Physics
College of William and Mary
Williamsburg, VA 23185

DIETER SIGMAR
Plasma Fusion Center
MIT, Cambridge, MA 02139

## ABSTRACT

Parameters (choice of incident radiation, scattering and orientation angles) are sought so that the one dimensional alpha particle distribution can be deduced from the experimental coherent scattering data. In order to be able to deduce the alpha distribution function, we must have the total scattering function totally dominated by the contribution from the electrons shielding the alphas, $S_\alpha(\omega) \approx S_{tot}(\omega)$ in the GHz frequency range, as well as all the frequency dependence in $S_\alpha(\omega)$ is contained only in the one dimensional alpha distribution function. $T_e$ has disparate effects: high $T_e$ leads to lower $S_\alpha/S_{tot}$, while leading to more of the $\omega$ dependence of $S_\alpha$ being carried by the one dimensional alpha distribution $f_\alpha(\omega/k)$.

The $CO_2$ laser is a passive probe of the plasma because of its very high frequency, but coherent scattering can only be achieved for very acute forward scattering angles ($\theta \leq 1.2^0$). For electron temperatures $T_e \geq 10$ keV, it will be quite difficult to directly deduce the alpha distribution from $S_{tot}(\omega)$.

For the two gyrotron sources considered here (2.14 mm at 140 GHz; and 5 mm at 60 GHz), the lower incident frequencies lead to serious questions concerning penetration, refraction and absorption by the plasma. Assuming these problems can be overcome, coherent scattering can be achieved for any forward (or backward) scattering angles. We find that one could deduce the alpha distribution from the scattering data for forward scattering angles, although the $\omega$ range for the 5 mm source is quite limited and the associated $S_{tot}(\omega)$ has a rapidly decaying amplitude. For backward scattering angles, there is the possibility that the alpha distribution could be deduced from $S_{tot}$ from the 5 mm source, although $S_{tot}(\omega)$ is again rapidly decaying in the limited $\omega$ range

where $S_{\alpha}(\omega) \neq 0$.

# I. INTRODUCTION

In an earlier calculation[1], we considered the possibility of employing an incident $CO_2$ laser as a diagnostic for detecting alpha particles in a fusion plasma. Since the power radiated from a particular plasma species is inversely proportional to the mass squared of that species, nearly all the observed radiation will be emitted by the electrons. Thus, to be able to detect alpha particles, we must choose incident parameters so as to achieve coherent scattering from the electrons shielding the alphas.

Theoretically, coherent scattering[2] has been shown to occur when the Salpeter parameter $\alpha \equiv 1/k(\theta)\lambda_D > 1$, where $k = k_s - k_i$ is the effect of the equilibrium electron density fluctuations on the incident radiation wavenumber $k_i$, and $\lambda_D$ is the Debye length. For the typical scattering experiments under consideration here, $|k_s| \approx |k_i|$ so that

$$k(\theta) = |k| \approx 2\, k_i \sin\left(\frac{\theta}{2}\right) \tag{1}$$

where $\theta$ is the forward scattering angle. Thus, if the incident wavelength is increased (from the short wavelength 10.6μm $CO_2$ laser to the longer wavelength millimeter gyrotron sources) the scattering angle $\theta$ can be significantly increased and yet remain in the coherent scattering regime.

Now our earlier calculation[1] was restricted in scope to examining orientations which were nearly perpendicular to the toroidal magnetic field : $\varphi \approx \pi/2$, where $\hat{k}.\hat{B} \equiv \cos\varphi$. It was reported there that in a narrow cone around $k_{\parallel} = 0$ there existed a very strong lower hybrid resonance peak in the scattering function $S_{tot}$, with the dominant contribution arising from the electrons

shielding the alphas, $S_\alpha$. However, several errors[3] had been found in this paper[1], and these have been corrected by us and the corrected results have been presented at various meetings[4]. It was found that qualitatively the results are unchanged, but there were significant quantitative corrections. These will be discussed here.

Recently, Hughes and Smith[5] have made the suggestion that scattering data obtained from particular orientations could give direct information on the alpha particle distributon function. In this report, we shall examine this suggestion quite carefully for both $CO_2$ and millimeter gyrotron sources. In particular, we shall examine this suggestion for a JET-like Maxwellian plasma in which the

temperatures $T_i \approx T_e = 10$ keV,

electron density $n_{eo} = 1.2 \times 10^{14}$ cm$^{-3}$,

deuteron density $n_{io} = 1.185 \times 10^{14}$ cm$^{-3}$,

alpha particle density $n_{\alpha o} = 7.5 \times 10^{11}$ cm$^{-3}$

since the plasma is assumed to be charge neutral. For simplicity, we shall also assume a uniform toroidal magnetic field $B_0 = 34$ kG. It will be of some interest to examine the role of $T_e$ on the scattering function, and we shall consider both $T_e = 1$ keV and 15 keV. We find that the scattering results are quite insensitive to the deuteron temperature $T_i$.

## II. ALPHA PARTICLE CONTRIBUTION TO THE SCATTERING FUNCTION.

It can be shown[1,2] from equilibrium fluctuation theory that the alpha particle contribution to the scattering function is given by

$$S_\alpha(k,\omega) = \frac{|H_e|^2}{|\varepsilon_L|^2} \frac{4n_{\alpha o}}{n_{eo}} \frac{2\pi}{|k|} f^{(1)}_{\alpha o}\left(\frac{\omega}{k}\right) \tag{2}$$

Here, $f^{(1)}$ is the one-dimensional alpha particle distribution function with the only velocity dependence being in the direction of $k$ (i.e., the velocity components perpendicular to $k$ have been integrated out). In Eq. (2), $H_e$ is given by

$$H_e(k,\omega) = \alpha^2 \sum_\ell \Gamma_{e\ell}\left[1 + \frac{\omega}{k_\parallel v_e} Z\left(\frac{\omega-\ell\Omega_e}{k_\parallel v_e}\right)\right] \tag{3}$$

where $\Gamma_{e\ell} = \exp(-k_\perp^2\rho_e^2)\, I_\ell(k_\perp^2\rho_e^2)$ is a typically Bessel function gyroradius term for Maxwellian electrons, and $Z$ is the Fried-Conte function. $v_e$ is the electron thermal speed, $\Omega_e$ the electron gyrofrequency and $\rho_e$ is the electron gyroradius. The dielectric function $\varepsilon_L(k,\omega)$ is defined by

$$\varepsilon_L(k,\omega) = 1 + H_e(k,\omega) + H_i(k,\omega) + G_\alpha(k,\omega) \tag{4}$$

where

$$H_i(k,\omega) = \alpha^2 \frac{n_{io}}{n_{eo}} \frac{T_e}{T_i} \sum_\ell \Gamma_{i\ell}\left[1 + \frac{\omega}{k_\parallel v_i} Z\left(\frac{\omega-\ell\Omega_i}{k_\parallel v_i}\right)\right] \tag{5}$$

$\Gamma_{i\ell}$ is the anolagous Bessel function gyroradius term for Maxwellian deuterons.

Finally $G_\alpha$ is given by

$$G_\alpha(k,\omega) = \frac{\omega_{p\alpha}^2}{k^2} \int d^3v \frac{k.\partial f_{\alpha 0}/\partial v}{\omega - k.v + i\delta} \tag{6}$$

The expressions for the electron and deuteron contributions to the scattering function,

$$S_{tot}(\omega,k) = S_e(\omega,k) + S_i(\omega,k) + S_\alpha(\omega,k)$$

will not be presented here since they are somewhat lengthy and not relevant to the discussion at hand. They are given in Ref. 1.

We now turn to the suggestion made by Hughes and Smith[5], that it should be possible to choose orientations so that the alpha particle distribution function can be determined directly from the diagnostics.

First, it should be noted that when a certain parmeter regime is chosen i.e., the incident radiation wavelength $\lambda_i$, incident scattering angle $\theta$, and the orientation $\varphi$ relative to the toroidal magnetic field, then the wave number $k=k(\theta)$ is fully determined.

Suppose now that over a significant GHz frequency range a parameter regime can be found in which

(i) the alpha particle contribution to the scattering function is dominant

$$S_\alpha(k,\omega) \approx S_{tot}(k,\omega)$$

and,

(ii) that $S_\alpha$ itself can be accurately approximated in this frequency range by

$$S_\alpha(k,\omega) \approx S_\alpha^*(k,\omega),$$

where

$$S_{\alpha}^{*}(k,\omega) = C^{*}\left[\frac{4n_{\alpha o}}{n_{eo}}\frac{2\pi}{|k|}f_{\alpha o}^{(1)}\left(\frac{\omega}{k}\right)\right] \tag{7}$$

and $C^{*}$ is some appropriate normalization constant, independent of $\omega$. Then, in such a parameter regime, a frequency dependent measurement of the total scattering function $S_{tot}(k,\omega)$ will yield a direct measurement of the one-dimensional alpha particle distribution function $f_{\alpha o}^{(1)}(\omega/k)$. This occurs because the complete frequency dependence of the $S_{tot} \approx S_{\alpha}$ measuerment is now retained only in the one-dimensional alpha particle distribution function.

This is the basic idea of Hughes and Smith[5], who suggested looking at orientations where the magnetic effects contained in $S_{\alpha}$ are negligible. Now all these magnetic effects are contained in the frequency dependent factor $|H_e(k,\omega)|^2/|\varepsilon_L(k,\omega)|^2$ , Eq. (2), and occur because the large scattering volume forces one into a magnetized treatment of the electrons shielding the alphas. However, if one can find a parameter regime in which this factor $|H_e(k,\omega)|^2/|\varepsilon_L(k,\omega)|^2$ is independent of $\omega$, then the complete frequency dependence in $S_{\alpha}$ is carried only by the one-dimensional alpha particle distribution $f^{(1)}(\omega/k)$.

For the results to be presented here, we shall assume that the alpha particles can be described by the slow-down distribution

$$f_{\alpha o}(\mathbf{v}) = \frac{F_o}{v^3 + v_c^3} \quad , \quad \text{for } |\mathbf{v}| < v_{\alpha}$$

$$= 0 \quad , \quad \text{for } |\mathbf{v}| > v_{\alpha}$$

where the normalization constant $F_0$ and $v_{\alpha}$ are given by

$$F_o = \frac{3}{4\pi \ln(1+v_\alpha^3/v_c^3)} \quad ; \quad v_\alpha = \sqrt{\frac{2E_\alpha}{m_\alpha}} \text{ for } E_\alpha = 3.5 \text{ MeV}$$

$v_c$ is the speed at which the electron drag on the alphas equals that due to the deuteron drag on the alphas.

It should be noted that for the slow-down distribution, there is an upper bound to the frequency, $\omega_{cut}$, above which there can be no alpha contribution to the scattering function. Since $f_{\alpha o} = 0$ for $|v| > v_\alpha$, it is easily seen that $S_\alpha(\omega,k)=0$ for $\omega>\omega_{cut}(\theta)$, where

$$\omega_{cut}(\theta) \equiv k(\theta)\, v_\alpha \approx 2\, k_i\, v_\alpha\, \sin(\theta/2) \qquad (8)$$

We shall present results for the scattering function and the alpha contribution to it in the GHz range. Only in this frequency range can the alphas yield a dominant contribution to the total scattering function. Indeed, for frequencies $\omega$ < 1 GHz the electrons shielding the deuterons will yield the dominant contribution $S_i$; while typically for $\omega$ > min {$\omega_{cut}$, 9-12 GHz} the electron contribution $S_e$ will dominate $S_{tot}$.

## III. INCIDENT $CO_2$ LASER SCATTERING AT 10.6μm

### A. The lower hybrid resonance, and orientations with $k_{\parallel} \approx 0$

For orientations around $\varphi \approx \pi/2$, the scattering function $S_{tot}$ exhibits a strong lower hybrid resonance at $\omega_{LH}$, which has the following simple form in the cold plasma approximation

$$\omega_{LH}^2 = \left( 1 + \frac{m_i k_{\parallel}^2}{m_e k_{\perp}^2} \right) \frac{\Omega_e^2}{\Omega_e^2 + \omega_{pe}^2} \omega_{pi}^2$$

In Fig. 1, we show temperature and orientation effects on $S_{tot}$ [connected or dashed curves] and $S_{\alpha}$ [unconnected triangles and stars] for the case of $CO_2$ laser scattering at forward scattering angle $\theta=0.5$. In Fig. 1a one sees a strong $\omega_{LH}$ resonance in the scattering function for $\varphi=85^0$ (** curves) at a low electron temperature of $T_e=1$ keV in which almost all the contribution to the scattering function comes from the electrons screening the alphas, $S_{\alpha}$. However, this resonance is easily destroyed by decreasing the orientation angle $\varphi$, as seen in Fig. 1a for $\varphi=80^0$ (triangle curves), although with this orientation we still have $S_{\alpha} \approx S_{tot}$.

The lower hybrid resonance is also easily destroyed by higher electron

temperatures. From Fig. 1b, one finds that for $T_e$=10 keV and $\varphi$=85$^0$, the lower hybrid resonance peak in $S_{tot}$ is significantly lowered as well as broadened in frequency. Moreover, over most of the GHz range, $S_\alpha$ no longer provides the dominant contribution to $S_{tot}$. This is further exhibited in Fig. 1c for Te=15 keV.

If instead, one increases the orientation angle $\varphi$ to $\pi/2$, the lower hybrid resonance becomes more pronounced than at $\varphi$=85$^0$, but again the ratio $S_\alpha/S_{tot}$ rapidly decreasing with increasing $T_e$. In general, for fixed orientations $\varphi$, as one increases the forward scattering angle $\theta$, both the lower hybrid resonance $\omega_{LH}$ and the cut-off frequency $\omega_{cut}$ increase, while both $S_{tot}$ and $S_\alpha$ decrease and $S_\alpha/S_{tot}$ significantly decreases over the GHz frequency range of interest.

**B. Orientations away from the lower hybrid resonance: $\varphi << \pi/2$, $k_\parallel \neq 0$.**

In Figs. 2 and 3, we consider the effect of increasing the forward scattering angle from $\theta$=0.5$^0$ to 1.0$^0$, for various $T_e$ but for orientations $\varphi$ significantly away from $\pi/2$ so that $k_\parallel$ is finite. On comparing these results with those from Fig. 1, it is seen that within a large frequency range of interest, $S_{tot}$ slightly decreases while $S_\alpha$ remains unchanged as $\varphi$ decreases in this range of finite $k_\parallel$ [e.g., compare Figs. 1b, 2b, and 3b]. As $T_e$ increases,

[Figs. 3a, 3b, and 3c], there is a marked flattening of the decay of $S_{tot}$ with frequency but the contribution from $S_\alpha$ decreases faster with $\omega$.

On increasing the forward scattering angle from $\theta=0.5^0$ to $\theta=1.0^0$ the Salpeter (or coherent scattering) parameter decreases. This results in a further decreases in the total signal $S_{tot}$, as one would expect. Moreover, as $T_e$ increases, there is significantly less flattening in the frequency decay of $S_{tot}$ unlike the case with $\theta=0.5^0$ [e.g., compare Figs. 3b and 3c]. However one finds in general that

$$\left.\frac{S_\alpha(\mathbf{k},\omega)}{S_{tot}(\mathbf{k},\omega)}\right|_{\theta\,=\,1.0} > \left.\frac{S_\alpha(\mathbf{k},\omega)}{S_{tot}(\mathbf{k},\omega)}\right|_{\theta\,=\,0.5}$$

which is somewhat unexpected.

## C. Parameter regime for detecting the alpha distribution function

We now attempt to find a parameter regime for the incident $CO_2$ laser from which a frequency dependent measurement of the scattering function, Stot, will yield direct information on the one-dimensional alpha particle distribution. In particular the full magnetized alpha contribution, $S_\alpha$ [Eq. (2)] , will be compared to that which would be obtained if magnetic effects are neglected, $S_\alpha^*$ [Eq. (7)]. For convenience, the normalization constant, C*, in Eq. (7) is chosen so that

$$\left.\frac{S_\alpha^*(\mathbf{k},\omega)}{S_\alpha(\mathbf{k},\omega)}\right|_{\omega\,=\,1.8\ GHz} \equiv 1 \qquad (9)$$

C* is strongly dependent on $\theta$ and $T_e$, but fairly insensitive to the orientation

angle $\varphi$. The normalization, Eq. (9), is somewhat arbitrarily assigned at the frequency $\omega$=1.8 GHz and any other choice of frequency would be appropriate provided it is sufficiently large so that the magnetized deuteron response $S_i$ at this frequency is negligible. Also, it should be noted that the setting of the right hand side of Eq. (9) to unity at this frequency is also of no importance. What is important is whether or not there exists a frequency range in which $S_\alpha^*(k,\omega)/S_\alpha(k,\omega)$ is independent of $\omega$.

In Fig. 4, we plot this ratio $S_\alpha^*(k,\omega)/S_\alpha(k,\omega)$ at forward scattering angle $\theta$=0.5$^0$ for various orientation angles $\varphi$ and electron temperatures $T_e$. Clearly, as $k_{||}$ increases (i.e., $\varphi$ decreases from $\pi/2$) the magnetic effects become less important. Also magnetic effects become less important as the electron temperature increases. From Fig. 4c and 4d, it appears that for $T_e$>7 keV and for $\varphi \leq 45^0$ there does exist a frequency range $\omega \geq 5$ GHz in which the $S_\alpha^*/S_\alpha$ curve is flat. However for $\varphi$=45$^0$ and Te=10 keV we see from Fig. 3b that the contribution from the alphas to the total scattering function $S_{tot}$ montonically decreases from about 86% at $\omega$=5 GHz, 71% at 7.4 GHz, to 51% at $\omega$=9 GHz.

From our earlier discussion on the Hughes and Smith[5] suggestion, it was shown that the one dimensional alpha particle distribution function can be inferred directly from the total scattering function data provided there existed a frequency range such that

$$\frac{S_\alpha^*(\omega)}{S_\alpha(\omega)} \approx \text{const.} \qquad (10)$$

with $k(\theta)$ fixed for given scattering angle $\theta$, and

$$S_\alpha(\omega) \approx S_{tot}(\omega). \qquad (11)$$

It thus appears that for a fusion plasma with $T_e \geq 10$ keV, the use of the $CO_2$ laser as an alpha particle distribution function diagnostic will be quite difficult since either Eq. (10) or (11) are usually violated. Unfortunately, as is evident from Fig. 3, increasing the forward scattering angle does not help since it leads to a drastically reduced alpha contribution to the scattering function: $S_\alpha/S_{tot} << 1$.

We have noted that choosing orientations with $k_\parallel \approx 0$ will lead, for low $T_e$, to a resonance in the scattering function with $S\alpha \approx Stot$ (e.g., Fig. 1a). But, as can be seen from Fig. 4a, the $S_\alpha^*(\omega)/S_\alpha(\omega)$ curve has a strong dependence on $\omega$. Hence, even under these conditions, it is difficult to directly determine the alpha particle distribution function since Eq. (10) is not satisfied.

As $T_e$ increases, the resonance peak in $S_{tot}$ decreases in amplitude and broadens in frequency, with $S_\alpha/S_{tot}$ decreasing. Moreover, it appears that relativistic effects will become important for $T_e \geq 20$ keV, especially for orientations $\varphi \rightarrow \pi/2$ since the Doppler broadening factor $k_\parallel c/\omega \rightarrow 0$. Relativistic effects[4,5] will smear out the previously sharp electron gyrofrequency since now the gyrofrequency is dependent on the particle's momentum, $\Omega_{ce} \approx \Omega_{ce}(p)$, where the relativistic momentum $p = \gamma m_0 v$. This, in turn, will further smear out any lower hybrid resonance peak in the scattering amplitudes. We are forced to conclude that there do not appear to be any significant advantages to be gained by choosing orientations with $k_\parallel \approx 0$ in the

detection of alpha particles. It will also be seen that this conclusion holds not only for the $CO_2$ laser but also for the gyrotron sources.

## IV. GYROTRON SCATTERING AT 2.14 mm AND 5.00 mm

Although one is necessarily restricted to very small forward angle scattering with the $CO_2$ laser in order to achieve coherent scattering from the electrons, the very high incident frequency of the $CO_2$ laser does allow a passive probing of the plasma. If instead one resorts to the longer wavelength millimeter radiation, then coherent scattering can be achieved at any forward (or even backward) scattering angle. However, there are now new difficulties introduced since the incident gyrotron frequency is on the order of the electron gyrofrequency (or its second harmonic). These added complications include the question of incident beam penetration into the plasma and the problems of refraction and absorption by the plasma. A careful study of these questions is in order, but in this report we shall concentrate on the properties of the scattering functions $S_\alpha$ and $S_{tot}$ as functions of scattering angle $\theta$, orientation angle $\varphi$ and electron temperature $T_e$. Preliminary simplified calculations of Woskov[6] seem to indicate that the use of gyrotron sources at 60 GHz (5.00 mm) and at 140 GHz (2.14 mm) should avoid most of these new complications. Hughes and Smith[5] have also considered gyrotron sources at these two frequencies.

For orientations $\varphi \approx \pi/2$, the cold plasma dispersion relation yields two propagating modes, the X-mode and the O-mode. To propagate into the plasma below the gyrofrequency $\Omega_e$, one would choose the X-mode (5.00 mm) which is elliptically polarized. However, the elliptical polarization introduces a form factor into $S_{tot}$ which leads to a reduced final signal. This form factor has been calculated for the cold plasma by Bretz[7]. If one wants to propagate the gyrotron beam into the plasma between the gyroharmonics, then one would choose the O-mode (2.14 mm) which is linearly polarized.

It should also be remembered that for the slow-down alpha distribution $f_{\alpha 0}=0$ for $v > v_{\alpha}$. Thus for frequencies with

$$\frac{\omega}{k} \approx \frac{\omega}{2k_i \sin(\theta/2)} > v_{\alpha}$$

there will be no electron-shielded alphas to scatter from. Thus

$$S_{\alpha}(k,\omega) = 0 \qquad \text{for } \omega > kv_{\alpha},$$

with the cutoff frequency $\omega_{cut}(\theta) \equiv k(\theta)\ v_{\alpha}$. Hence, in comparing the appropriate cutoffs for the 2.14 mm and 5.00 mm gyrotron sources at the same forward scattering angle $\theta$, we find

$$\omega_{cut}\Big|_{2.14\ mm} = 4.28 \times \omega_{cut}\Big|_{5\ mm} \tag{12}$$

It will be seen that these gyrotron cutoff frequencies will impose restrictions on the GHz frequency range from which to obtain scattering data, unlike the situation for the shorter wavelength $CO_2$ laser where

$$\omega_{cut}\Big|_{CO_2} >> \omega_{cut}\Big|_{2.14\ mm}$$

and for which there are no such similar limitations in the GHz frequency range.

## A. The lower hybrid resonance, and orientations with $k_{\parallel} \approx 0$

In Fig. 5 we consider the scattering functions for the 2.14 mm gyrotron radiation at forward scattering angle $\theta=90^0$, and for the same orientations $\varphi$ and temperatures $T_e$ as in Fig. 1 for the $CO_2$ laser source. For $T_e=1$ keV (Fig. 5a), one again sees the strong lower hybrid resonance in $S_{tot}$ at $\varphi=85^0$ with $S_{\alpha} \approx S_{tot}$. There is a striking similarity between these results and those results from the $CO_2$ laser at $\theta=0.5^0$, (Fig. 1a), up to the cutoff frequency for

the 2.14 mm gyrotron source, $\omega_{cut}(\theta) \approx$ 8.4 GHz. As $T_e$ increases to 10 keV (Fig. 5b) and 15 keV (Fig. 5c), the resonance peak in the scattering function broadens and lowered with the $S_\alpha/S_{tot}$ ratio now being significantly less than one. Again, there is strong similarity with the $CO_2$ results (Figs. 1b and 1c). As the orientation decreases to $\varphi=80^0$, the lower hybrid resonance no longer occurs in the frequency range 1.8 GHz $< \omega < \omega_{cut}$, as for the case of the $CO_2$ laser (c.f. Figs. 1a and 5a). Again, as $T_e$ is increased, the alpha contribution $S_\alpha$ to $S_{tot}$ is significantly reduced (c.f., Figs. 1b and 5b, 1c and 5c).

On increasing the scattering angle to $135^0$ (i.e., backward scattering angles), there is even a more striking similarity with the results of $CO_2$ scattering although the resonance peak in the scattering function at $\varphi=85^0$ is significantly lower in the 2.14 mm gyrotron case (c.f., Figs. 6a and 1a). The similarites continue for both $\varphi=80^0$ and $\varphi=85^0$ as can be seen from Figs. 6b and 1b, 6c and 1c.

## B. Orientations away from the lower hybrid resonance: $\varphi << \pi/2$, $k_{||} \neq 0$.

We now consider the effects of different orientations $\varphi$ and temperatures $T_e$ on the scattering functions for the 2.14 mm gyrotron for forward scattering angles $\theta=90^0$ and $135^0$ [Fig. 7 for $\varphi=75^0$, Fig. 8 for $\varphi=45^0$, and Fig. 9 for $\varphi=0^0$]. The results are qualitatively similar to those for the $CO_2$ laser.

For $T_e$=1 keV, $S_\alpha \approx S_{tot}$ for both $\theta=90^0$ and the backscatter angle $\theta=135^0$, but

$S|_{\theta=135} > S|_{\theta=90}$ in the Ghz frequency range, and changing the orientation angle has little effect (c.f., Figs. 7a, 8a, and 9a).

As $T_e$ increases, both $S_\alpha$ and $S_{tot}$ increase but $S_\alpha(\omega)/S_{tot}(\omega)$ is a decreasing function of $\omega$ (c.f., for example Figs. 8a, 8b, and 8c).

## C. Comparison between the 2.14 mm and 5 mm gyrotron sources

In Figs. 10 and 11 we contrast the effect of orientation on the 2.14 mm (140 GHz) and the 5 mm (60 GHz) gyrotron sources. At forward scattering angle of $\theta=45^0$ and $T_e=10$ keV, one finds that for both gyrotrons $S_\alpha \approx S_{tot}$, and decreasing the orientation from $\varphi=75^0$ to $\varphi=45^0$ has little effect (Fig. 10). Since for the 5 mm gyrotron the cutoff frequency $\omega_{cut}$ is only 1.9 GHz, we have plotted the scattering function for this gyrotron source from $\omega=1$ Ghz. It is interesting to note that the 2.14 mm source has a larger scattering function than the 5 mm source, as well as a larger non-zero frequency range [c.f., Eq. (12)]. However, a disadvantage of these relatively small forward scattering angles is that the cutoff frequency $\omega_{cut}$ is quite low.

As $\theta$ increases, $\omega_{cut}$ also increases. However, for backscatter angles we now see that for the 2.14 mm gyrotron $S_\alpha/S_{tot}$ is significantly less than one and is a monotone decreasing function of $\omega$. In Fig. 11, we consider $T_e=10$ keV and $\theta=135^0$. As the orientation angle decreases from $\varphi=75^0$ to $\varphi=0^0$, the alpha contribution to the scattering function increases :

$$\left.\frac{S_\alpha(\omega)}{S_{tot}(\omega)}\right|_{\varphi = 75^\circ} < \left.\frac{S_\alpha(\omega)}{S_{tot}(\omega)}\right|_{\varphi = 45^\circ} \tag{13}$$

There is only a small difference between the results for $\varphi=45^0$ and $0^0$. Indeed, we find that the contribution from the alphas to the scattering function is also monotonically decreasing:

2.14 mm : $S_\alpha/S_{tot}$ : $\theta=135^0$

| | $\varphi=45^0$ | $\varphi=0^0$ |
|---|---|---|
| $\omega$=5 GHz: | 85% | 88% |
| $\omega$=7.4 GHz: | 70% | 75% |
| $\omega$=9 GHz: | 53% | 59% |

For the 5 mm gyrotron source, however, the results are somewhat more encouraging, since in the frequency range 1.4 GHz $\leq \omega \leq$ 4.4 GHz we see that $S_\alpha/S_{tot} \geq 0.94$ , for backscatter angle $\theta=135^0$ and for both orientations $\varphi=45^0$ and $0^0$, (see Fig. 11b and 11c). Unfortunately, there are two drawbacks in the use of the longer wavelength gyrotron, the first being quite serious:

(i) $S_{tot}(\omega)$ is a very rapidly decreasing function of $\omega$ with, typically, $S_{tot}(\omega)|_{5mm} << S_{tot}(\omega)|_{2.14mm}$ for most of the frequency range,

(ii) the cutoff frequency is quite low $\omega_{cut}$=4.8 GHz. Indeed,

One again sees the strong effect of electron temperature on $S_\alpha$ and $S_{tot}$ in Fig. 11d for backscatter angle of $\theta=135^0$ and $T_e$=1 keV. Even for orientations up

$\varphi=75^0$, $S_\alpha \approx S_{tot}$ for all $\omega$ up to $\omega_{cut}$ for both 2.14 mm and 5 mm sources.

## D. Parameter regime for detecting the alpha distribution function

To be able to deduce the alpha particle distribution function from the scattering data, we must find a frequency range in which both Eq. (10) and (11) are satisfied simultaneoulsy. From Fig. 12a-12c, for the 2.14 mm gyrotron at forward scattering angle $\theta=45^0$, it can be seen that Eq. (10), $S_\alpha^*(\omega)/S_\alpha(\omega) \approx$ const., is satisfied for nearly the whole GHz range (up to $\omega_{cut}$) for $T_e \geq 10$ keV and for orientations $\varphi \leq 45^0$. Similar results hold for the 5 mm gyrotron (Figs. 12d-12f). From Fig. 10, we also see that in this regime, Eq. (11) is also satisfied: $S_\alpha(\omega) \approx S_{tot}(\omega)$.

Thus it appears that one should be able to deduce the one-dimensional alpha distribution from the scattering data for either gyrotron source for forward scattering angles (here shown at $\theta=45^0$) and orientations $\varphi \leq 45^0$.

We now consider the effect of increasing the scattering angle $\theta$, Figs. 13 and 14. Again, provided the orientation $\varphi \leq 45^0$ and Te $\geq$ 10 keV, $S_\alpha^*(\omega)/S_\alpha(\omega) \approx$ const. However, $S_\alpha(\omega)/S_{tot}(\omega)$ decreases (at fixed $\omega$) as $\theta$ increaases. This decrease is significant for the 2.14 mm source, but not very significant for the 5 mm gurotron (i.e., if one ignores the much reduced final signal amplitude $S_{tot}$, and the effect on the cutoff frequency $\omega_{cut}$). For example, for $\theta=90^0$ (with $\omega_{cut}=8.4$ GHz)

| 2.14 mm : $S_\alpha/S_{tot}$ : $\theta=90^0$ | | |
|---|---|---|
| | $\varphi=45^0$ | $\varphi=0^0$ |
| $\omega$=5 GHz: | 91% | 93% |
| $\omega$=7.4 GHz: | 69% | 75% |
| $\omega$=8 GHz: | 50% | 57% |

Thus, for backscatter angles the 5 mm gyrotron source can give detailed information on the one dimensional alpha distribution function, provided the signal amplitude is sufficiently large for experimental detection, while the 2.14 mm source will have quite limited applicability.

## V. SUMMARY

In this calculation we have considered the possibility of using the short wavelength $CO_2$ laser or the longer wavelength gyrotron sources as a diagnostic for the detection of alpha particles in a JET-like plasma. In particular we have examined closely the suggestion of Hughes and Smith[5] that judicial choice of scattering parameters could yield direct information on the one dimensional alpha particle distribution function.

One of the main advantages of the $CO_2$ laser is its very high incident frequency. This allows a passive probing of the plasma. The price one has to pay is that coherent scattering can only be obtained for very acute forward scattering angles $\theta \leq 1.0^0$. On the other hand, the gyrotron sources have incident frequencies in the vicinity of the electron gyrofrequency or its second harmonic so that questions of penetration, accessibility and refraction of the incident beam become very important. (These analyses have not yet been performed for a hot plasma, and have not been attempted here.) The advantage of the longer wavelength gyrotron sources over the $CO_2$ laser is that one can achieve coherent scattering not only for any forward scattering angles but also for backweard scattering angles ($\theta > \pi/2$). Since in the D-T fusion reaction the alphas are born with 3.5 MeV energy there will effectively arise a cutoff phase velocity above which there are no alpha particles. For the gyrotron sources this will imply a cutoff frequency $\omega_{cut}$ in the GHz range such that for given $\theta$,

$$f_\alpha^{(1)}(v) = 0 \quad , \text{ for } v > \omega_{cut}/k(\theta)$$

where $k(\theta)$ is related to the incident wave number $k_i$ by the relation $k(\theta) \approx 2k_i \times$ $\times \sin(\theta/2)$. However for the $CO_2$ laser, because of its higher incident wave number, the associated $\omega_{cut}$ is far outside the GHz range and plays no role.

In order to be able to determine the alpha particle distribution function from the scattering data, we find that Eqs. (10) and (11) must be satisfied simultaneously in an appropriate GHz frequency range. One finds in general that the electron temperature $T_e$ has opposing effects in satisfying Eqs. (10) and (11): as $T_e$ increases, at fixed $\theta$ and $\varphi$,

$S_\alpha(\omega)/S_{tot}(\omega)$ decreases , as one expects on physical grounds, while

$S_\alpha^*(\omega)/S_\alpha(\omega) \rightarrow$ const.

Moreover, for $S_\alpha^*(\omega)/S_\alpha(\omega) \approx$ const. it is necessary that $k_{||}^2>0$. Thus one must stay away from orientations $\varphi\approx\pi/2$ at which $k_{||}\approx 0$.

On the other hand, only for orientations $\varphi\approx\pi/2$, is there a strong lower hybrid resonance peak in the scattering function at $\omega_{LH}$. However, as $T_e$ increases the peak in S decreases while the resonance itself is broadened. However $S_\alpha/S_{tot}$ decreases as $T_e$ increases. For these orientations, relativistic effects would become important for $T_e>20$ keV and these would smear out even further the $\omega_{LH}$ resonance. Thus, making measurements around perpendicular orientation seems to have little applicability in determining the alpha particle distribution function (whether one uses the $CO_2$ laser or the gyrotron sources).

One of the important diferences between the 2.14 mm and 5 mm gyrotrons is that the final signal, $S_{tot}(\omega)$, is significantly lower for the 5 mm source in most of the appropriate $\omega$ range which is also significantly reduced over that for the 2.14 mm gyrotron.

Finally, for orientations with $\varphi<\pi/2$, one finds that for the 5 mm gyrotron one can determine the alpha particle distribution for both forward and backward scattering angles. However, for the 2.14 mm gyrotron it is more beneficial to use forward rather than backward scattering angles. These results are all based on an electrostatic calculation. A full electromagnetic calculation is necessary so as to take proper account of polarization effects.

**Acknowledgments**

The authors are grateful to Roger Richards of O. R. N. L for pointing out to us a mistake in our original numerical code, and to Paul Woskov of M . I. T for pointing out to us the shortcoming of treating the electrons shielding the alphas as unmagnetized.

This work was supported by the Department of Energy.

REFERENCES

1. L. Vahala, G. Vahala, and D. J. Sigmar, Nucl. Fusion **26**, 51 (1986)

2. J. Sheffield, **Plasma Scattering of Electromagentic Radiation**, New York, Academic Press, 1975;

3. Roger Richards (ORNL) pointed out to us a numerical error, while Paul Woskoboinikow (MIT) indicated that it would be more correct to treat the electrons shielding the alphas as magnetized, rather than as unmagnetized. These errors effect the results for perpendicular orientations more than those for off-perpendicular orientations. They were corrected by us and presented at the annual Sherwood Theory meeting, paper 3A29, (1987) in April 6-8 at San Diego.

4. L. Vahala and G. Vahala, paper 3A29, Sherwood Theory Meeting, April 6-8 (1987) ; and L. Vahala and G. Vahala, Bull. Am. Phys. Soc. **32**, 1896 (1987).

5. T. P. Hughes and S. R. P. Smith, submitted to Nucl. Fusion

6. P. Woskov, MIT report PFC/RR-87-16

7. N. Bretz, Princeton University report PPPL-2396 (1986)

FIGURE CAPTIONS

Fig. 1 The effect of $T_e$ and orientation angle $\varphi$ on the frequency dependence of the total scattering function $S_{tot}(\omega)$ and the alpha contribution $S_\alpha(\omega)$ for incident $CO_2$ laser at forward scattering angle $\theta=0.5^0$. The **** curves are for $\varphi=85^0$ : the curve -*-*- is for $S_{tot}$, while the unconncected * * * is the $S_\alpha$ curve. The ΔΔΔΔ curves are for $\varphi=80^0$: $S_{tot}$ -Δ-Δ-Δ , while $S_\alpha$ is the unconnected triangles curve.

**(a)** For $T_e$=1 keV, there is a sharp lower hybrid resonance in $S_{tot}$ provided $\varphi=85^0$ but this resonance in absent for $\varphi=80^0$. For both orientations $S_\alpha(\omega)\approx S_{tot}(\omega)$ except near $\omega\approx 1.8$ GHz where the deuteron contribution dominates. **(b)** $T_e$=10 keV. **(c)** $T_e$=15 keV. Note that as $T_e\uparrow$, $S_\alpha(\omega)/S_{tot}(\omega)\downarrow\downarrow$ , $\omega_{LH}\rightarrow$ , and the resonance broadens. Thus for relevant $T_e$, Eq. (10) is not satisfied, and so one will not be able to deduce the one dimensional alpha particle distribution function directly from the scattering data.

Fig. 2 $CO_2$ scattering. $\varphi=60^0$. Forward scattering angles: $\theta=1.0^0$ (****) , and $\theta=0.5^0$ (ΔΔΔΔ). **(a)** $T_e$=1 keV, **(b)** $T_e$=10 keV, **(c)** $T_e$=15 keV. Again, as $T_e\uparrow$, $S_\alpha(\omega)/S_{tot}(\omega)\downarrow\downarrow$.

Fig. 3 Same as Fig. 2, but for increased $k_{||}$ ($\varphi=45^0$).

Fig. 4 The electron temperature effect on $S_\alpha^*(\omega)/S_\alpha(\omega)$ for $CO_2$ scattering for various orientations $\varphi$: (a) $\varphi=75^0$, (b) $\varphi=60^0$, (c) $\varphi=45^0$, (d) $\varphi=0^0$. Forward scattering angle $\theta=0.5^0$. $T_e$= 1keV ($\Delta\Delta\Delta\Delta$) ; $T_e$=10 keV (oooo) ; $T_e$= 15 keV (****). As $T_e\uparrow$ , frequency dependence of $S_\alpha^*(\omega)/S_\alpha(\omega)$ $\downarrow$. As $\varphi\downarrow$ , frequency dependence of $S_\alpha^*(\omega)/S_\alpha(\omega)$ $\downarrow$. The normalization of the curves is chosen arbitrarily at $\omega$=1.8 GHz.

Fig. 5 $S_\alpha(\omega)$ and $S_{tot}(\omega)$ for the 2.14 mm gyrotron source at forward scattering angle $\theta=90^0$, and for $\varphi=85^0$ (****) and $\varphi=80^0$($\Delta\Delta\Delta\Delta$). (a) $T_e$=1 keV, (b) $T_e$=10 keV, (c) $T_e$=15 keV. These diagrams should be compared with Fig. 1 for the $CO_2$ laser. Note that the magnitudes of $S_{tot}$ and $S_\alpha$ are very similar, as is the behavior for $T_e\uparrow$ and for $\varphi\downarrow$.

Fig. 6 Same as Fig. 5, but for backward scattering angle $\theta=135^0$ and still $k_{\parallel}<<1$.

Fig. 7 2.14 mm gyrotron, $\varphi=75^0$ and $\theta=135^0$ (****) , $\theta=90^0$ ($\Delta\Delta\Delta\Delta$). Typically, $S_{tot}(\omega)\big|_{\theta=135} > S_{tot}(\omega)\big|_{\theta=90}$ . Similarly for $S_{\alpha(}\omega)$. Again, as $T_e$ $\uparrow$, $S_{tot}$ $\uparrow$,$S_\alpha$ $\uparrow$ but $S_\alpha/S_{tot}$ $\downarrow$. [N.B. compare with the $CO_2$ curves, Fig. 2] (a) $T_e$=1 keV, (b) $T_e$=10 keV, (c) Te=15 keV.

Fig. 8 Same as for Fig. 7, but for $\varphi=45^0$.

Fig. 9 Same as for Figs. 7 and 8, but for $\varphi=0^0$.

Fig. 10 $S_{tot}(\omega)$ and $S_\alpha(\omega)$ for the 2.14 mm (****) and 5 mm ($\Delta\Delta\Delta\Delta$) gyrotron sources. $\theta=45^0$, $T_e=10$ keV, and **(a)** $\varphi=75^0$, **(b)** $\varphi=45^0$. For the 5 mm gyrotron radiation, $S_i(\omega) \approx 0$ for $\omega=1$ GHz, so $S_{tot}$ and $S_\alpha$ are presented for 1 GHz $\leq \omega \leq$ $\omega$cut = 1.8 GHz frequency range. Note that for the 2.14 mm radiation, the signal strength is considerably greater than for the 5 mm source, and $\omega_{cut}$ is considerably higher (3.6 GHz). Notice that for both mm sources, $S_\alpha(\omega) \approx S_{tot}(\omega)$ : i.e., Eq. (11) is satisifed at $T_e=10$ keV.

Fig. 11 Same as Fig. 10, but for backscatter angle $\theta=135^0$, and **(a)** $\varphi=75^0$, (b) $\varphi=45^0$, (c) $\varphi=0^0$ at $T_e=$ 10 keV. The initial fall in $S_{tot}$ is due to the rapid decay of the deuteron contribution $S_i(\omega)$. $S_\alpha(\omega)/S_{tot}(\omega)$ $\downarrow\downarrow$ for the 2.14 mm source, but $S_\alpha(\omega)/S_{tot}(\omega)$ $\downarrow$ for the 5 mm source. However, $S_{tot}(\omega)$ $\downarrow\downarrow\downarrow$ with $\omega$. As $\varphi\downarrow$, $S_\alpha(\omega)/S_{tot}(\omega)$ $\uparrow$. Thus, Eq. (10) is quite well satisfied for the 5 mm source ($\Delta\Delta\Delta\Delta$), but not that well satisfied by the 2.14 mm source (****). In **(d)**, $T_e=1$ keV, and (d) should be compared to (a). In (d), $S_\alpha(\omega)/S_{tot}(\omega) \approx 1$.

Fig. 12 $T_e$ effects on $S_\alpha^*(\omega)/S_\alpha(\omega)$ at $\theta=45^0$ : $T_e$=1 kev ($\Delta\Delta\Delta\Delta$), $T_e$=10 keV (oooo), $T_e$=15 keV (****).

For 2.14 mm gyrotron : **(a)** $\varphi=75^0$, **(b)** $\varphi=60^0$, **(c)** $\varphi=0^0$,
for 5 mm gyrotron: **(d)** $\varphi=75^0$, **(e)** $\varphi=60^0$, **(f)** $\varphi=0^0$.

Provided $T_e \geq 10$ keV, $S_\alpha^*(\omega)/S_\alpha(\omega) \rightarrow$ const. as $\varphi\downarrow$ (for $\varphi<60^0$). Notice the low $\omega_{cut}$ for the sources ($\omega_{cut}$=1.9 GHz for 5 mm radiation, and $\omega_{cut}$=4.6 GHz for 2.14 mm radiation).

Fig. 13 Same as Fig. 12 except that $\theta=90^0$ and the orientations considered are $\varphi=75^0$ [**(a)**, **(e)**]; $\varphi=60^0$ [**(b)**, **(f)**]; $\varphi=45^0$ [**(c)**, **(g)**]; $\varphi=0^0$ [**(d)**, **(h)**]. As $\theta\uparrow$, $\omega_{cut}\uparrow$. Clearly for $\varphi=45^0$ and $\downarrow$, $S_\alpha^*(\omega)/S_\alpha(\omega)\approx$ const., provided $T_e \geq 10$ keV.

Fig. 14 Same as Fig. 13 except that $\theta=135^0$. As $\theta\uparrow$, $\omega_{cut}\uparrow$. Again for $\varphi=45^0$ and $\downarrow$, $S_\alpha^*(\omega)/S_\alpha(\omega)\approx$ const., provided $T_e \geq 10$ keV.

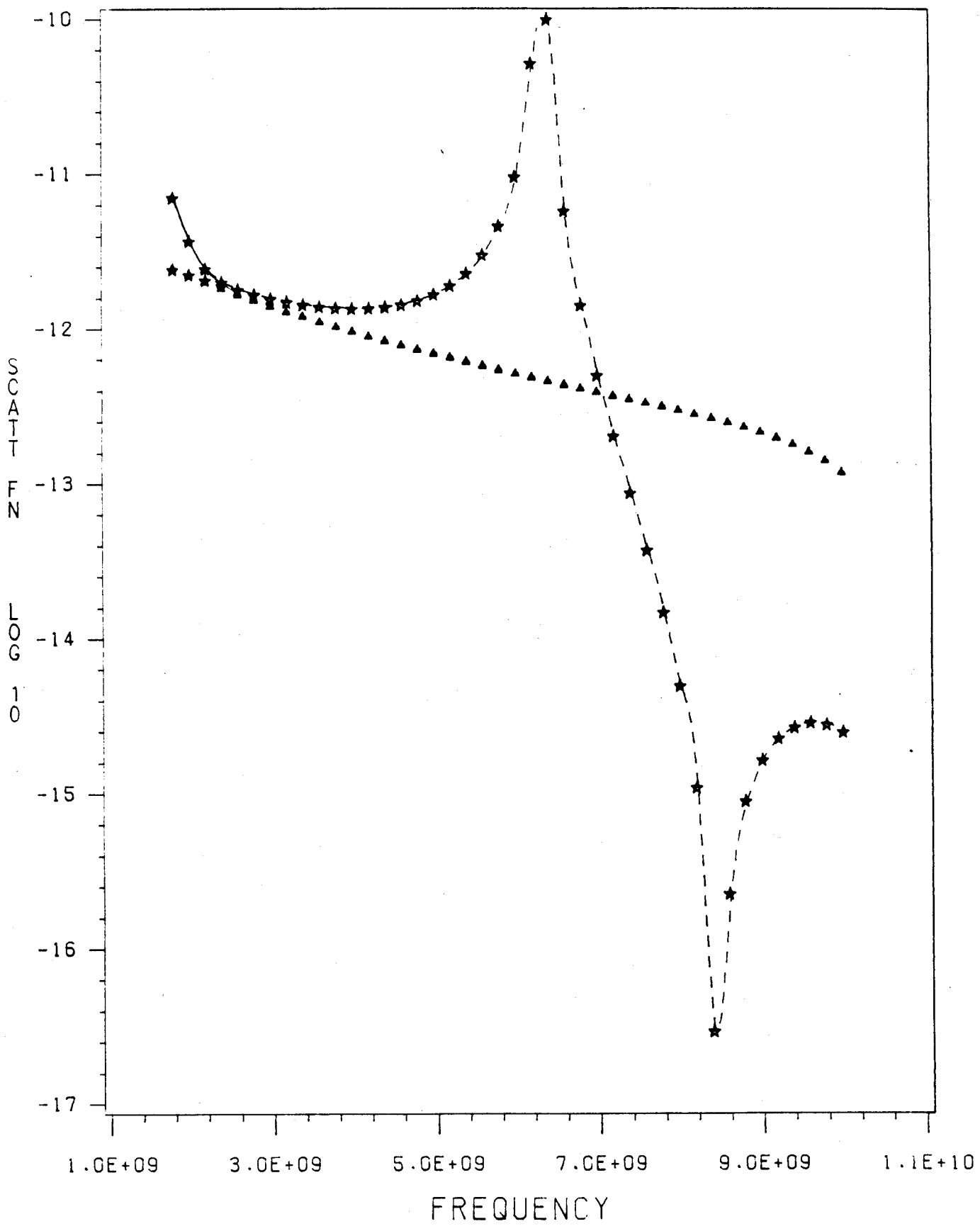
FORWARD SCATT. ANGLE=0.5 DEG, TE=1 KEV
K.B ANGLE : AA (80) , ** (85) DEG
-10
-11
-12
-13
-14
-15
-16
-17
SCATT FN
LOG 10
1.0E+09
3.0E+09
5.0E+09
7.0E+09
9.0E+09
1.1E+10
FREQUENCY

Fig. 1a

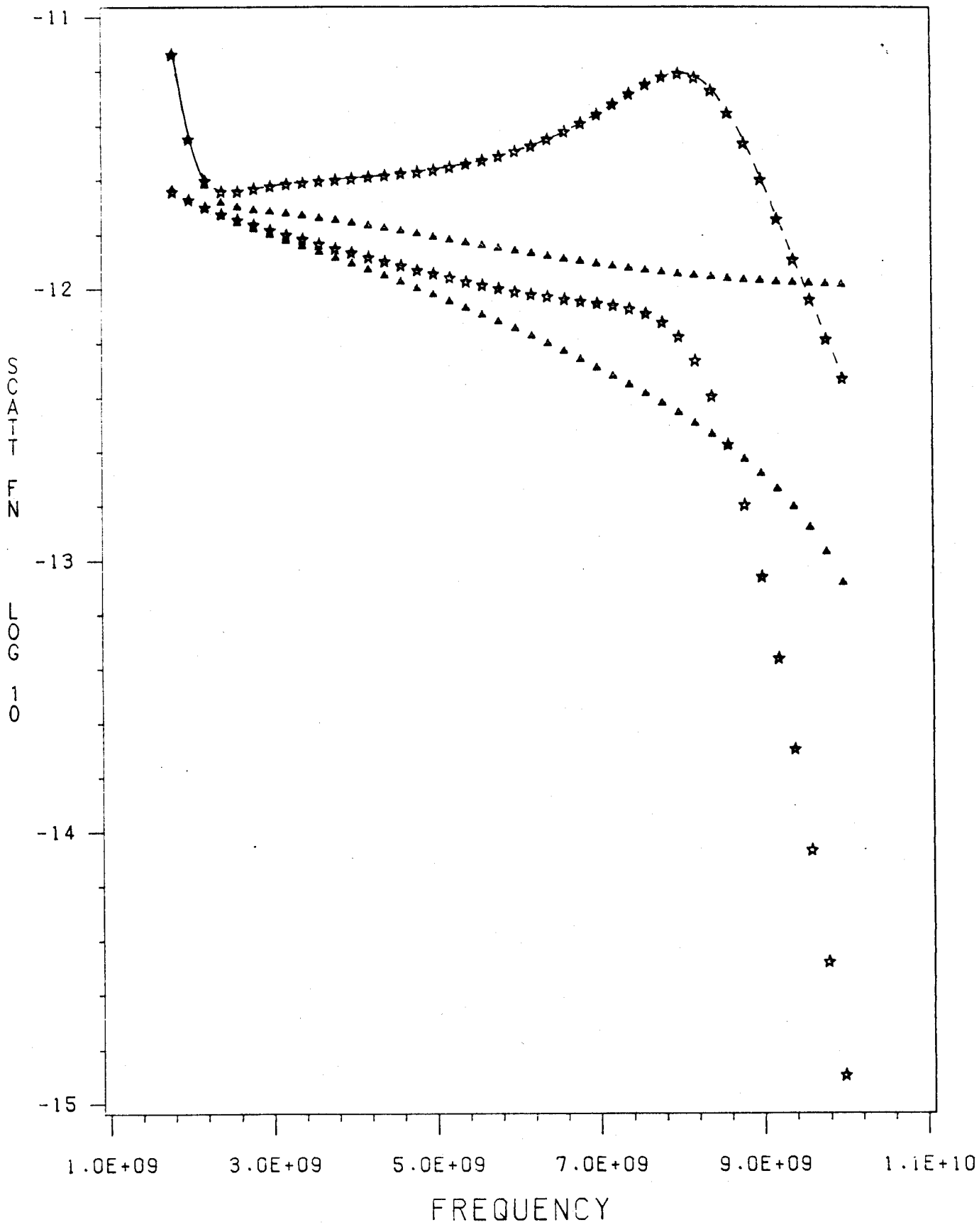
FORWARD SCATT. ANGLE=0.5 DEG, TE=10 KEV
K.B ANGLE : AA (80) , ** (85) DEG
-11
-12
-13
-14
-15
SCATT FN
LOG 10
1.0E+09
3.0E+09
5.0E+09
7.0E+09
9.0E+09
1.1E+10
FREQUENCY

Fig. 1b

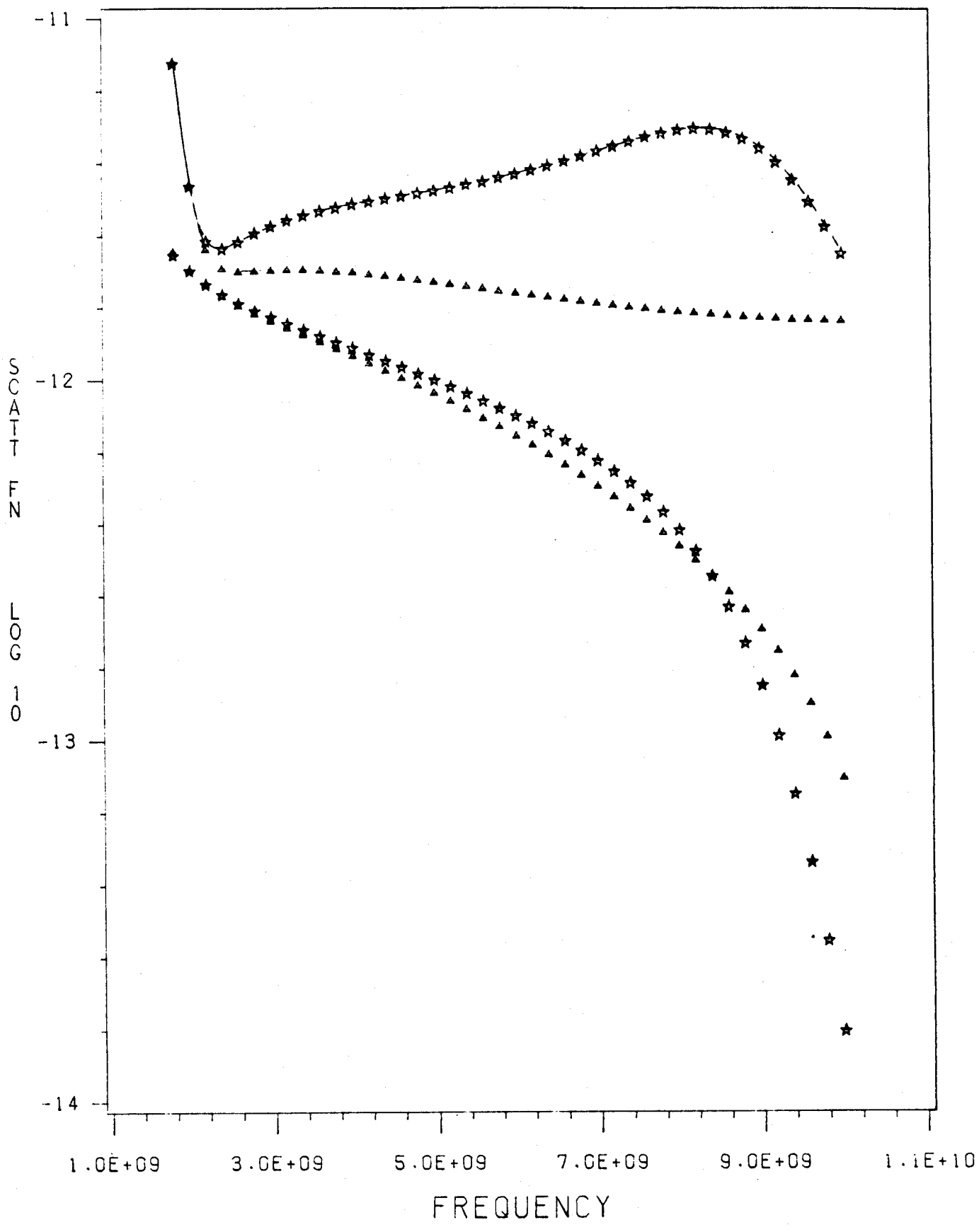
FORWARD SCATT. ANGLE=0.5 DEG, TE=15 KEV
K.B ANGLE : AA (80) , ** (85) DEG
-11
-12
-13
-14
SCATT FN
LOG 10
1.0E+09
3.0E+09
5.0E+09
7.0E+09
9.0E+09
1.1E+10
FREQUENCY

Fig. 1c

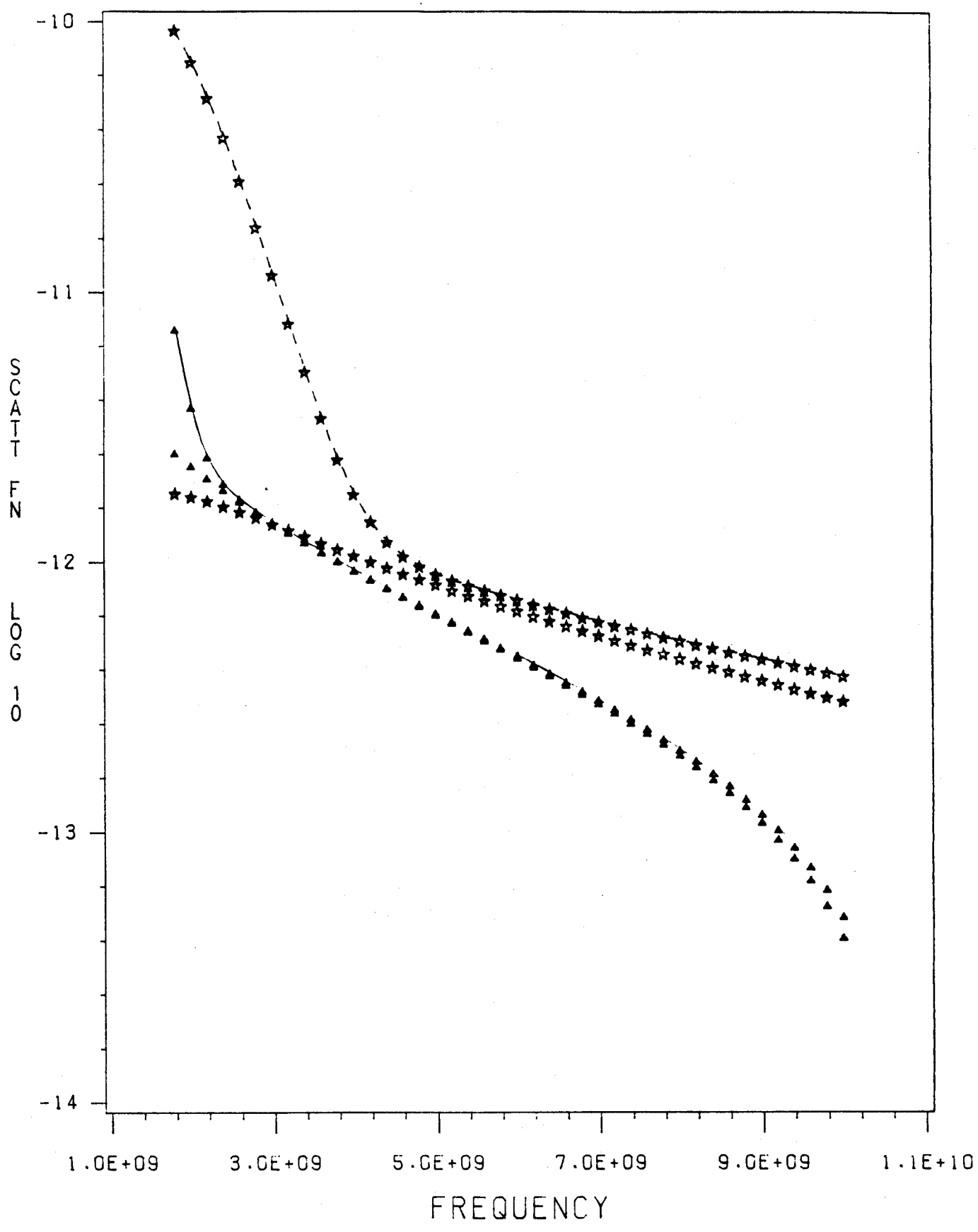
CO2 SCATT. AT K.B=60 DEG , TE=1 KEV
FORWARD SCATT. ANGLE: 1.0 DEG (**) , 0.5 (AA)
-10
-11
-12
-13
-14
SCATT FN
LOG 10
1.0E+09
3.0E+09
5.0E+09
7.0E+09
9.0E+09
1.1E+10
FREQUENCY

Fig. 2a

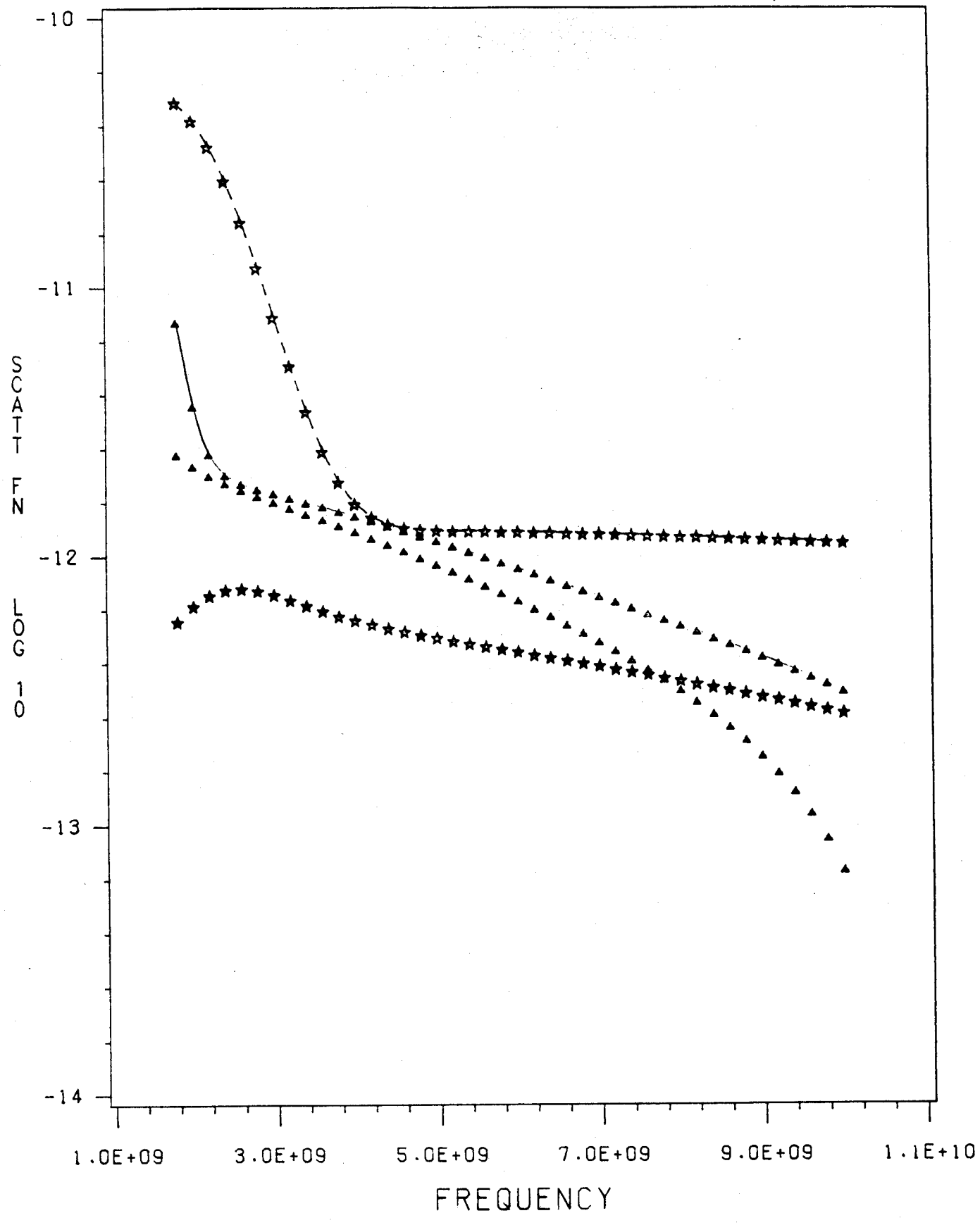
CO2 SCATT. AT K.B=60 DEG , TE=10 KEV
FORWARD SCATT. ANGLE: 1.0 DEG (**) , 0.5 (AA)
-10
-11
-12
-13
-14
SCATT FN
LOG 10
1.0E+09
3.0E+09
5.0E+09
7.0E+09
9.0E+09
1.1E+10
FREQUENCY

Fig. 2b

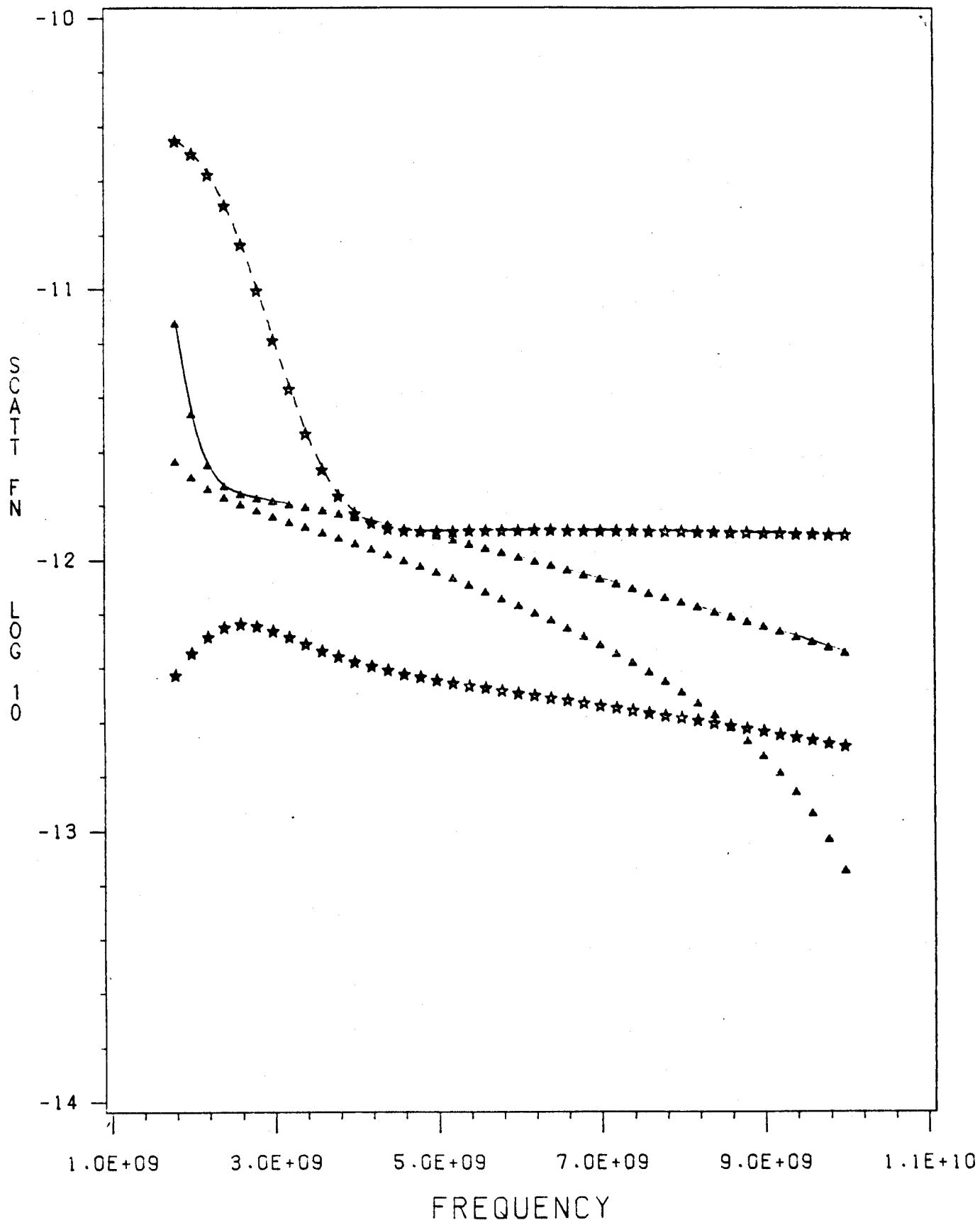
CO2 SCATT. AT K.B=60 DEG , TE=15 KEV
FORWARD SCATT. ANGLE: 1.0 DEG (**) , 0.5 (AA)
-10
-11
-12
-13
-14
SCATT FN
LOG 10
1.0E+09
3.0E+09
5.0E+09
7.0E+09
9.0E+09
1.1E+10
FREQUENCY

Fig. 2c

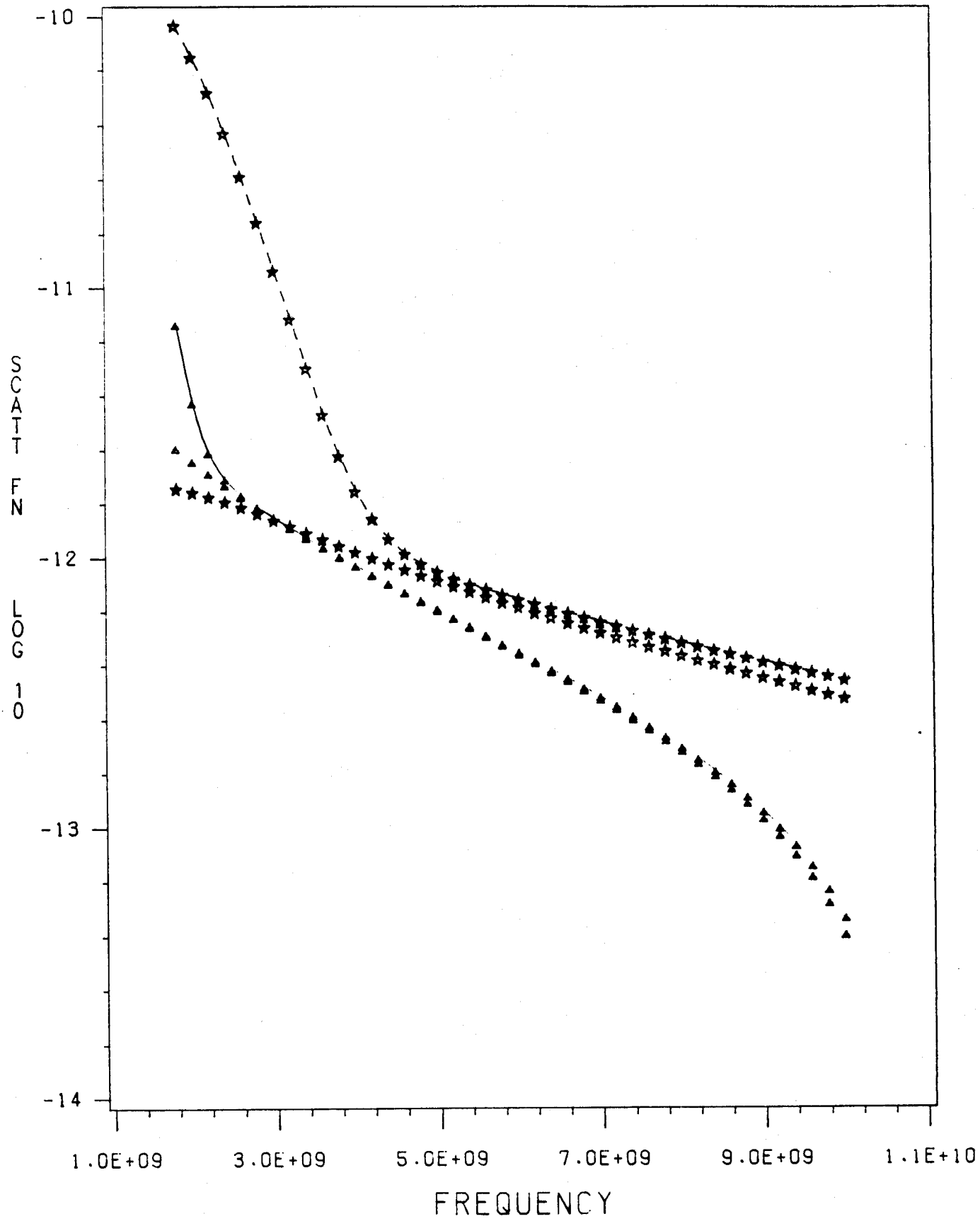
CO2 SCATT. AT K.B=45 DEG , TE=1 KEV
FORWARD SCATT. ANGLE: 1.0 DEG (**) , 0.5 (AA)
-10
-11
-12
-13
-14
SCATT FN
LOG 10
1.0E+09
3.0E+09
5.0E+09
7.0E+09
9.0E+09
1.1E+10
FREQUENCY

Fig. 3a

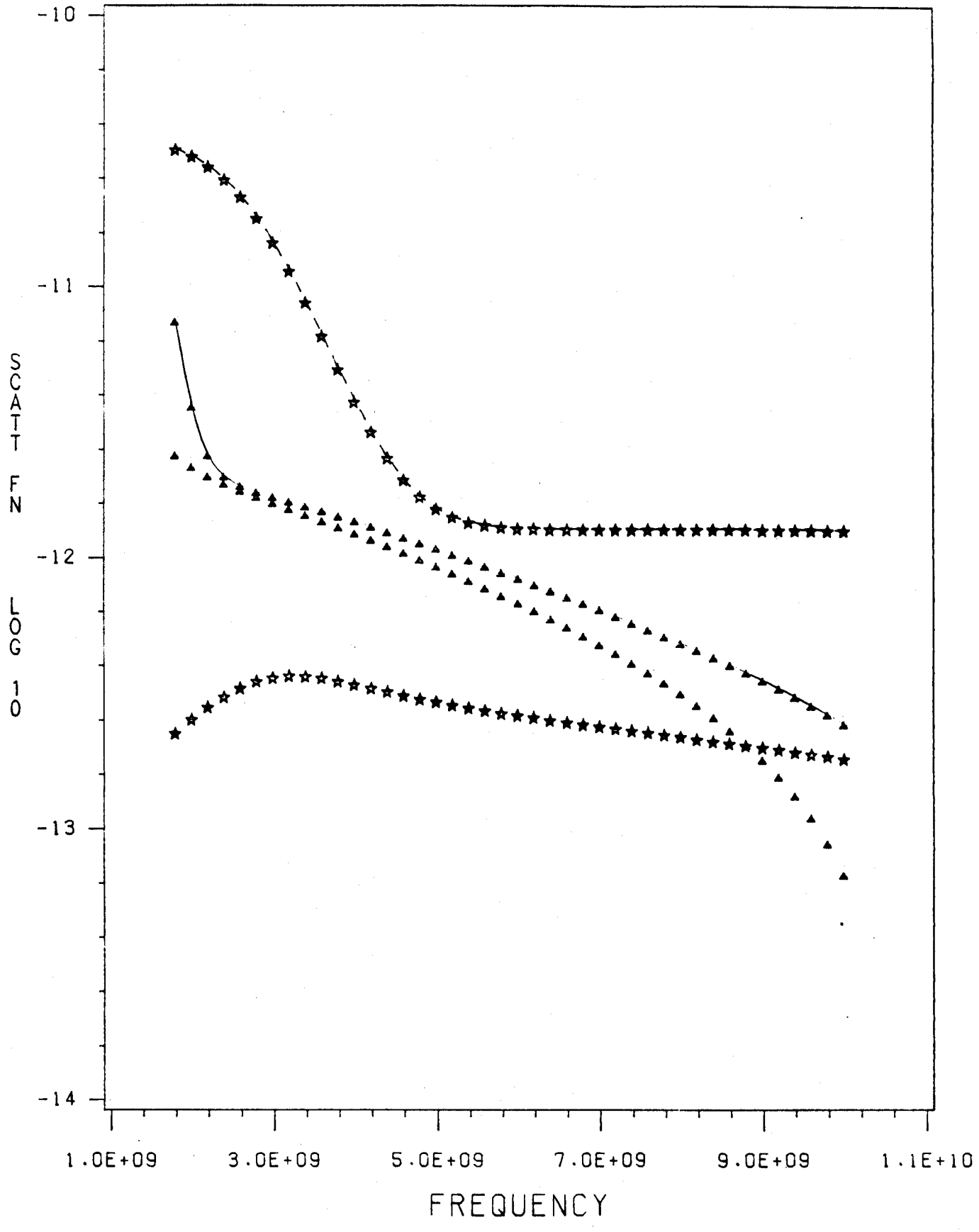
CO2 SCATT. AT K.B=45 DEG , TE=10 KEV
FORWARD SCATT. ANGLE: 1.0 DEG (**) , 0.5 (AA)
-10
-11
-12
-13
-14
SCATT FN
LOG 10
1.0E+09
3.0E+09
5.0E+09
7.0E+09
9.0E+09
1.1E+10
FREQUENCY

Fig. 3b

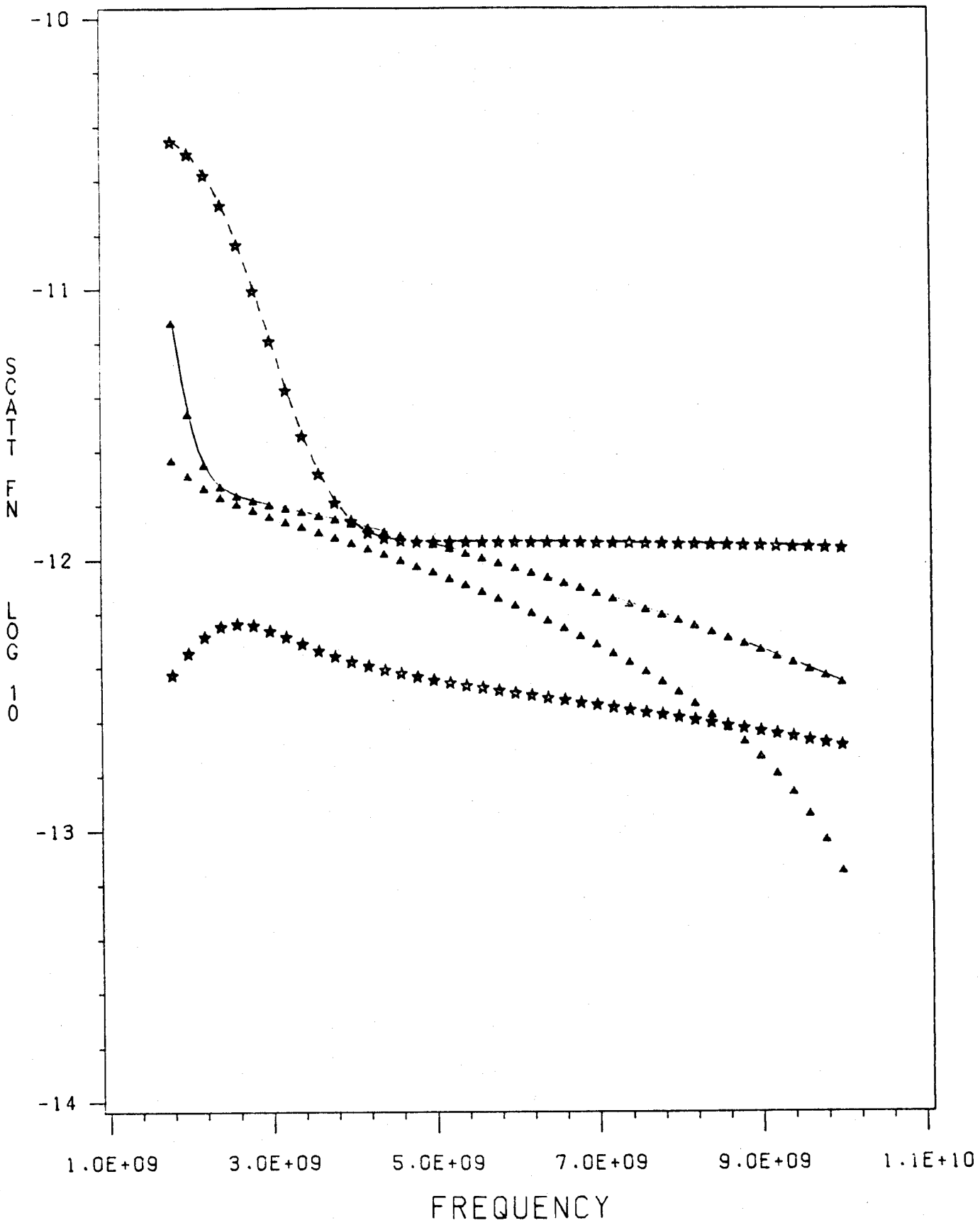
CO2 SCATT. AT K.B=45 DEG , TE=15 KEV
FORWARD SCATT. ANGLE: 1.0 DEG (**) , 0.5 (AA)
-10
-11
-12
-13
-14
SCATT FN
LOG 10
1.0E+09
3.0E+09
5.0E+09
7.0E+09
9.0E+09
1.1E+10
FREQUENCY

Fig. 3c

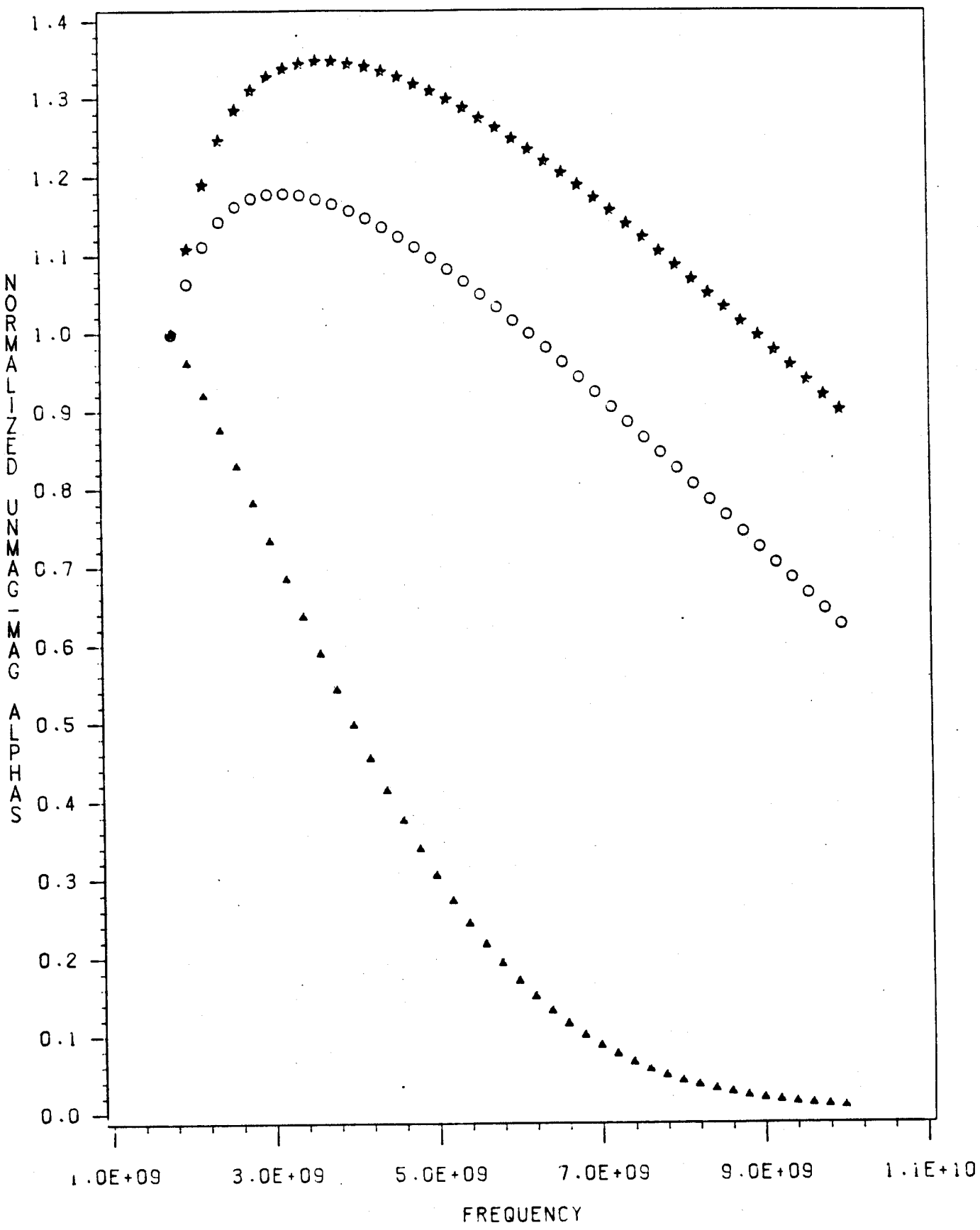
TE EFFECTS AT 0.5 DEG, K.B=75 DEG
CO2 , TE: ** 15 KEV, OO 10 KEV, AA 1 KEV
NORMALIZED UNMAG-MAG ALPHAS
1.4
1.3
1.2
1.1
1.0
0.9
0.8
0.7
0.6
0.5
0.4
0.3
0.2
0.1
0.0
1.0E+09
3.0E+09
5.0E+09
7.0E+09
9.0E+09
1.1E+10
FREQUENCY

Fig. 4a

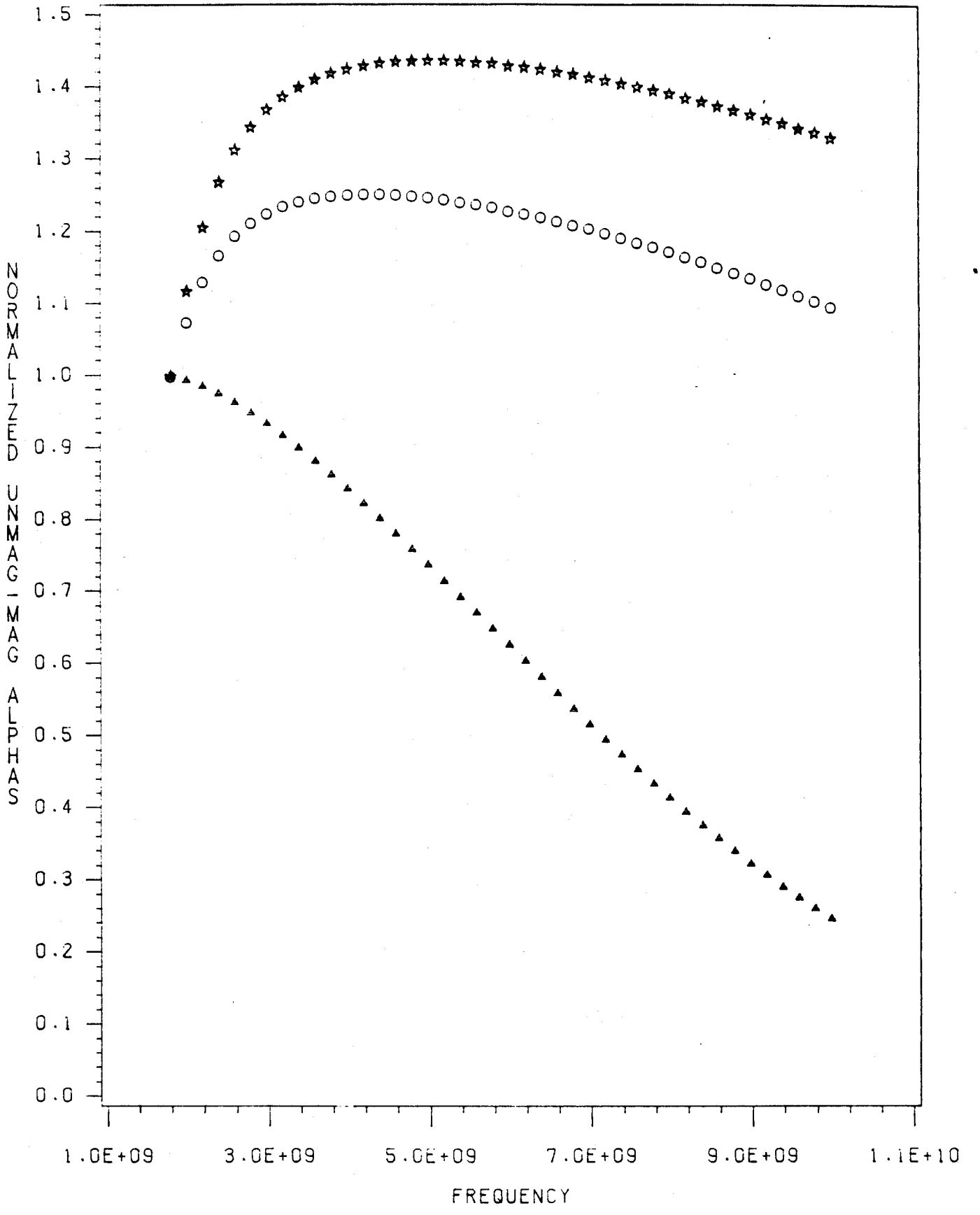
TE EFFECTS AT 0.5 DEG, K.B=60 DEG
CO2 , TE: ** 15 KEV, OO 10 KEV, AA 1 KEV
NORMALIZED UNMAG-MAG ALPHAS
1.5
1.4
1.3
1.2
1.1
1.0
0.9
0.8
0.7
0.6
0.5
0.4
0.3
0.2
0.1
0.0
1.0E+09
3.0E+09
5.0E+09
7.0E+09
9.0E+09
1.1E+10
FREQUENCY

Fig. 4b

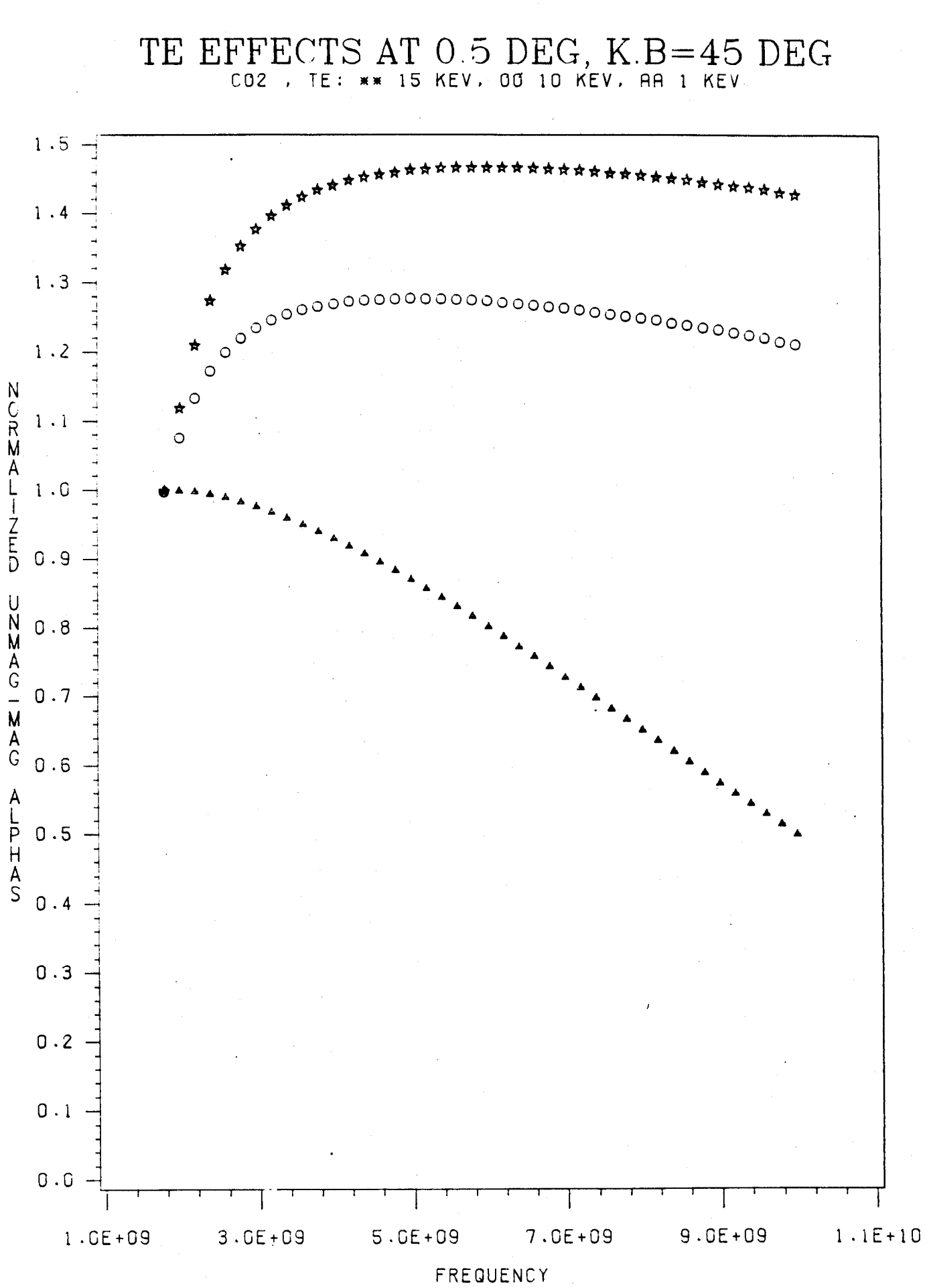
TE EFFECTS AT 0.5 DEG, K.B=45 DEG
CO2 , TE: ** 15 KEV, OO 10 KEV, AA 1 KEV
NORMALIZED UNMAG-MAG ALPHAS
1.5
1.4
1.3
1.2
1.1
1.0
0.9
0.8
0.7
0.6
0.5
0.4
0.3
0.2
0.1
0.0
1.0E+09
3.0E+09
5.0E+09
7.0E+09
9.0E+09
1.1E+10
FREQUENCY

Fig. 4c

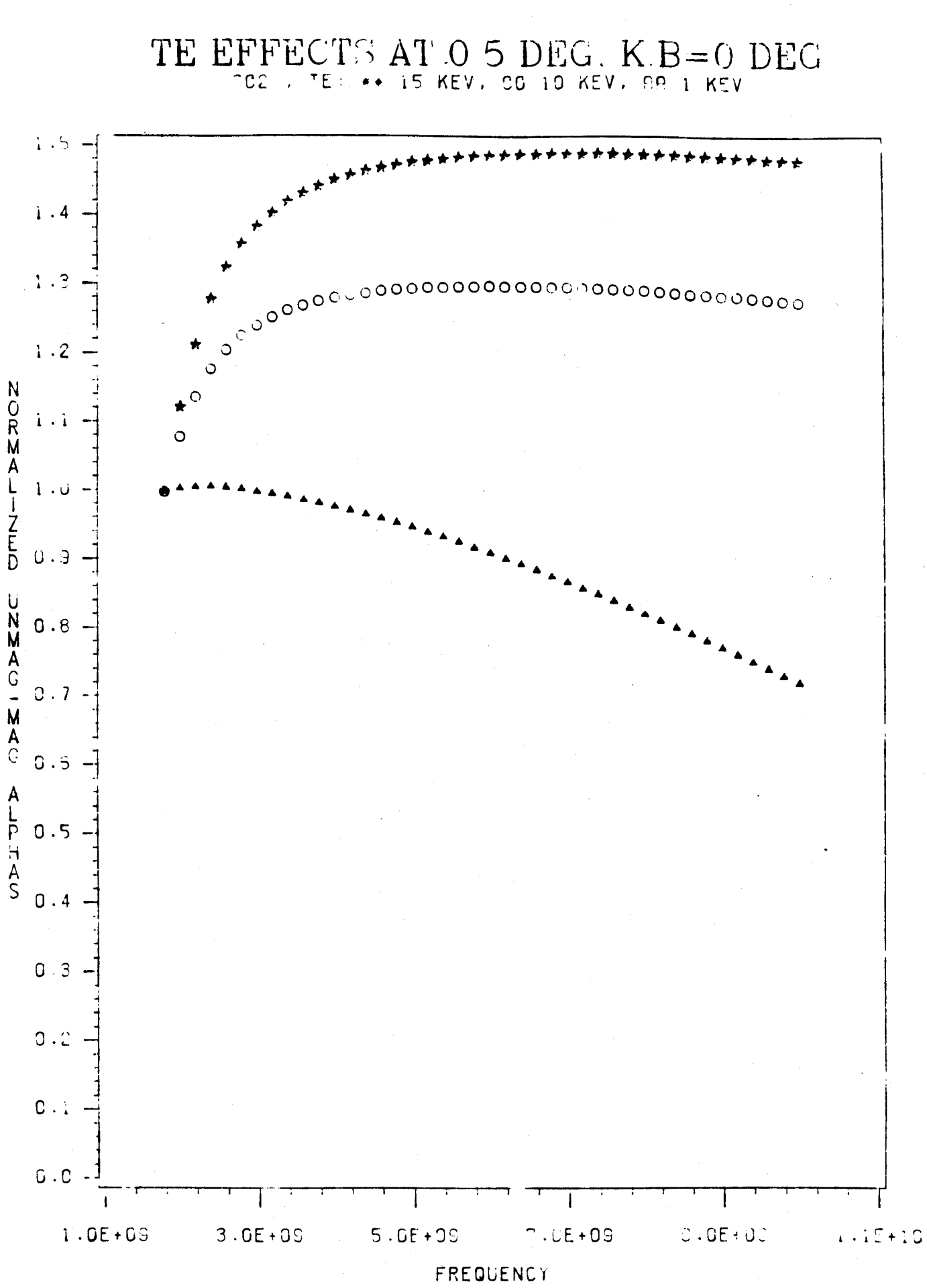
TE EFFECTS AT 0 5 DEG. K.B=0 DEG
15 KEV, 10 KEV, 1 KEV
NORMALIZED UNMAG-MAG ALPHAS
1.5
1.4
1.3
1.2
1.1
1.0
0.9
0.8
0.7
0.6
0.5
0.4
0.3
0.2
0.1
0.0
1.0E+09
3.0E+09
5.0E+09
FREQUENCY

**Fig. 4d**

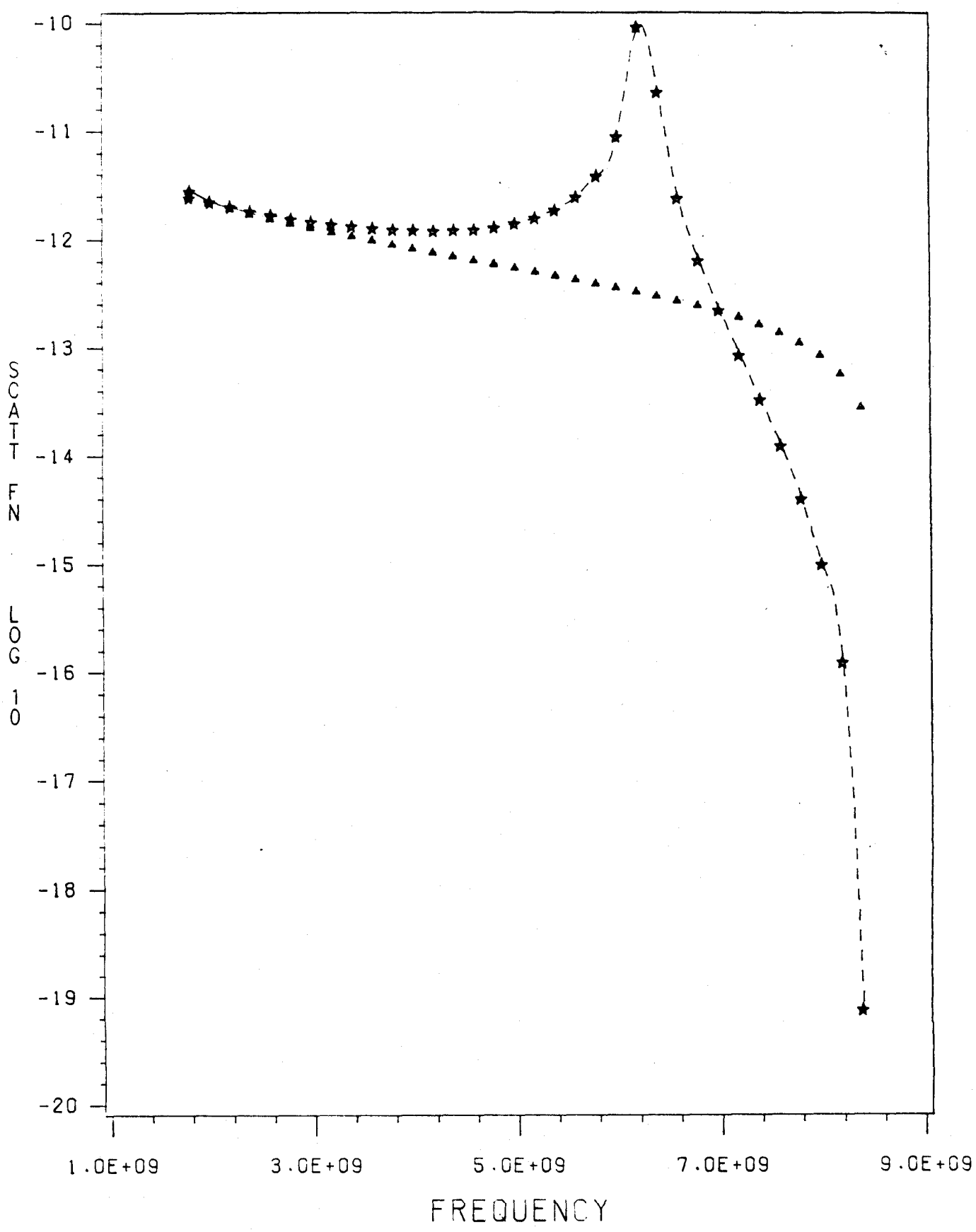
2.14 MM : THETA=90 DEG, TE=1 KEV
K.B ANGLE : AA (80) , ** (85) DEG
-10
-11
-12
-13
-14
-15
-16
-17
-18
-19
-20
SCATT FN
LOG 10
1.0E+09
3.0E+09
5.0E+09
7.0E+09
9.0E+09
FREQUENCY

Fig. 5a

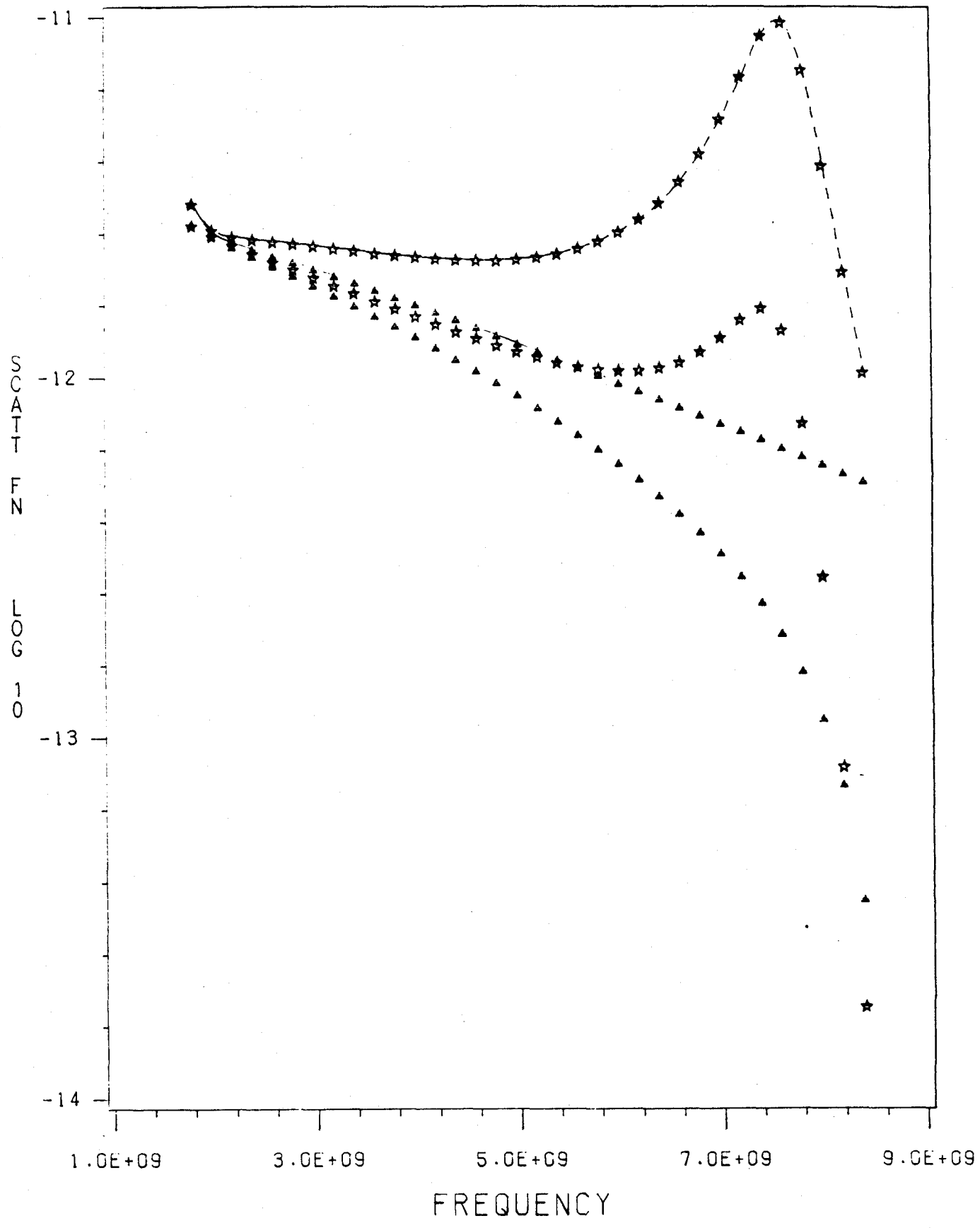
2.14 MM : THETA=90 DEG, TE=10 KEV
K.B ANGLE : AA (80) , ** (85) DEG
-11
-12
-13
-14
SCATT FN
LOG 10
1.0E+09
3.0E+09
5.0E+09
7.0E+09
9.0E+09
FREQUENCY

Fig. 5b

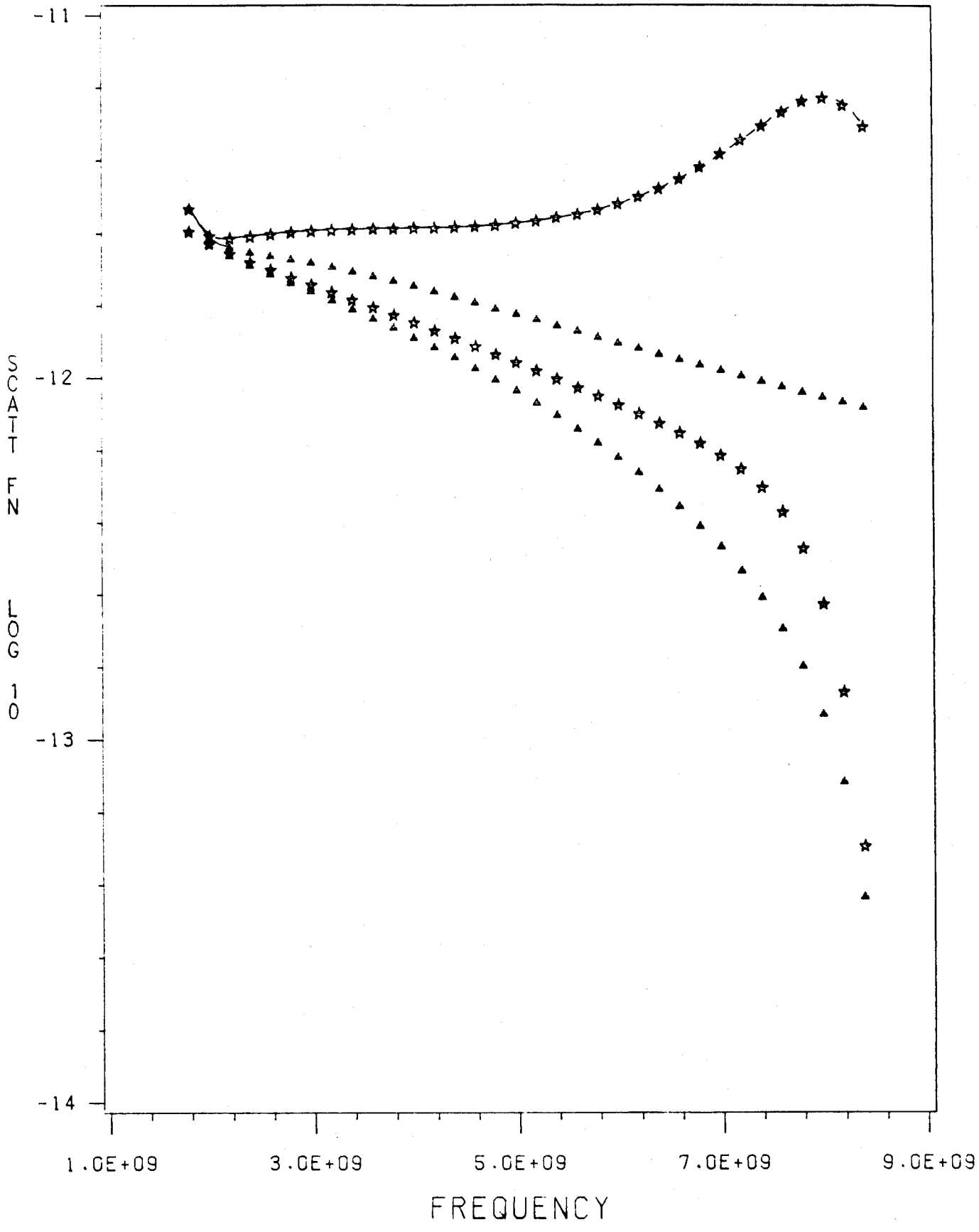
2.14 MM : THETA=90 DEG, TE=15 KEV
K.B ANGLE : ** (80) , ** (85) DEG
-11
-12
-13
-14
SCATT FN
LOG 10
1.0E+09
3.0E+09
5.0E+09
7.0E+09
9.0E+09
FREQUENCY

Fig. 5c

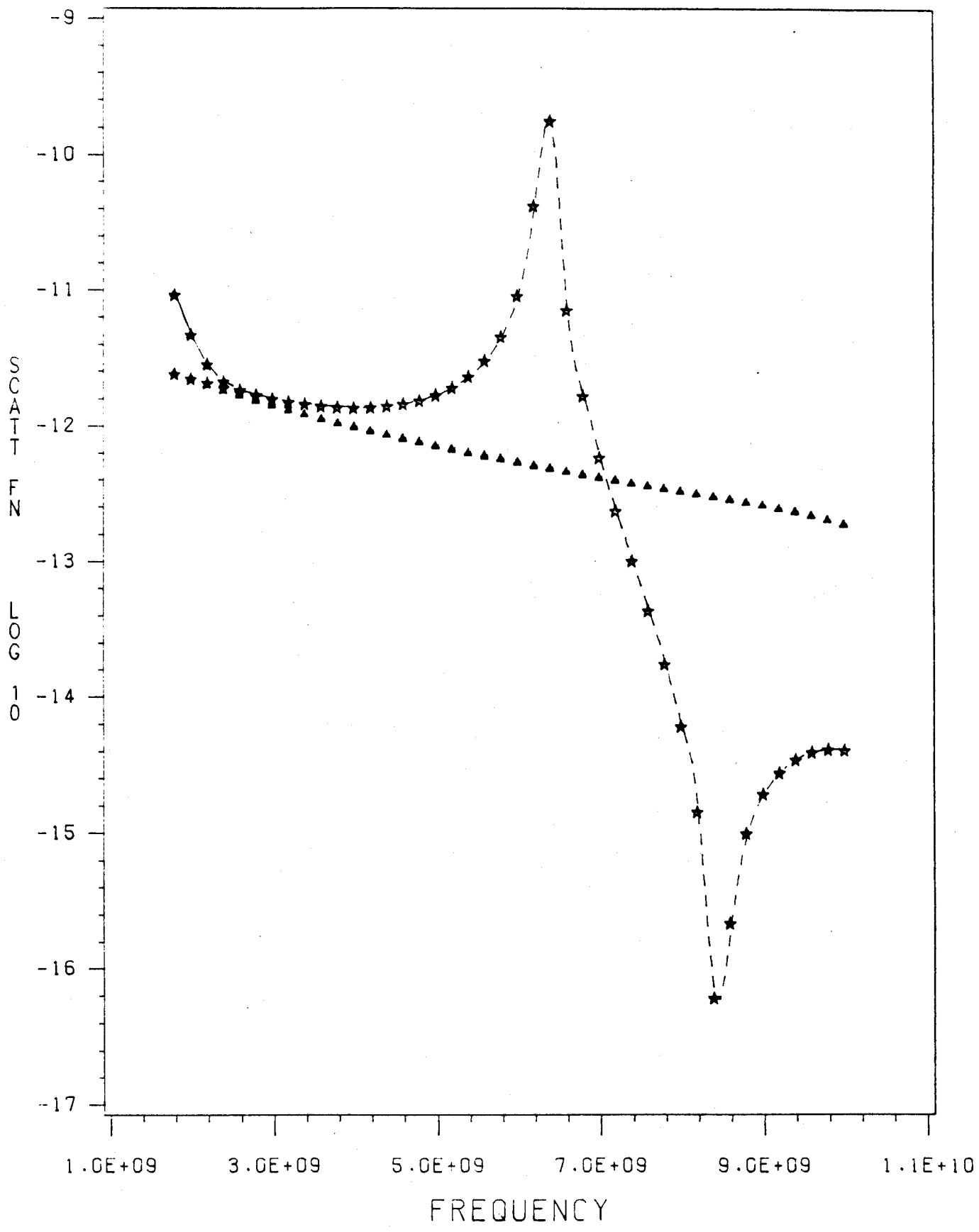
2.14 MM : THETA=135 DEG, TE=1 KEV
K.B ANGLE : AA (80) , ** (85) DEG
-9
-10
-11
-12
-13
-14
-15
-16
-17
SCATT FN
LOG 10
1.0E+09
3.0E+09
5.0E+09
7.0E+09
9.0E+09
1.1E+10
FREQUENCY

Fig. 6a

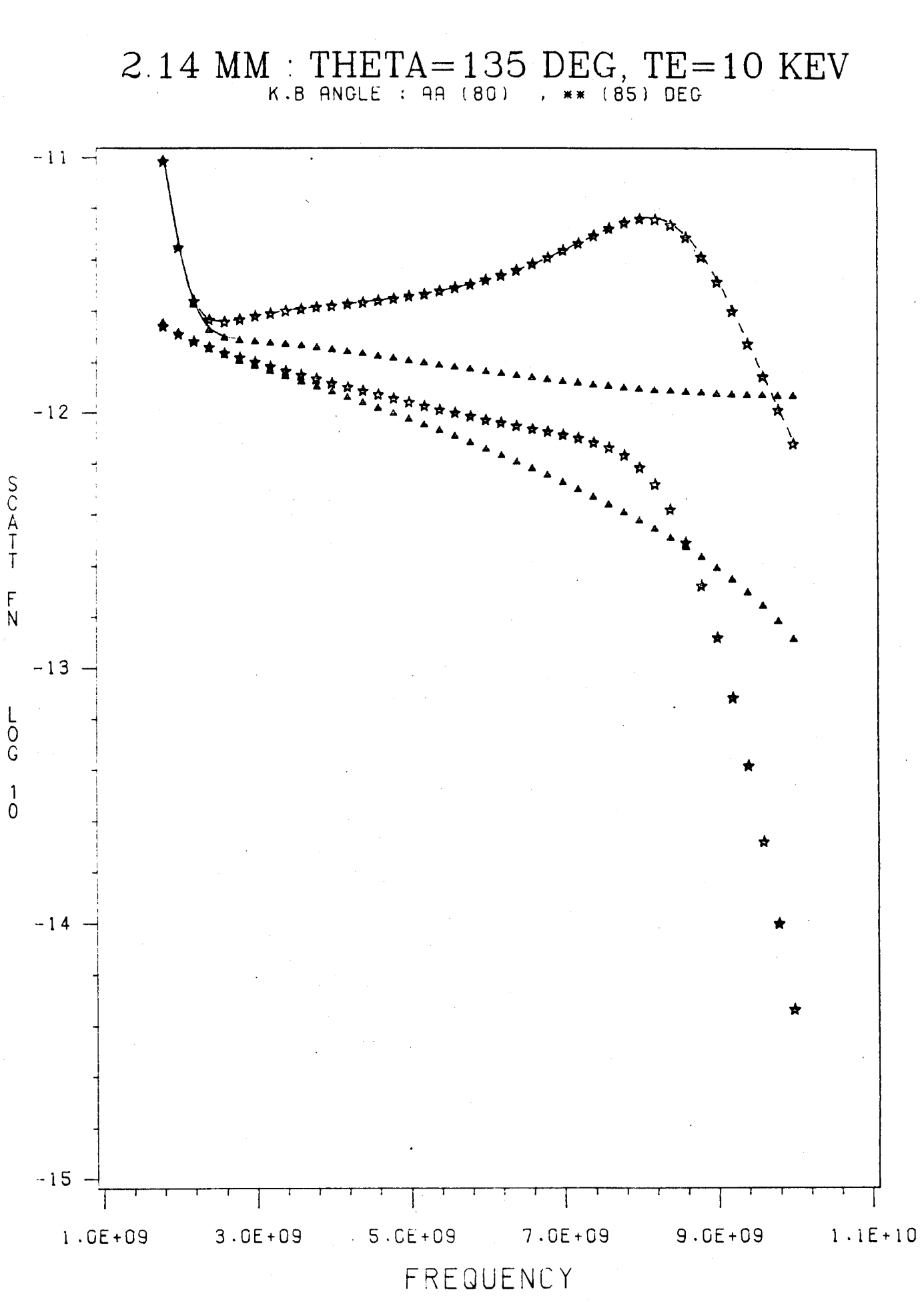
2.14 MM : THETA=135 DEG, TE=10 KEV
K.B ANGLE : AA (80) , ** (85) DEG
-11
-12
-13
-14
-15
SCATT FN
LOG 10
1.0E+09
3.0E+09
5.0E+09
7.0E+09
9.0E+09
1.1E+10
FREQUENCY

Fig. 6b

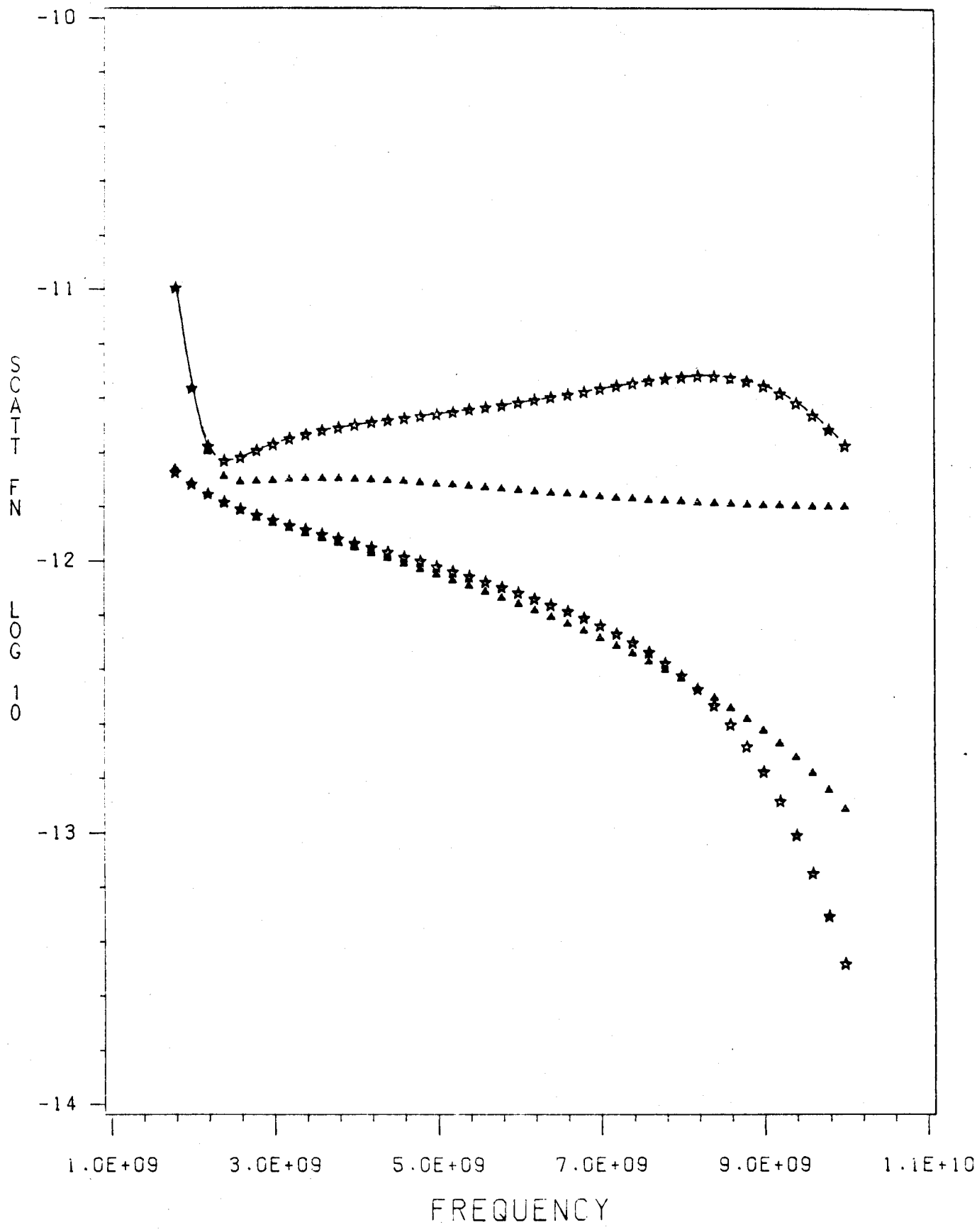
2.14 MM : THETA=135 DEG, TE=15 KEV
K.B ANGLE : 9A (80) , ** (85) DEG
-10
-11
-12
-13
-14
SCATT FN
LOG 10
1.0E+09
3.0E+09
5.0E+09
7.0E+09
9.0E+09
1.1E+10
FREQUENCY

Fig. 6c

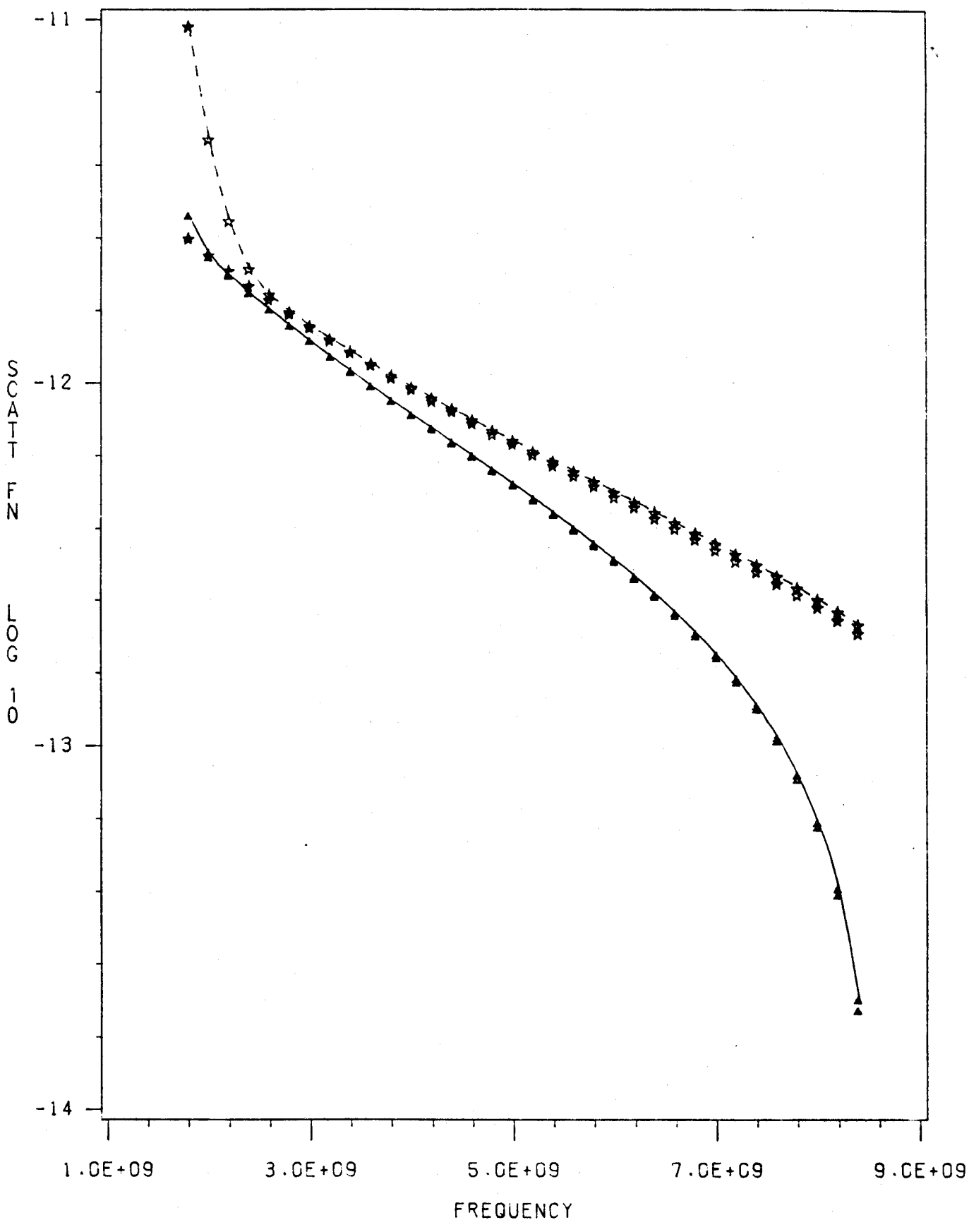
2.14 MM ; K.B ANGLE=75 DEG ; TE=1 KEV
FORWARD SCATT. ANGLE : 90 DEG (AA), 135 DEG (**)
-11
-12
-13
-14
SCATT FN
LOG 10
1.0E+09
3.0E+09
5.0E+09
7.0E+09
9.0E+09
FREQUENCY

Fig. 7a

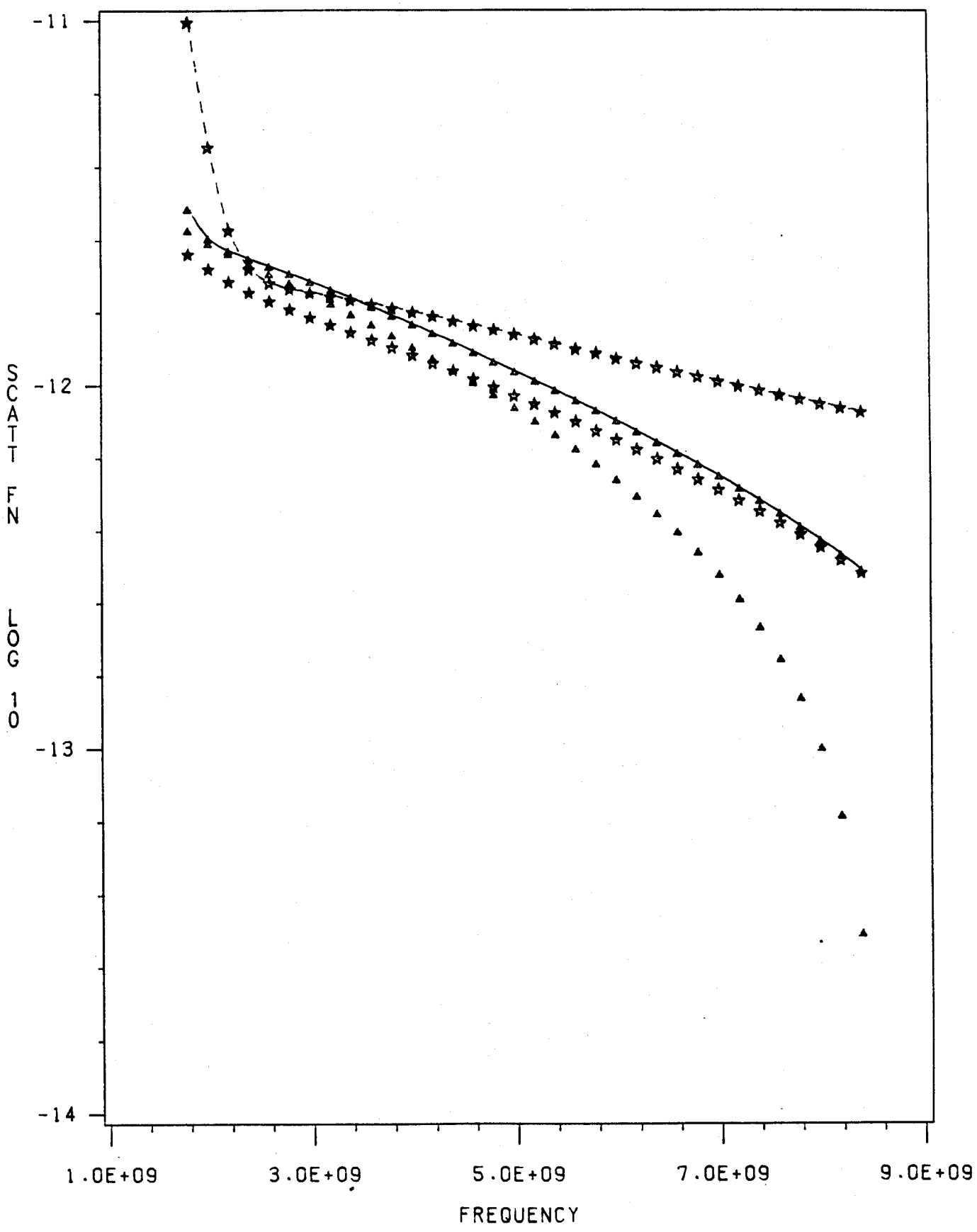
2.14 MM ; K.B ANGLE=75 DEG ; TE=10 KEV
FORWARD SCATT. ANGLE : 90 DEG (AA), 135 DEG (**)
-11
-12
-13
-14
SCATT FN
LOG 10
1.0E+09
3.0E+09
5.0E+09
7.0E+09
9.0E+09
FREQUENCY

Fig. 7b

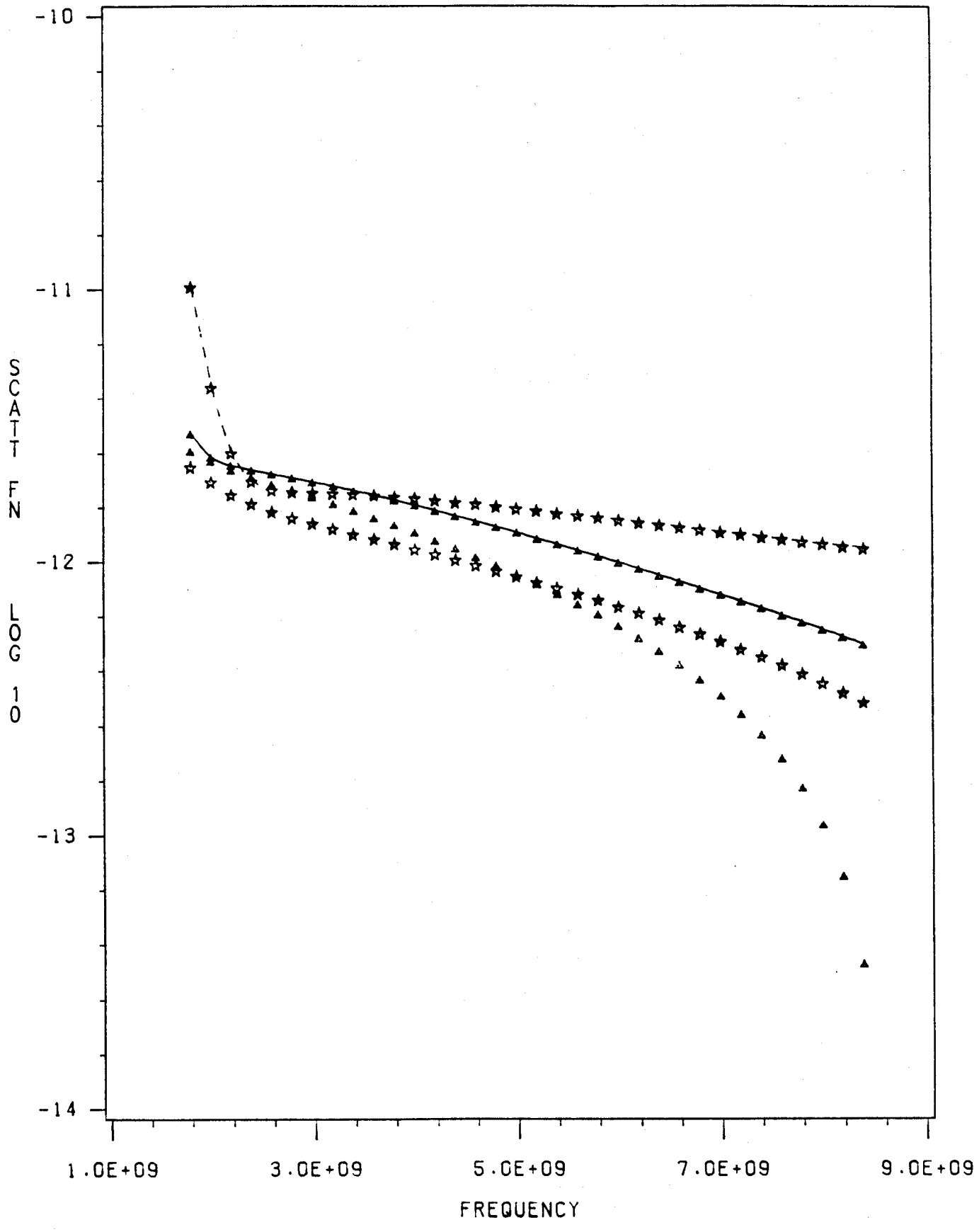
2.14 MM ; K.B ANGLE=75 DEG ; TE=15 KEV
FORWARD SCATT. ANGLE : 90 DEG (AA), 135 DEG (**)
-10
-11
-12
-13
-14
SCATT FN
LOG 10
1.0E+09
3.0E+09
5.0E+09
7.0E+09
9.0E+09
FREQUENCY

Fig. 7c

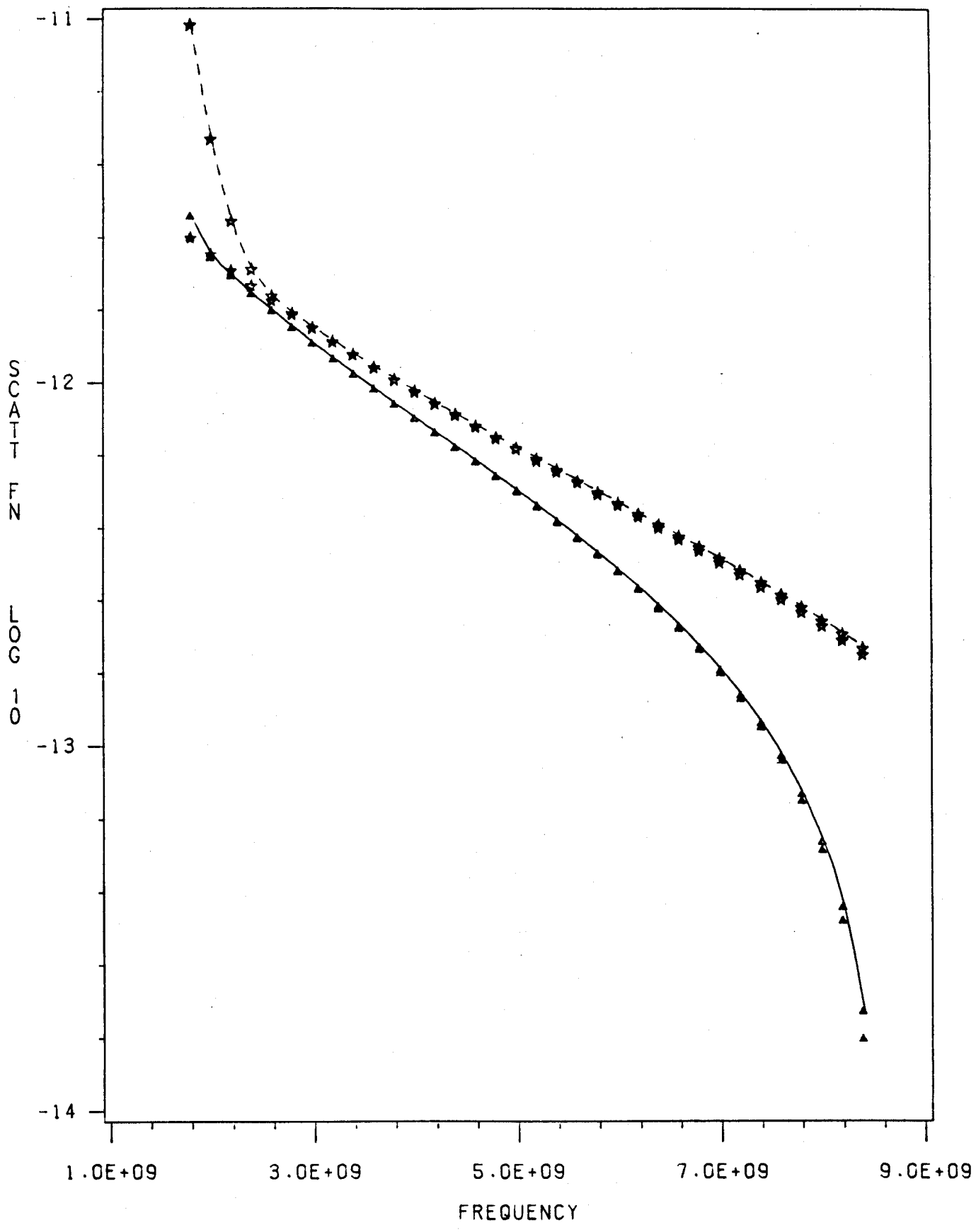
2.14 MM ; K.B ANGLE=45 DEG ; TE=1 KEV
FORWARD SCATT. ANGLE : 90 DEG (AA), 135 DEG (**)
-11
-12
-13
-14
SCATT FN
LOG 10
1.0E+09
3.0E+09
5.0E+09
7.0E+09
9.0E+09
FREQUENCY

Fig. 8a

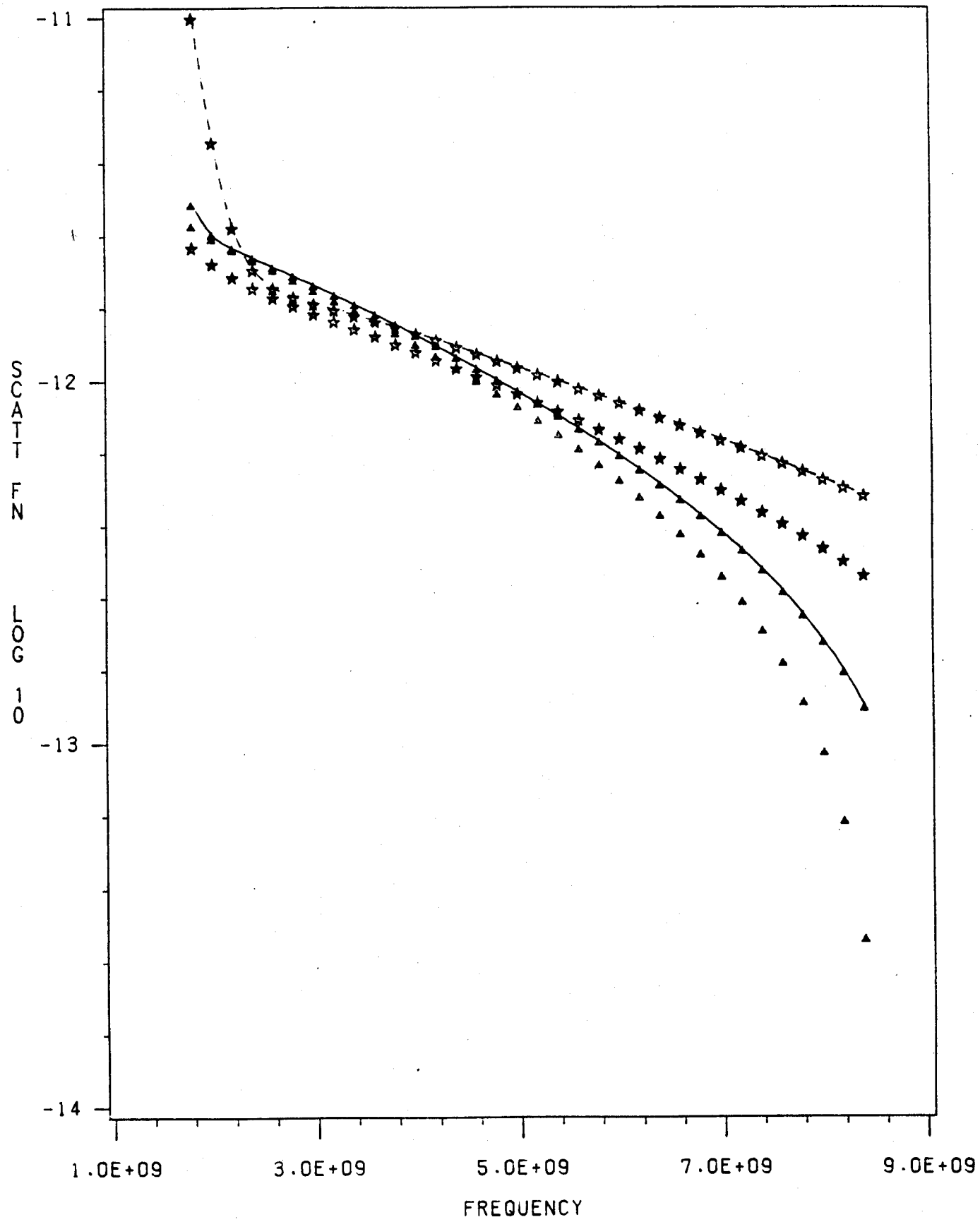
2.14 MM ; K.B ANGLE=45 DEG ; TE=10 KEV
FORWARD SCATT. ANGLE : 90 DEG (AA), 135 DEG (**)
-11
-12
-13
-14
SCATT FN
LOG 10
1.0E+09
3.0E+09
5.0E+09
7.0E+09
9.0E+09
FREQUENCY

Fig. 8b

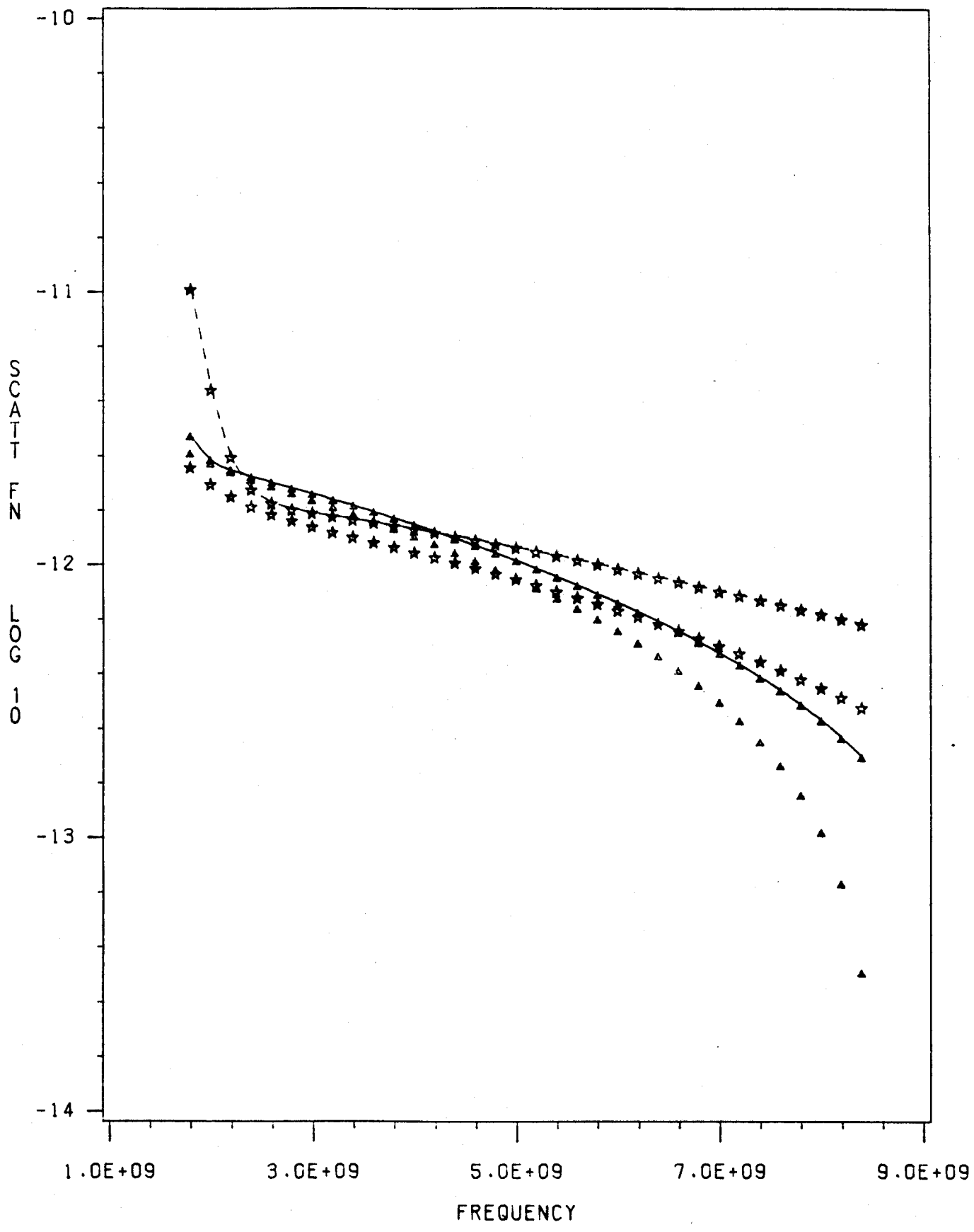
2.14 MM ; K.B ANGLE=45 DEG ; TE=15 KEV
FORWARD SCATT. ANGLE : 90 DEG (AA), 135 DEG (**)
-10
-11
-12
-13
-14
SCATT FN
LOG 10
1.0E+09
3.0E+09
5.0E+09
7.0E+09
9.0E+09
FREQUENCY

Fig. 8c

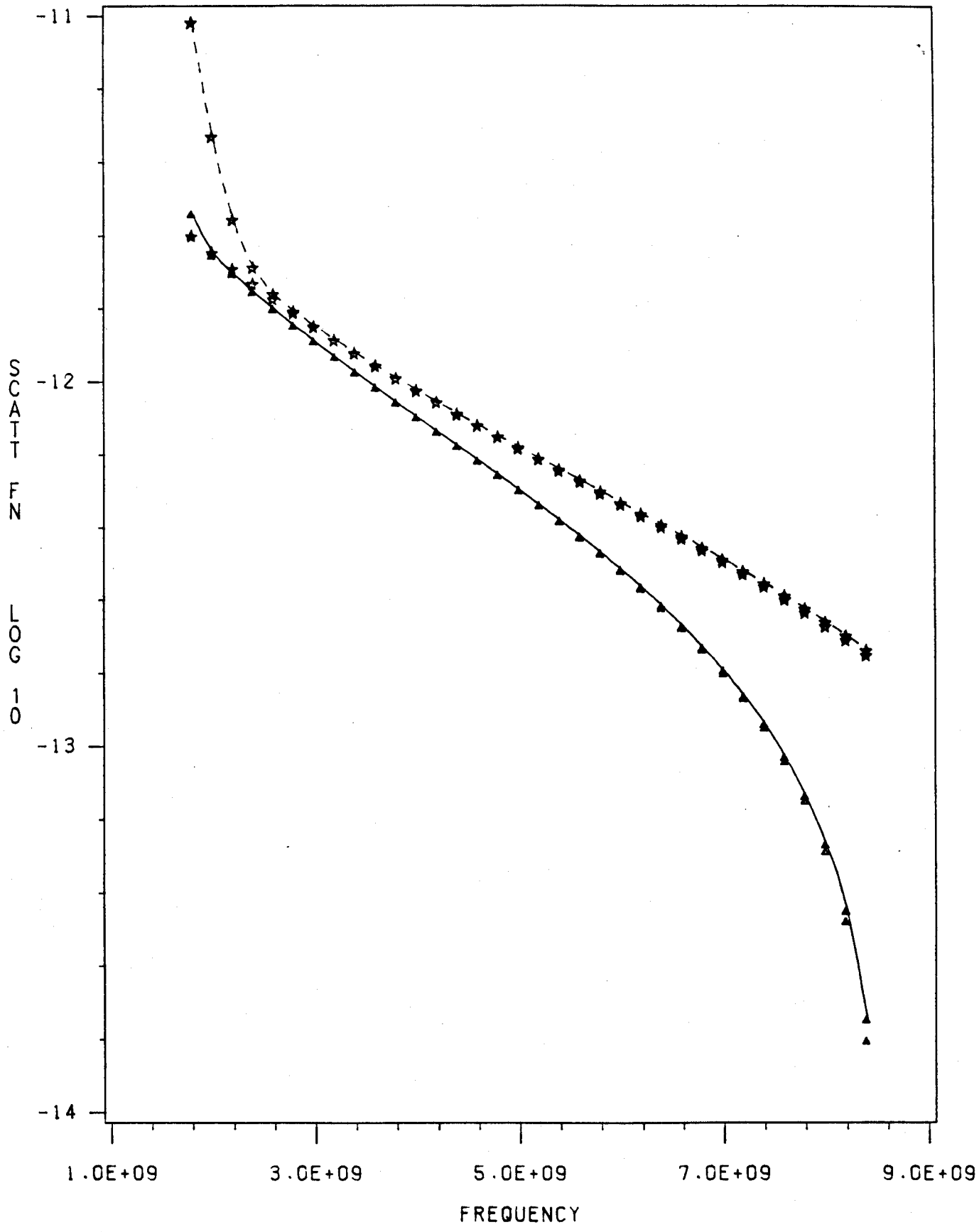
2.14 MM ; K.B ANGLE=0 DEG ; TE=1 KEV
FORWARD SCATT. ANGLE : 90 DEG (AA), 135 DEG (**)
-11
-12
-13
-14
SCATT FN
LOG 10
1.0E+09
3.0E+09
5.0E+09
7.0E+09
9.0E+09
FREQUENCY

Fig. 9a

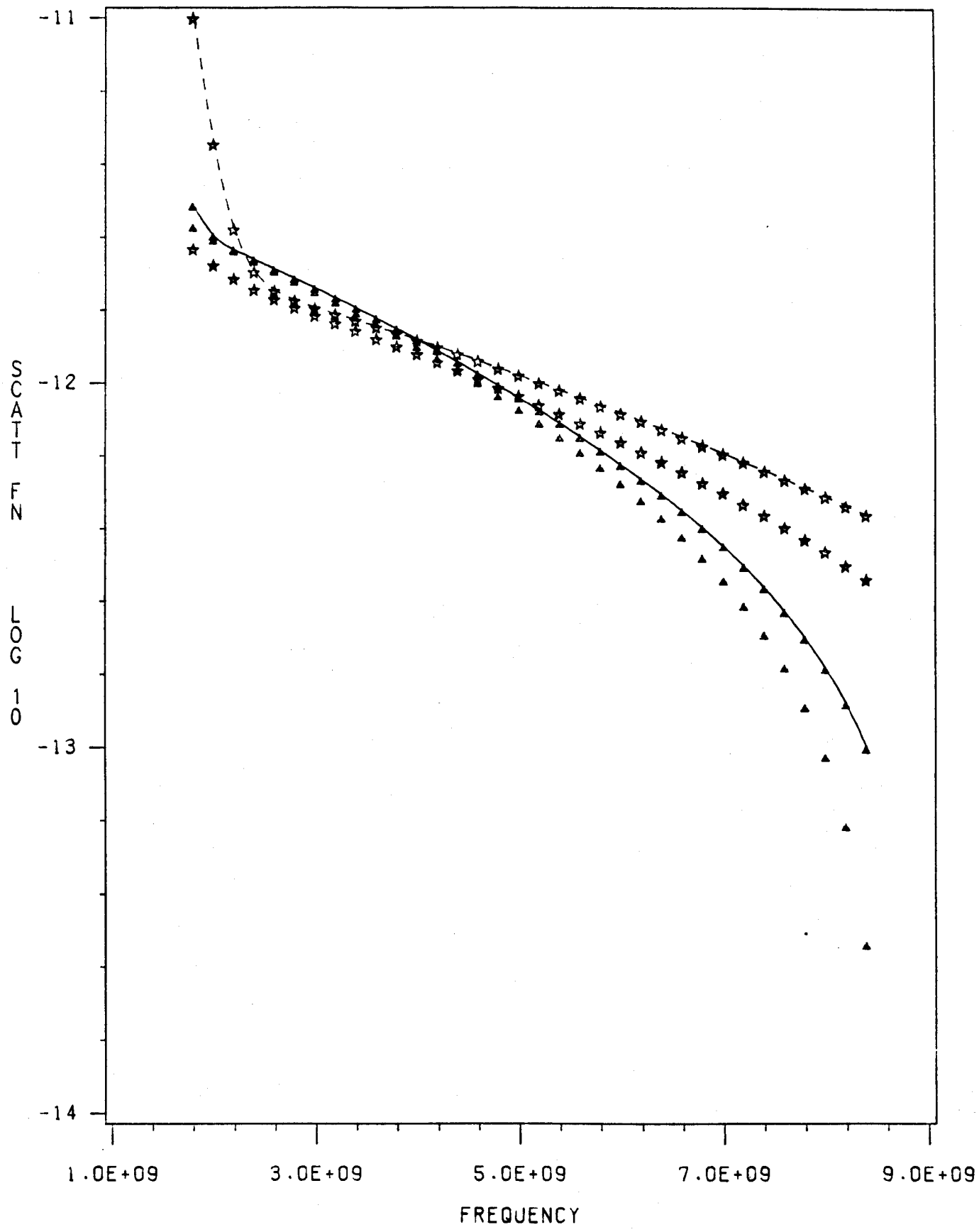
2.14 MM ; K.B ANGLE=0 DEG ; TE=10 KEV
FORWARD SCATT. ANGLE : 90 DEG (AA), 135 DEG (**)
-11
-12
-13
-14
SCATT FN
LOG 10
1.0E+09
3.0E+09
5.0E+09
7.0E+09
9.0E+09
FREQUENCY

Fig. 9b

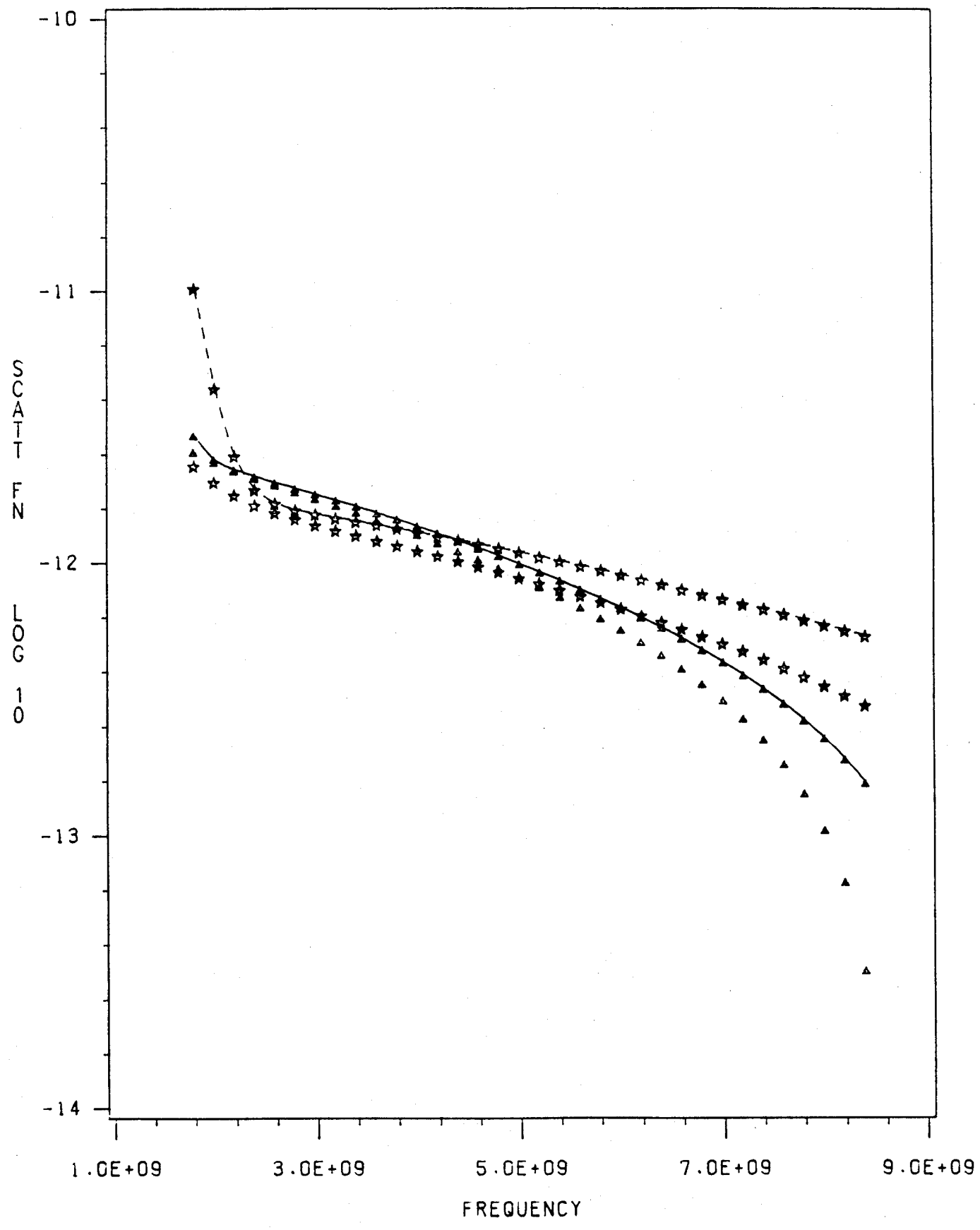
2.14 MM ; K.B ANGLE=0 DEG ; TE=15 KEV
FORWARD SCATT. ANGLE : 90 DEG (AA), 135 DEG (**)
-10
-11
-12
-13
-14
SCATT FN
LOG 10
1.0E+09
3.0E+09
5.0E+09
7.0E+09
9.0E+09
FREQUENCY

Fig. 9c

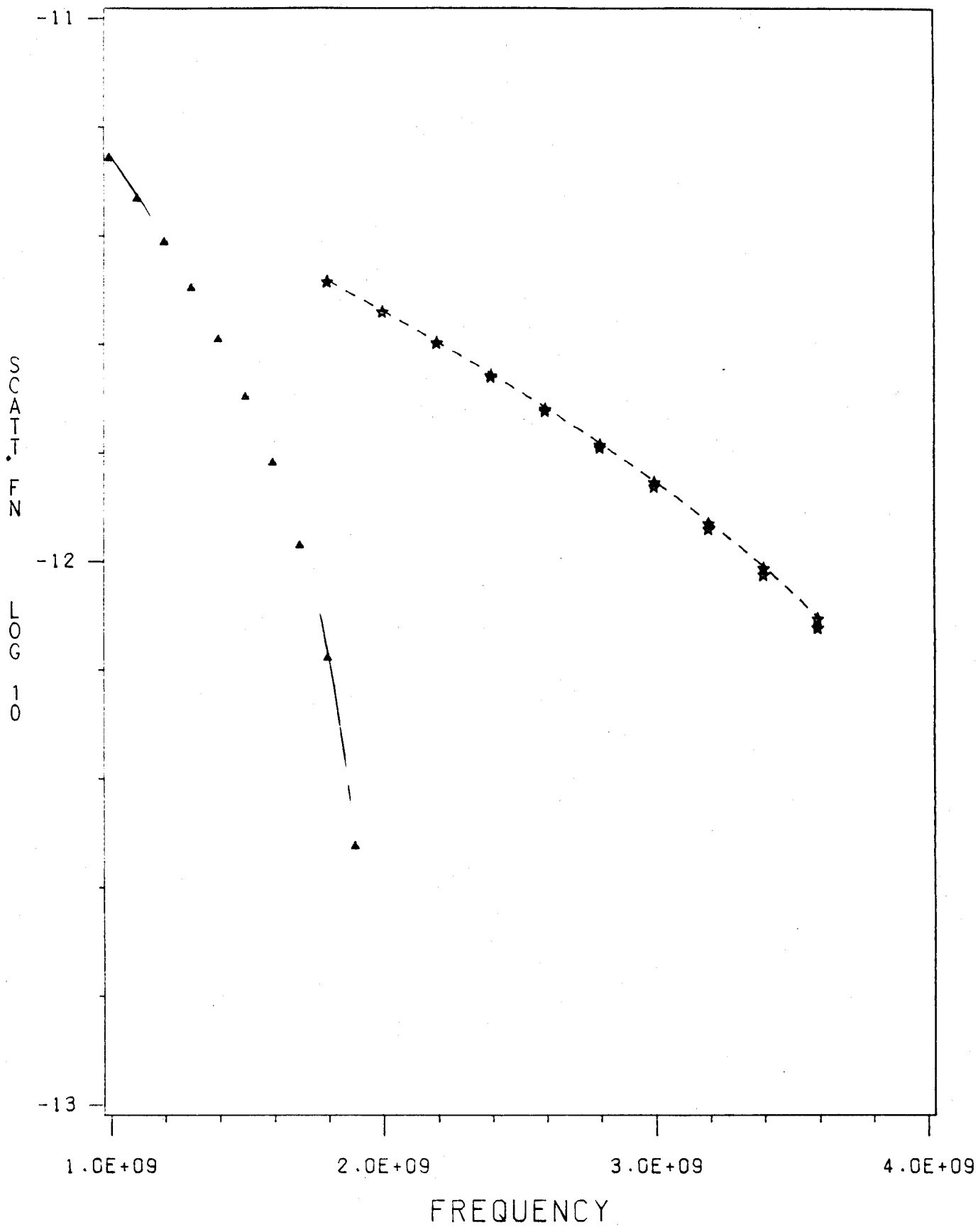
MM SCATT. AT 45 DEG , K.B=75 DEG
TE=10 KEV : 2.14 MM (**) , 5 MM (AA)
-11
-12
-13
SCATT. FN
LOG 10
1.0E+09
2.0E+09
3.0E+09
4.0E+09
FREQUENCY

Fig. 10a

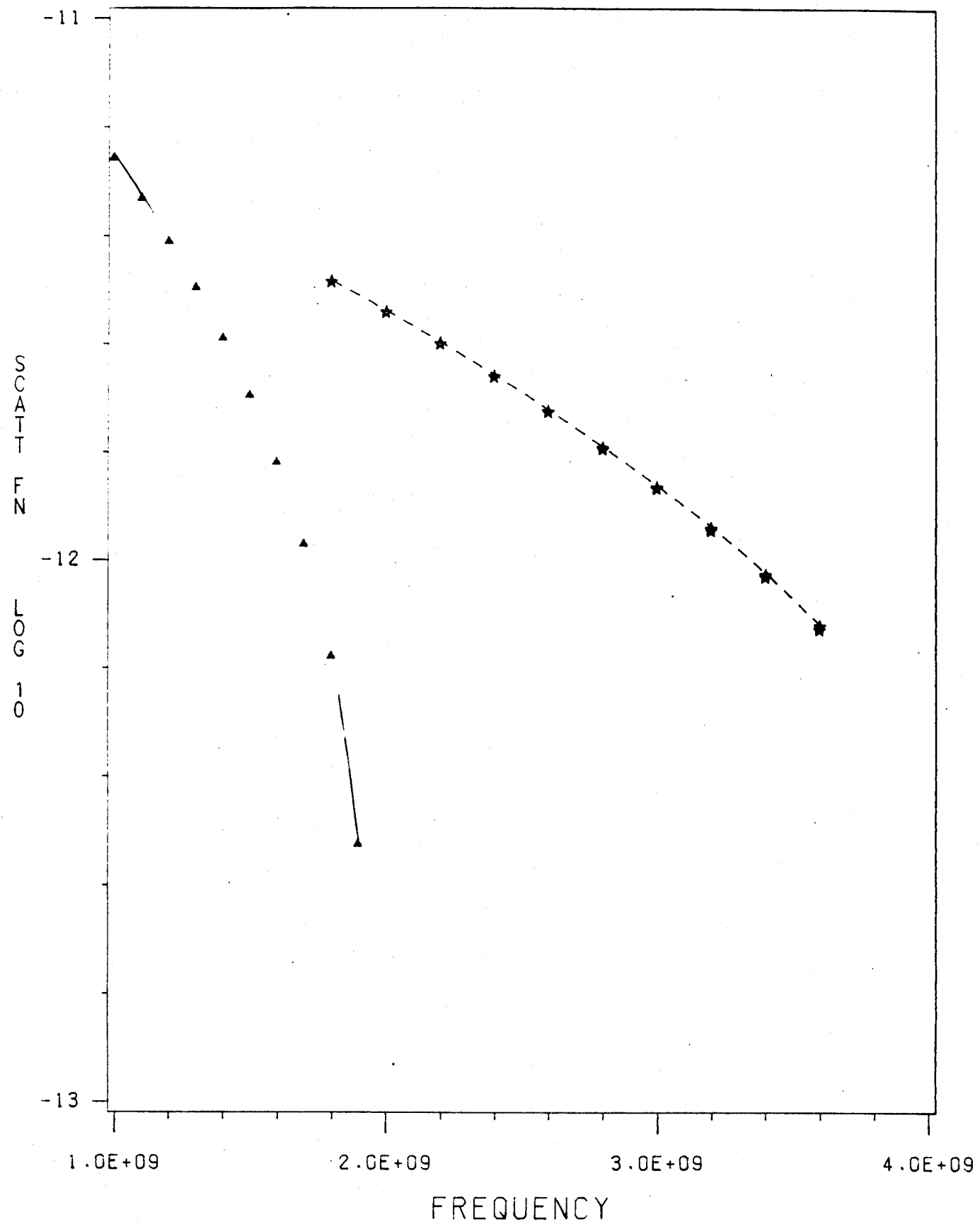
MM SCATT. AT 45 DEG , K.B=45 DEG
TE=10 KEV : 2.14 MM (**) , 5 MM (AA)
-11
-12
-13
SCATT FN
LOG 10
1.0E+09
2.0E+09
3.0E+09
4.0E+09
FREQUENCY

Fig. 10b

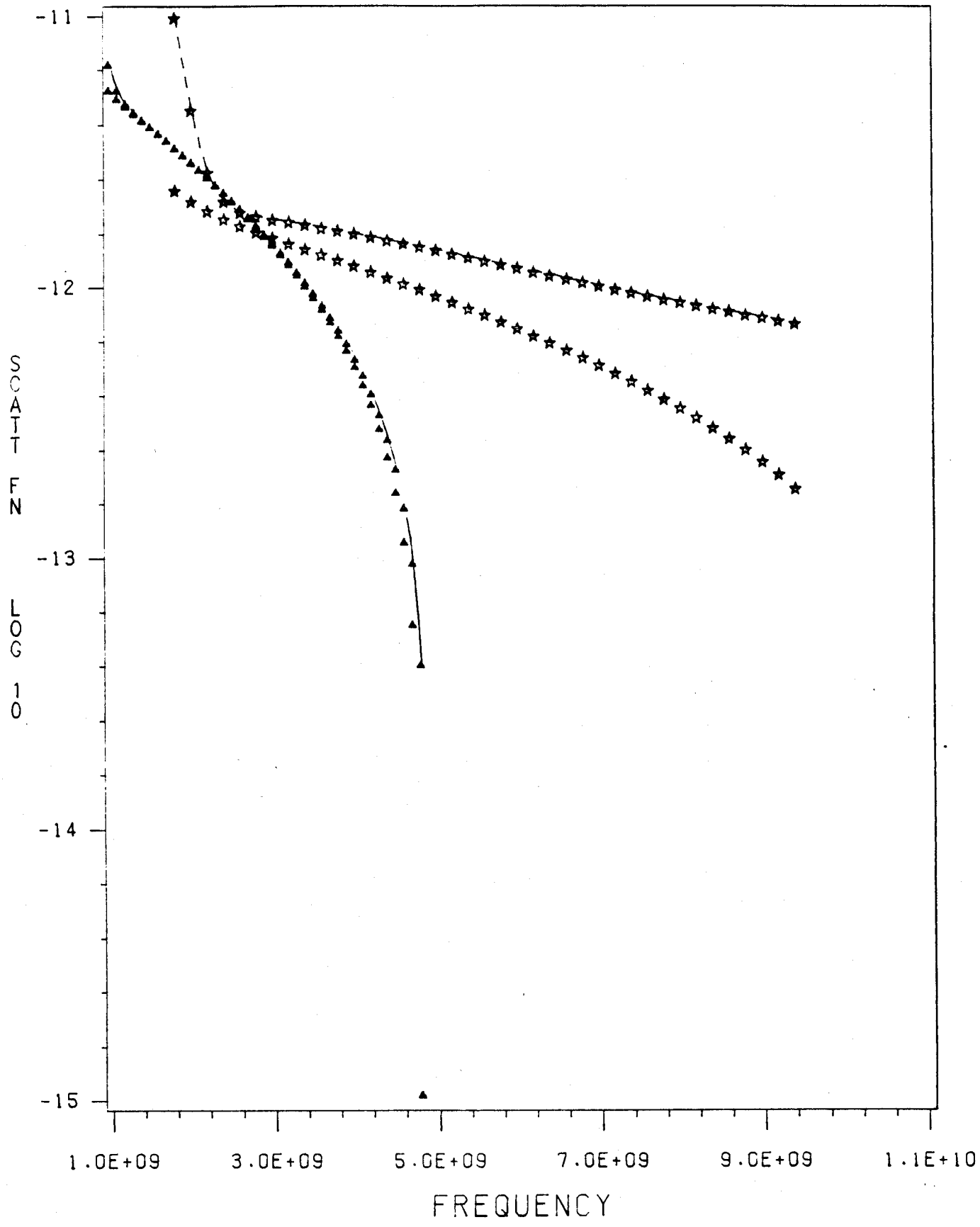
MM SCATT. AT 135 DEG , K.B=75 DEG
TE=10 KEV : 2.14 MM (**) , 5 MM (AA)
-11
-12
-13
-14
-15
SCATT FN LOG 10
1.0E+09
3.0E+09
5.0E+09
7.0E+09
9.0E+09
1.1E+10
FREQUENCY

Fig. 11a

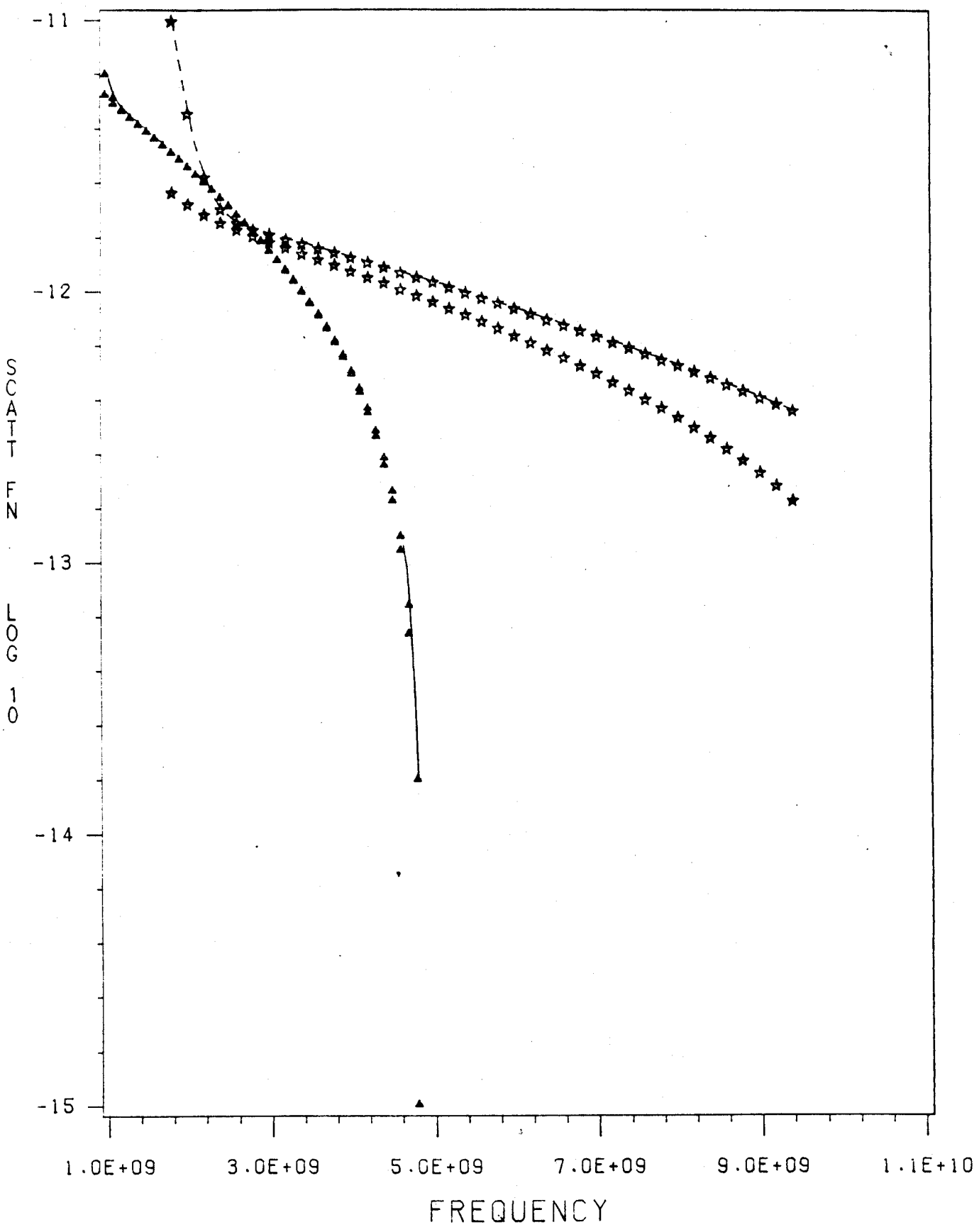
MM SCATT. AT 135 DEG , K.B=45 DEG
TE=10 KEV : 2.14 MM (**) , 5 MM (AA)
-11
-12
-13
-14
-15
SCATT FN
LOG 10
1.0E+09
3.0E+09
5.0E+09
7.0E+09
9.0E+09
1.1E+10
FREQUENCY

Fig. 11b

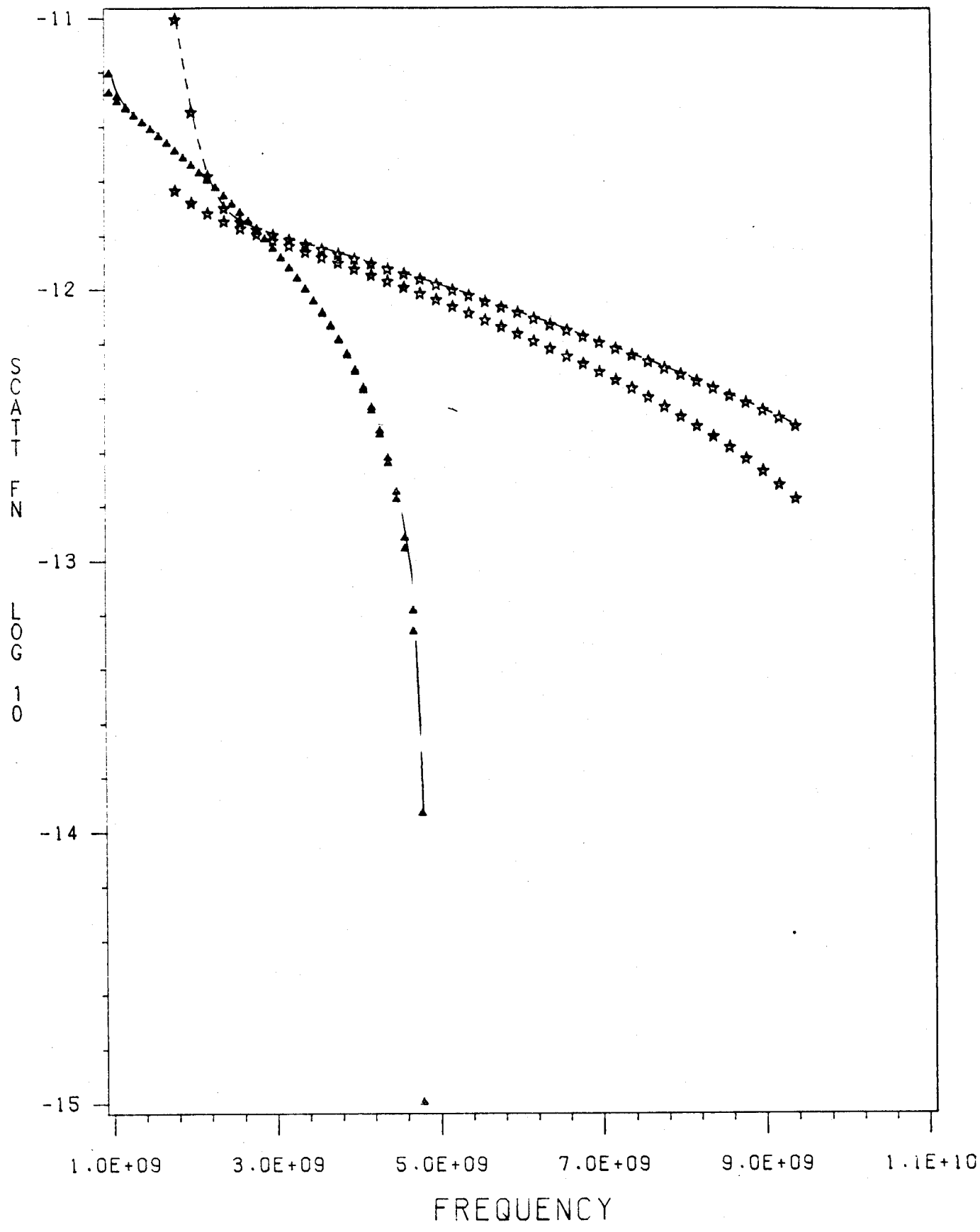
MM SCATT. AT 135 DEG , K.B=0 DEG
TE=10 KEV : 2.14 MM (**) , 5 MM (AA)
-11
-12
-13
-14
-15
SCATT FN
LOG 10
1.0E+09
3.0E+09
5.0E+09
7.0E+09
9.0E+09
1.1E+10
FREQUENCY

Fig. 11c

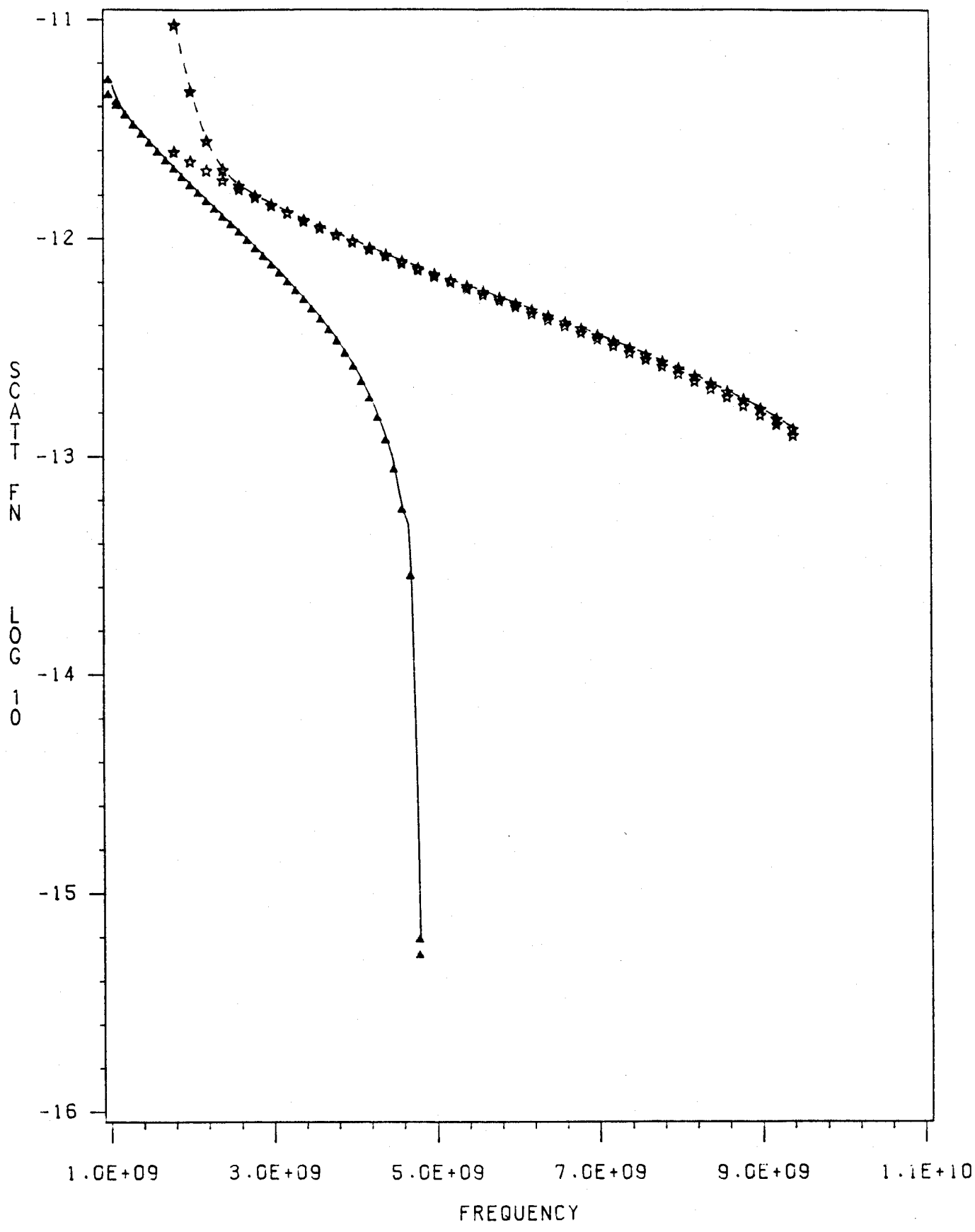
MM SCATT. AT 135 DEG , K.B=75 DEG
TE=1 KEV : 2.14 MM (**) , 5 MM (AA)
-11
-12
-13
-14
-15
-16
SCATT FN
LOG 10
1.0E+09
3.0E+09
5.0E+09
7.0E+09
9.0E+09
1.1E+10
FREQUENCY

Fig. 11d

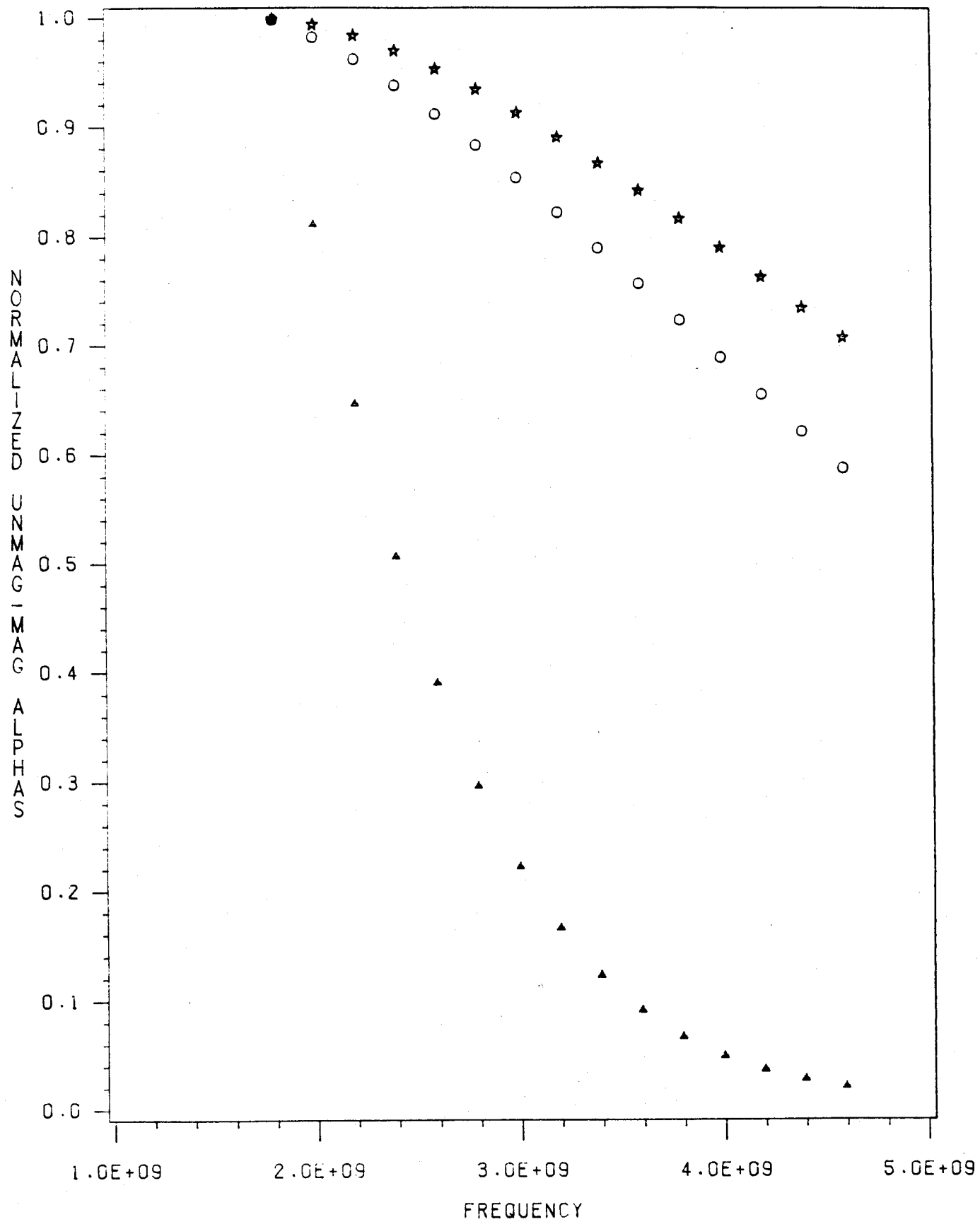
TE EFFECTS AT 45 DEG, K.B=75 DEG
2.14 MM , TE: ** 15 KEV, OO 10 KEV, AA 1 KEV
NORMALIZED UNMAG-MAG ALPHAS
1.0
0.9
0.8
0.7
0.6
0.5
0.4
0.3
0.2
0.1
0.0
1.0E+09
2.0E+09
3.0E+09
4.0E+09
5.0E+09
FREQUENCY

Fig. 12a

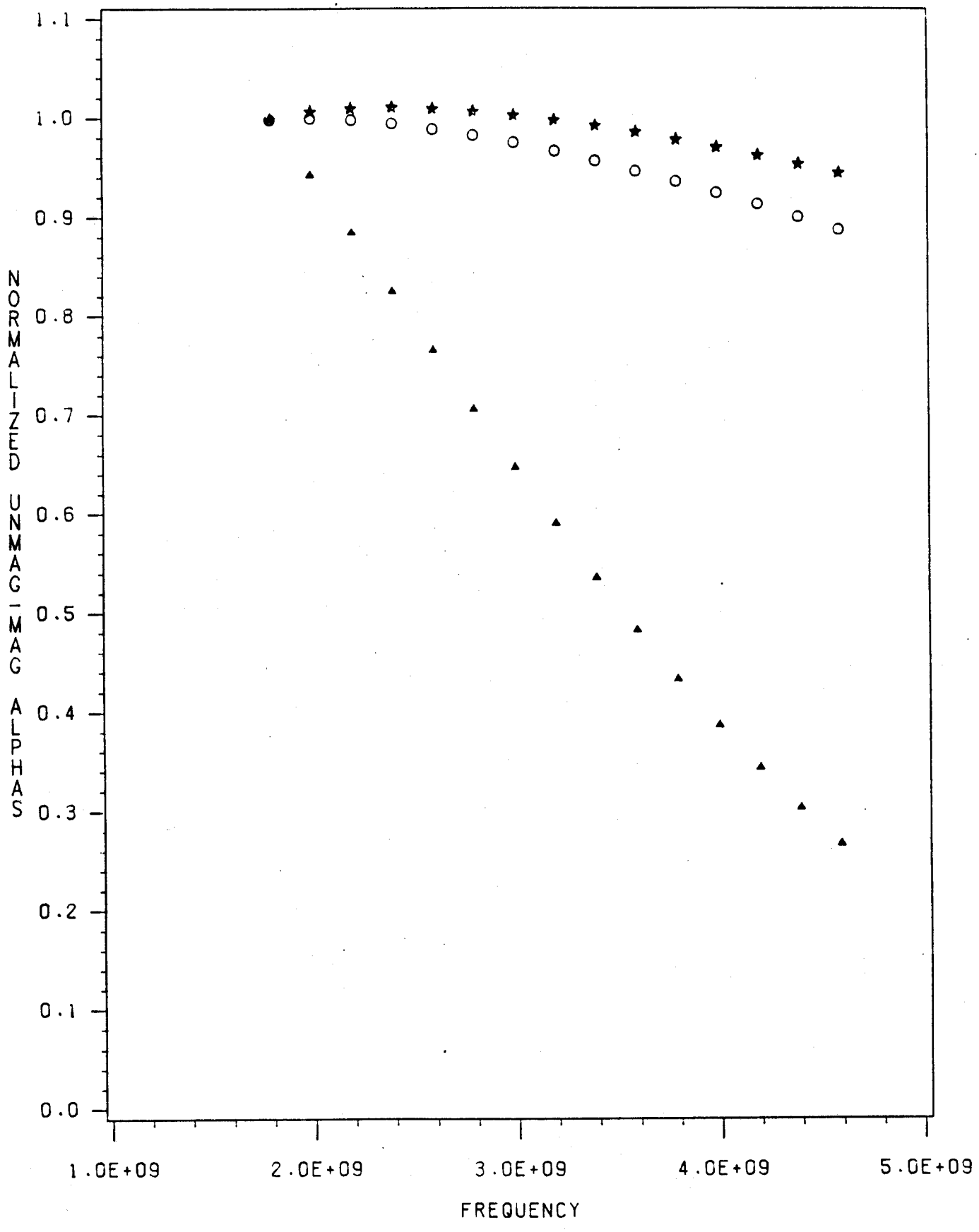
TE EFFECTS AT 45 DEG, K.B=60 DEG
2.14 MM , TE: ** 15 KEV, OO 10 KEV, AA 1 KEV
NORMALIZED UNMAG-MAG ALPHAS
1.1
1.0
0.9
0.8
0.7
0.6
0.5
0.4
0.3
0.2
0.1
0.0
1.0E+09
2.0E+09
3.0E+09
4.0E+09
5.0E+09
FREQUENCY

Fig. 12b

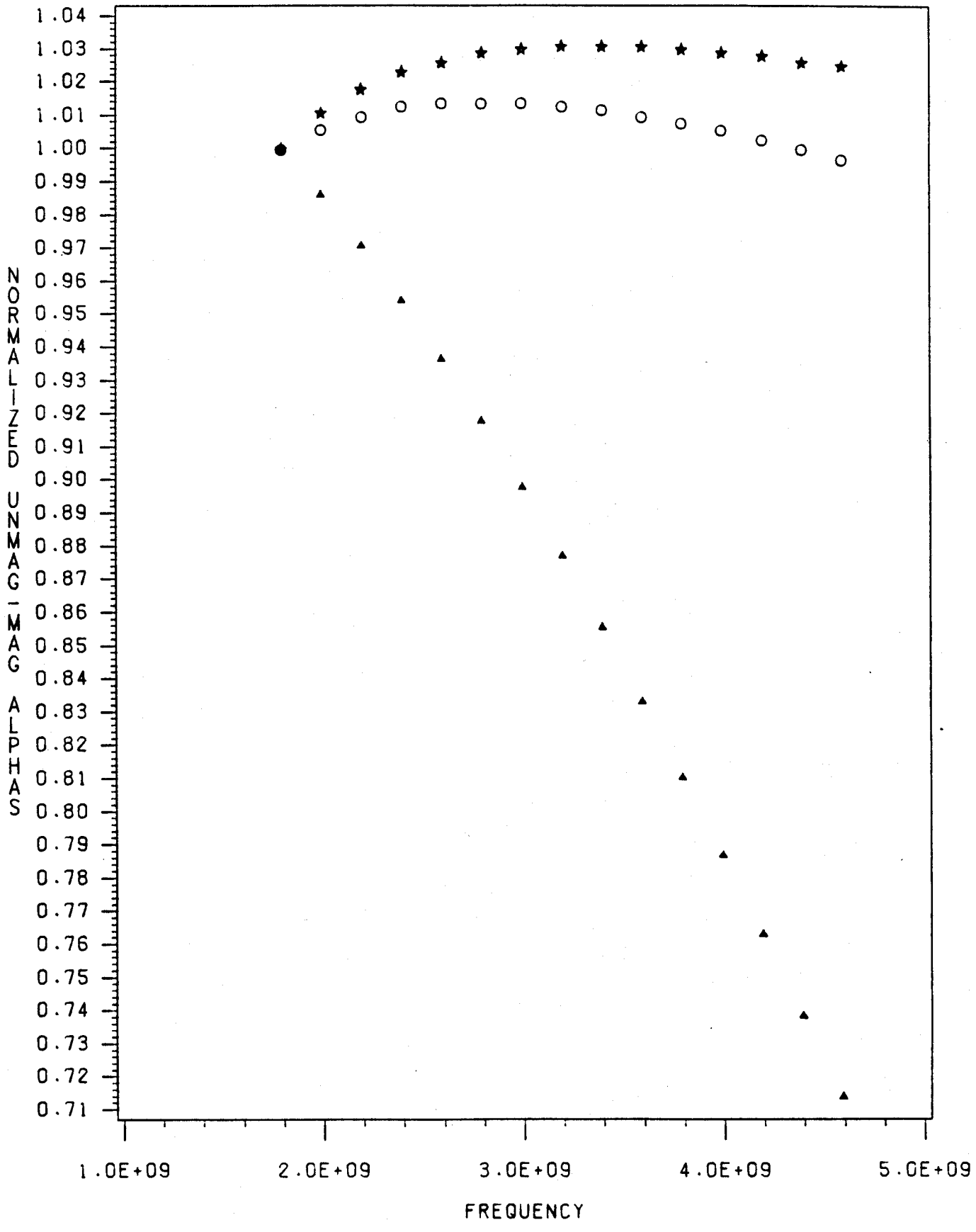
TE EFFECTS AT 45 DEG, K.B=0 DEG
2.14 MM , TE: ** 15 KEV, 00 10 KEV, AA 1 KEV
NORMALIZED UNMAG-MAG ALPHAS
1.04
1.03
1.02
1.01
1.00
0.99
0.98
0.97
0.96
0.95
0.94
0.93
0.92
0.91
0.90
0.89
0.88
0.87
0.86
0.85
0.84
0.83
0.82
0.81
0.80
0.79
0.78
0.77
0.76
0.75
0.74
0.73
0.72
0.71
1.0E+09
2.0E+09
3.0E+09
4.0E+09
5.0E+09
FREQUENCY

Fig. 12c

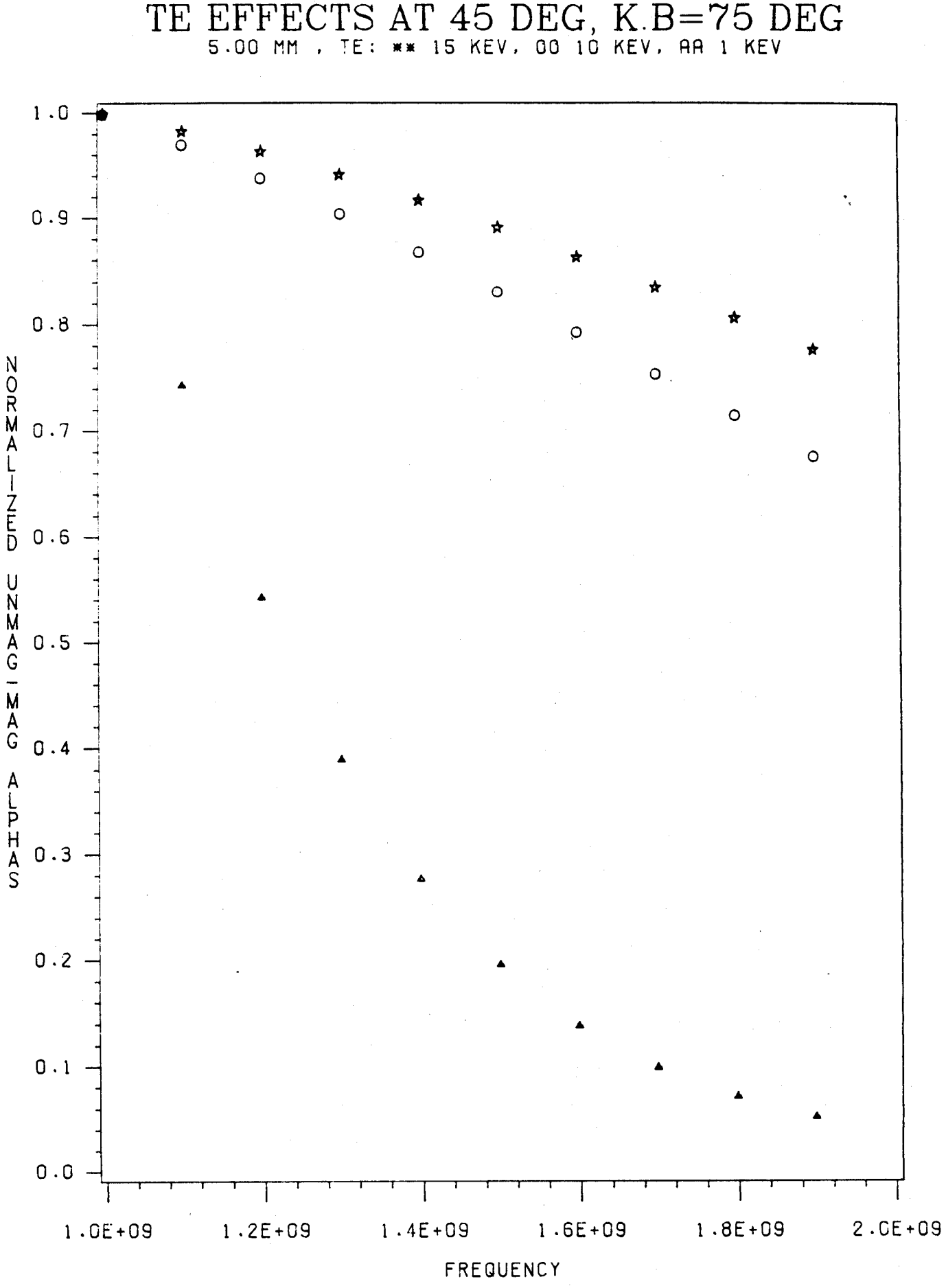
TE EFFECTS AT 45 DEG, K.B=75 DEG
5.00 MM , TE: ** 15 KEV, 00 10 KEV, AA 1 KEV
NORMALIZED UNMAG-MAG ALPHAS
1.0
0.9
0.8
0.7
0.6
0.5
0.4
0.3
0.2
0.1
0.0
1.0E+09
1.2E+09
1.4E+09
1.6E+09
1.8E+09
2.0E+09
FREQUENCY

Fig. 12d

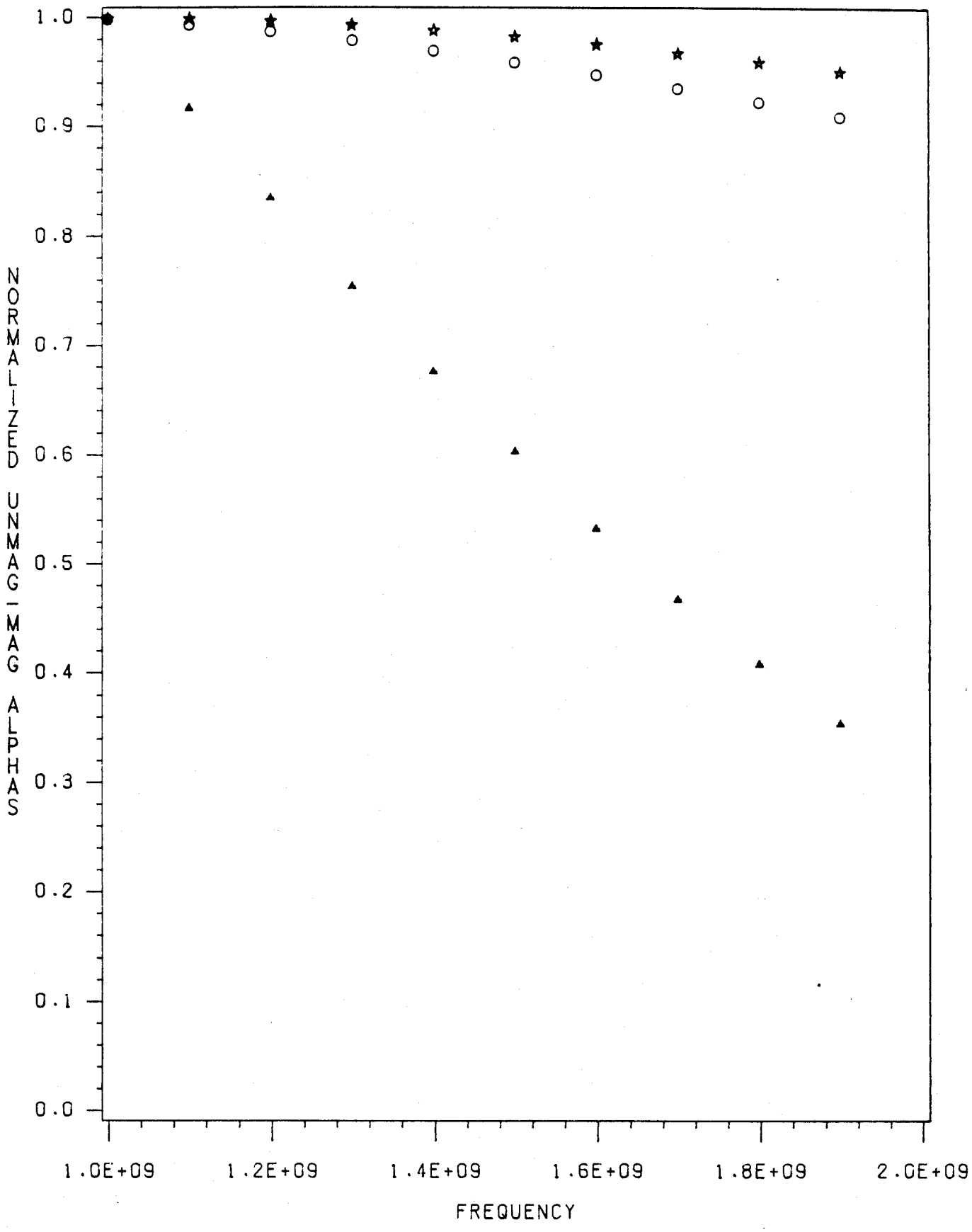
TE EFFECTS AT 45 DEG, K.B=60 DEG
5.00 MM , TE: ** 15 KEV, 00 10 KEV, AA 1 KEV
NORMALIZED UNMAG-MAG ALPHAS
1.0
0.9
0.8
0.7
0.6
0.5
0.4
0.3
0.2
0.1
0.0
1.0E+09
1.2E+09
1.4E+09
1.6E+09
1.8E+09
2.0E+09
FREQUENCY

Fig. 12e

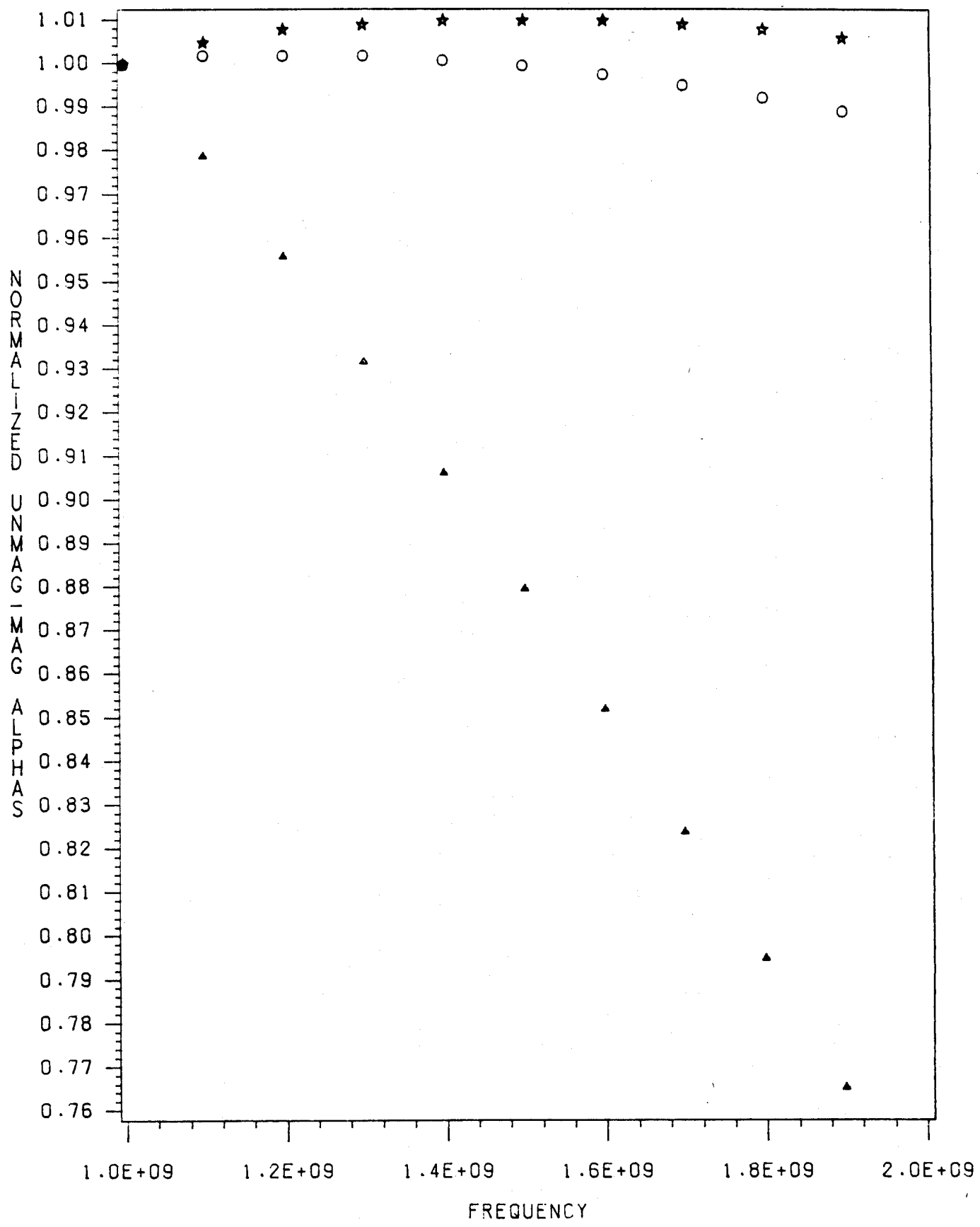
TE EFFECTS AT 45 DEG, K.B=0 DEG
5.00 MM , TE: ** 15 KEV, 00 10 KEV, AA 1 KEV
NORMALIZED UNMAG-MAG ALPHAS
1.01
1.00
0.99
0.98
0.97
0.96
0.95
0.94
0.93
0.92
0.91
0.90
0.89
0.88
0.87
0.86
0.85
0.84
0.83
0.82
0.81
0.80
0.79
0.78
0.77
0.76
1.0E+09
1.2E+09
1.4E+09
1.6E+09
1.8E+09
2.0E+09
FREQUENCY

Fig. 12f

# TE EFFECTS AT 90 DEG, K.B=75 DEG

2.14 MM , TE: ** 15 KEV, 00 10 KEV, AA 1 KEV

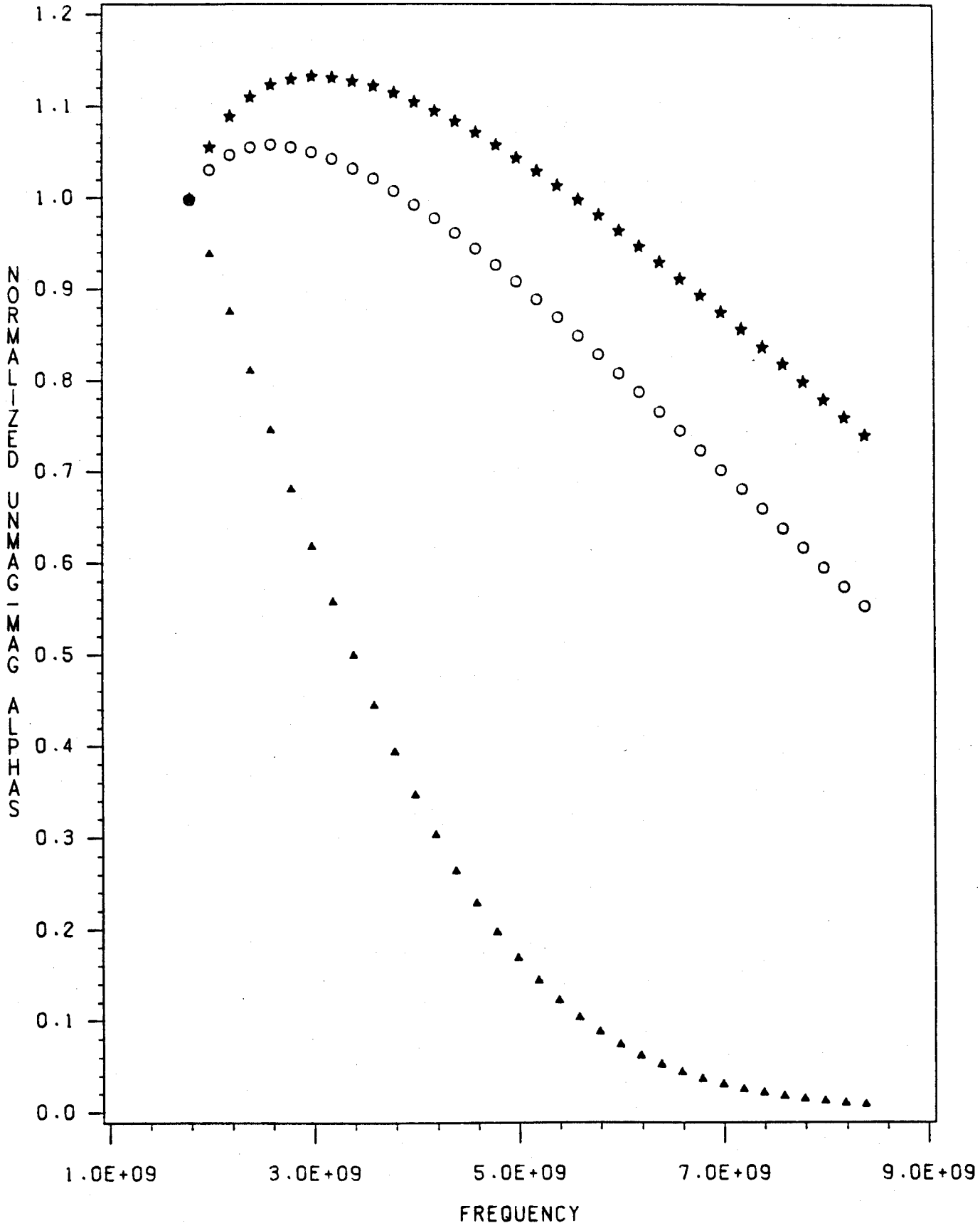


Fig. 13a

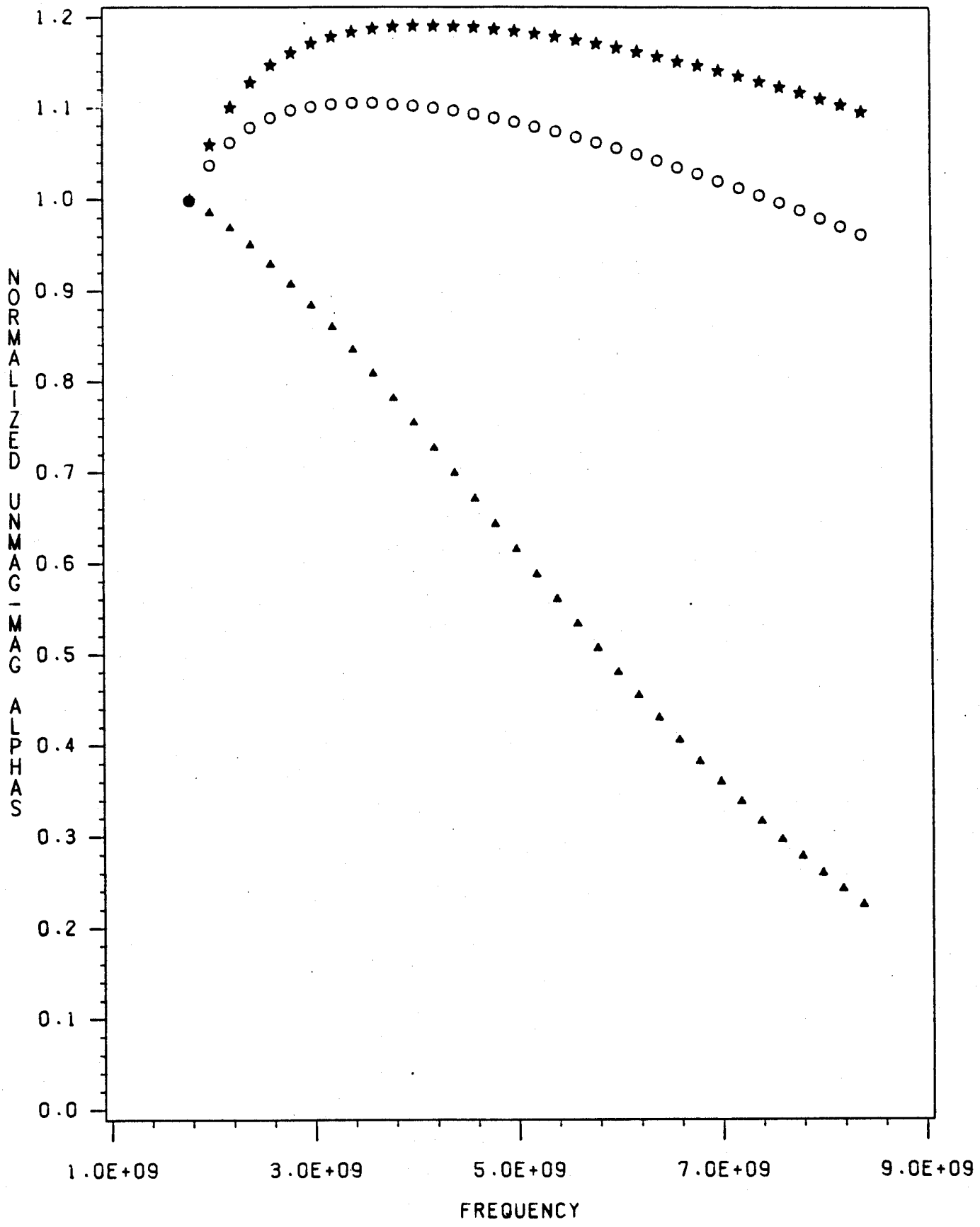
TE EFFECTS AT 90 DEG., K.B=60 DEG
2.14 MM , TE: ** 15 KEV, 00 10 KEV, AA 1 KEV
NORMALIZED UNMAG-MAG ALPHAS
1.2
1.1
1.0
0.9
0.8
0.7
0.6
0.5
0.4
0.3
0.2
0.1
0.0
1.0E+09
3.0E+09
5.0E+09
7.0E+09
9.0E+09
FREQUENCY

Fig. 13b

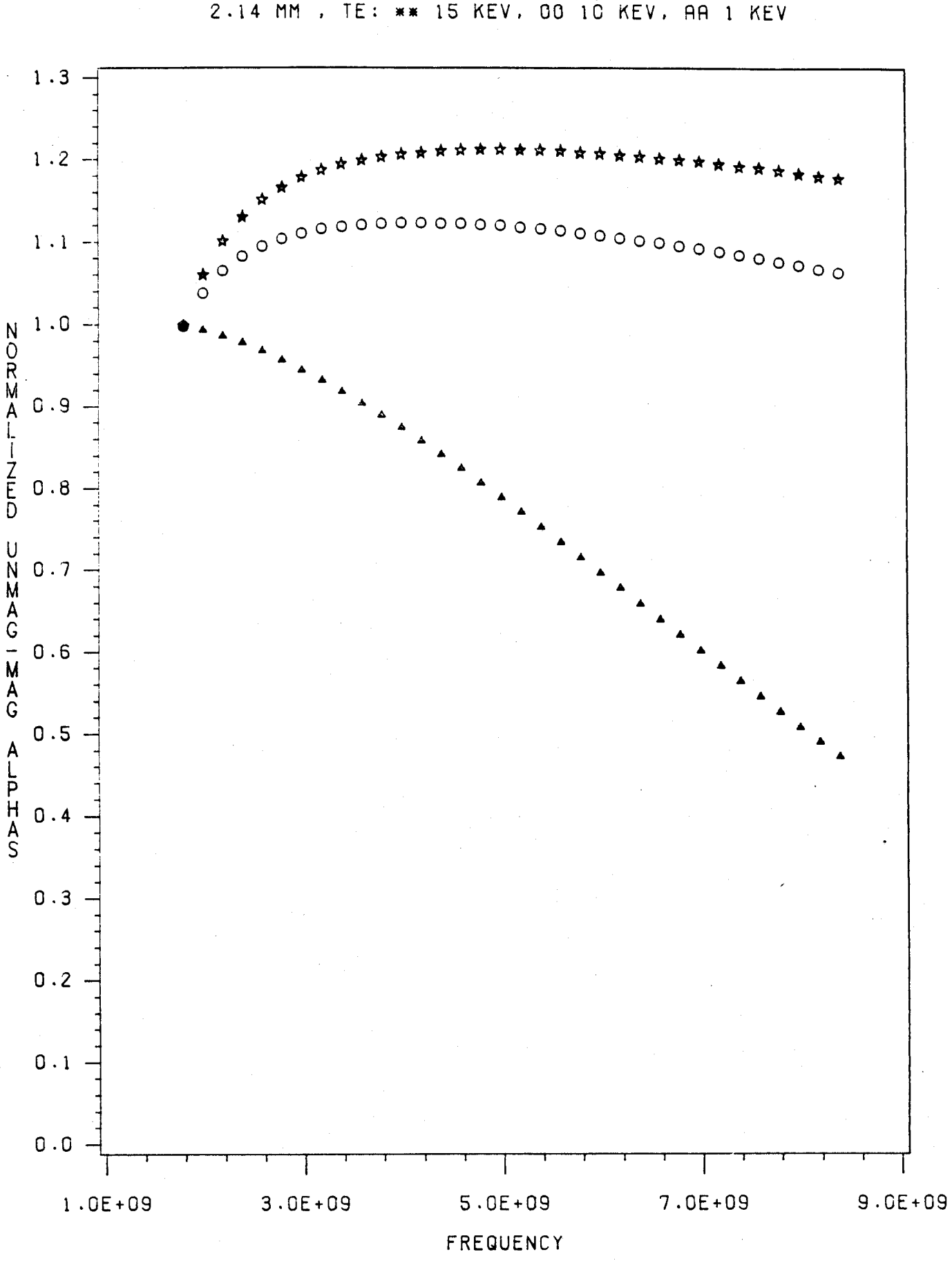
TE EFFECTS AT 90 DEG, K.B=45 DEG
2.14 MM , TE: ** 15 KEV, OO 10 KEV, AA 1 KEV
NORMALIZED UNMAG-MAG ALPHAS
1.3
1.2
1.1
1.0
0.9
0.8
0.7
0.6
0.5
0.4
0.3
0.2
0.1
0.0
1.0E+09
3.0E+09
5.0E+09
7.0E+09
9.0E+09
FREQUENCY

Fig. 13c

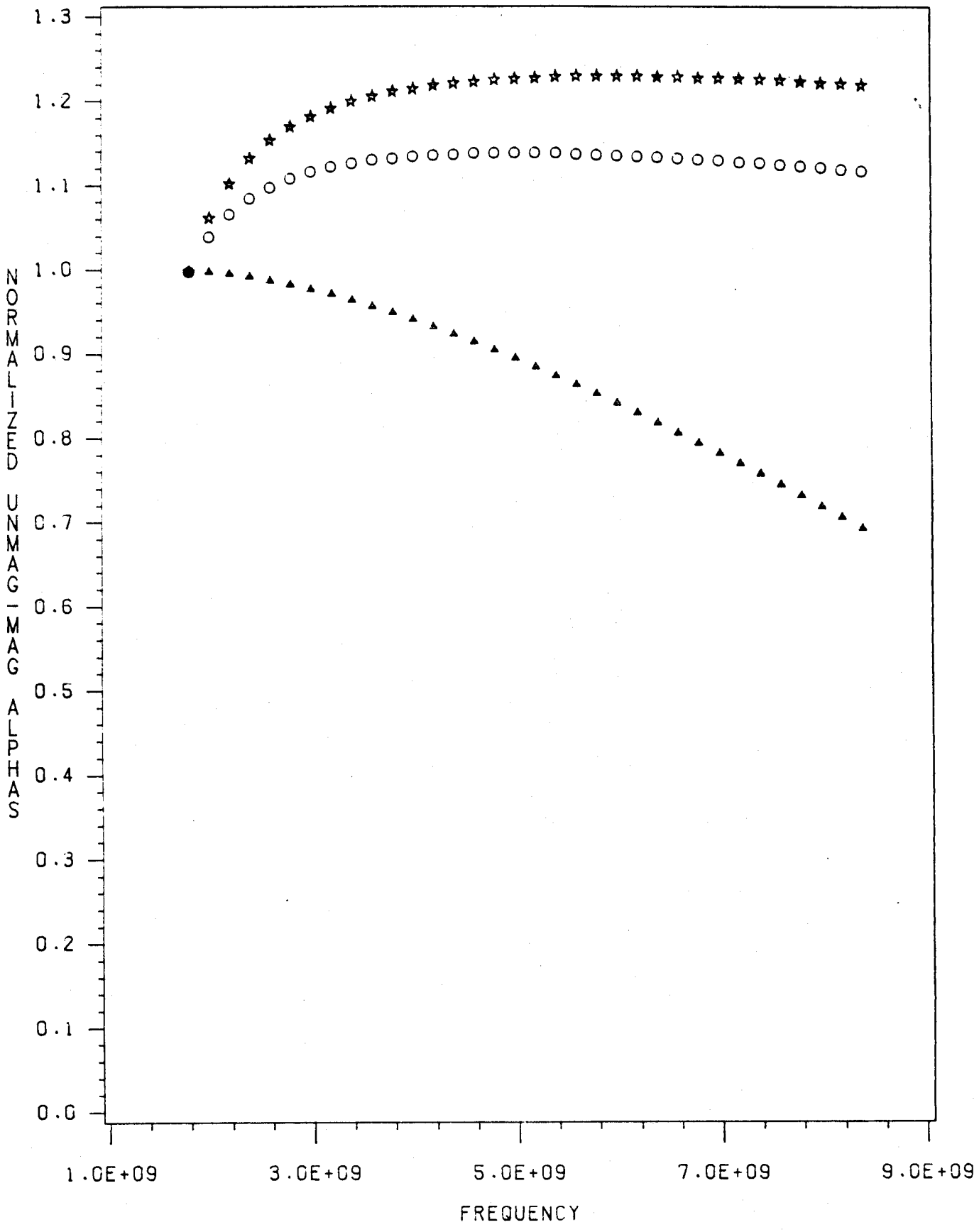
TE EFFECTS AT 90 DEG, K.B=0 DEG
2.14 MM , TE: ** 15 KEV, OO 10 KEV, AA 1 KEV
NORMALIZED UNMAG-MAG ALPHAS
1.3
1.2
1.1
1.0
0.9
0.8
0.7
0.6
0.5
0.4
0.3
0.2
0.1
0.0
1.0E+09
3.0E+09
5.0E+09
7.0E+09
9.0E+09
FREQUENCY

Fig. 13d

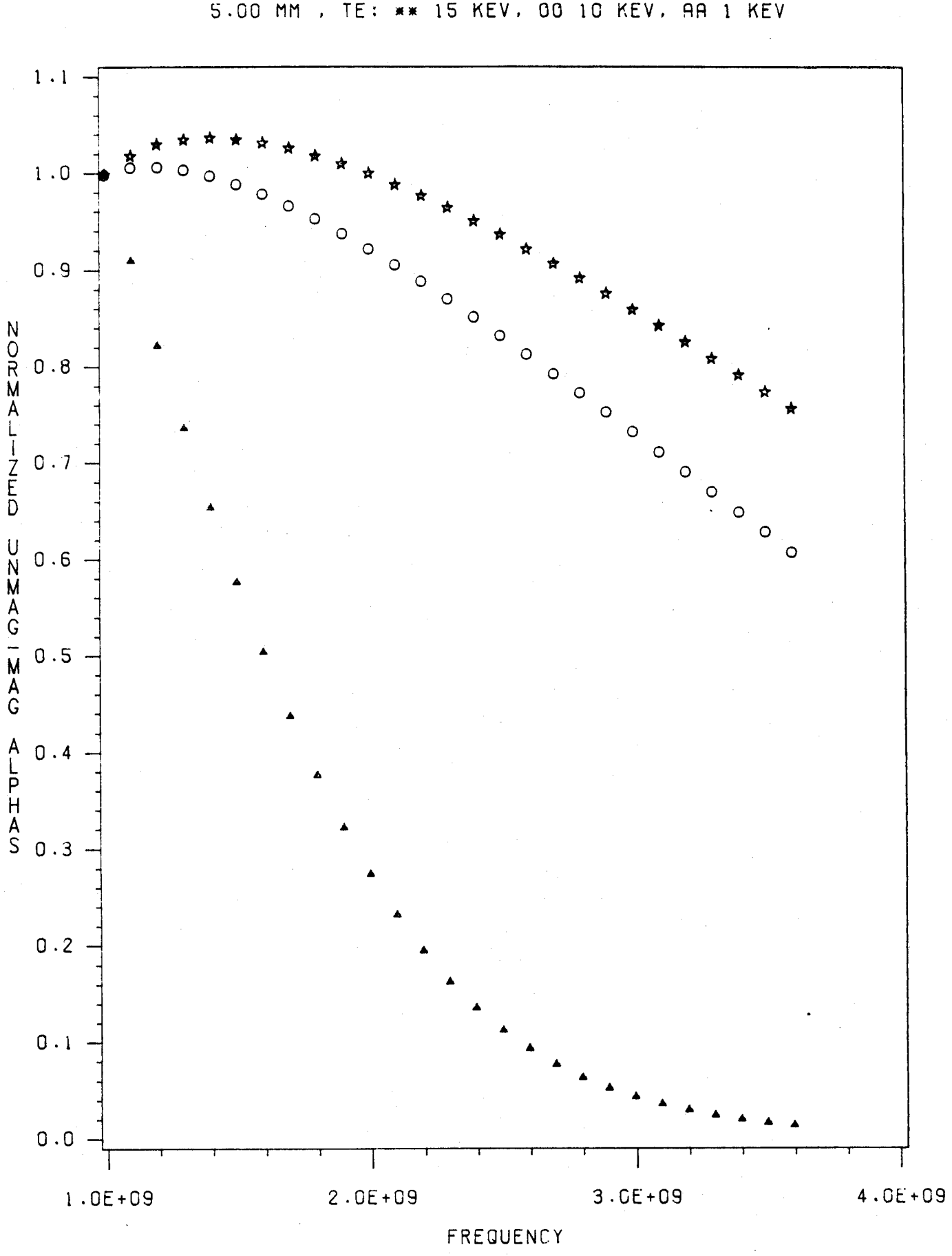
TE EFFECTS AT 90 DEG, K.B=75 DEG
5.00 MM , TE: ** 15 KEV, 00 10 KEV, AA 1 KEV
NORMALIZED UNMAG-MAG ALPHAS
1.1
1.0
0.9
0.8
0.7
0.6
0.5
0.4
0.3
0.2
0.1
0.0
1.0E+09
2.0E+09
3.0E+09
4.0E+09
FREQUENCY

Fig. 13e

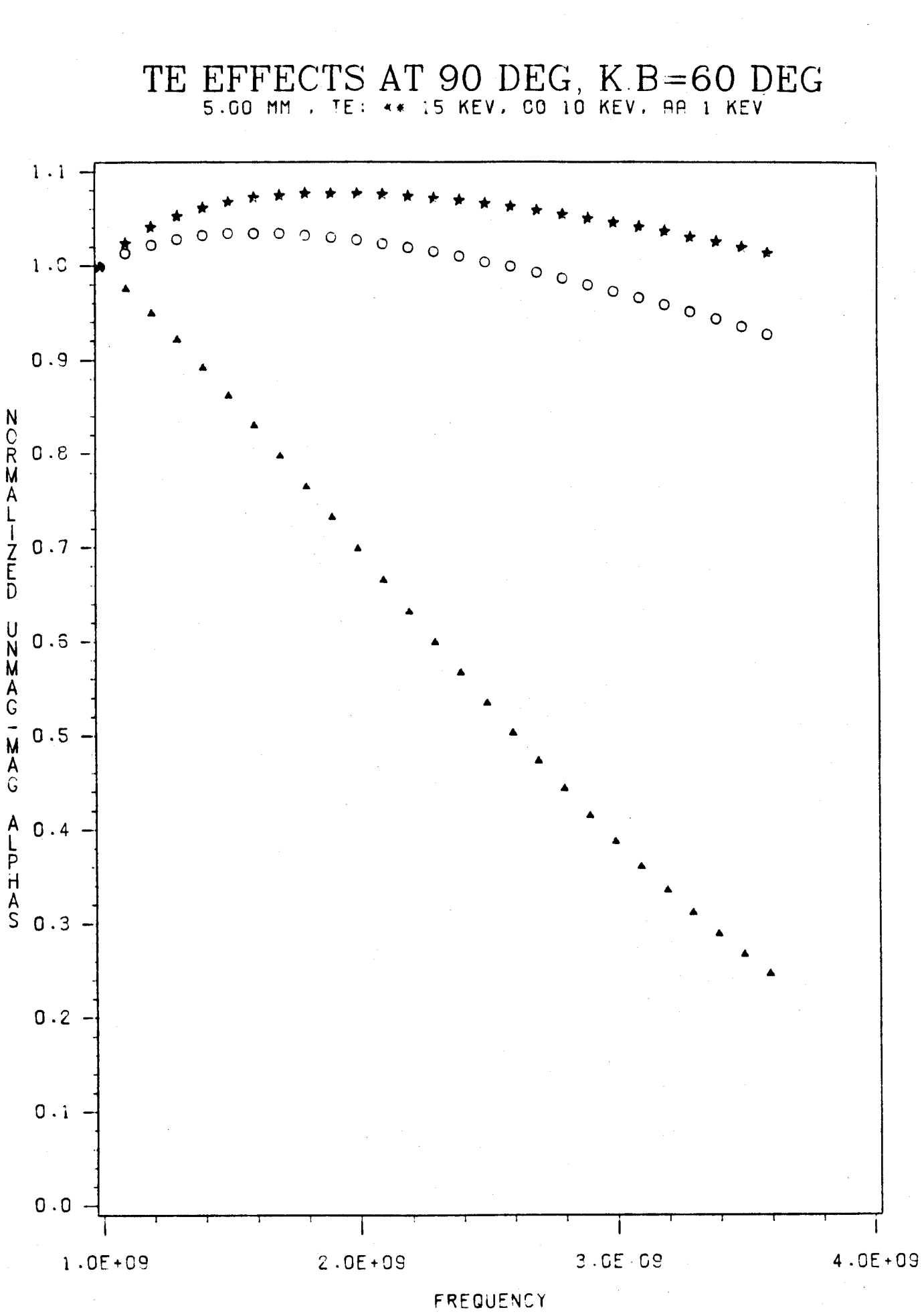
TE EFFECTS AT 90 DEG, K.B=60 DEG
5.00 MM , TE: ** 15 KEV, CO 10 KEV, AR 1 KEV
NORMALIZED UNMAG-MAG ALPHAS
1.1
1.0
0.9
0.8
0.7
0.6
0.5
0.4
0.3
0.2
0.1
0.0
1.0E+09
2.0E+09
3.0E+09
4.0E+09
FREQUENCY

Fig. 13f

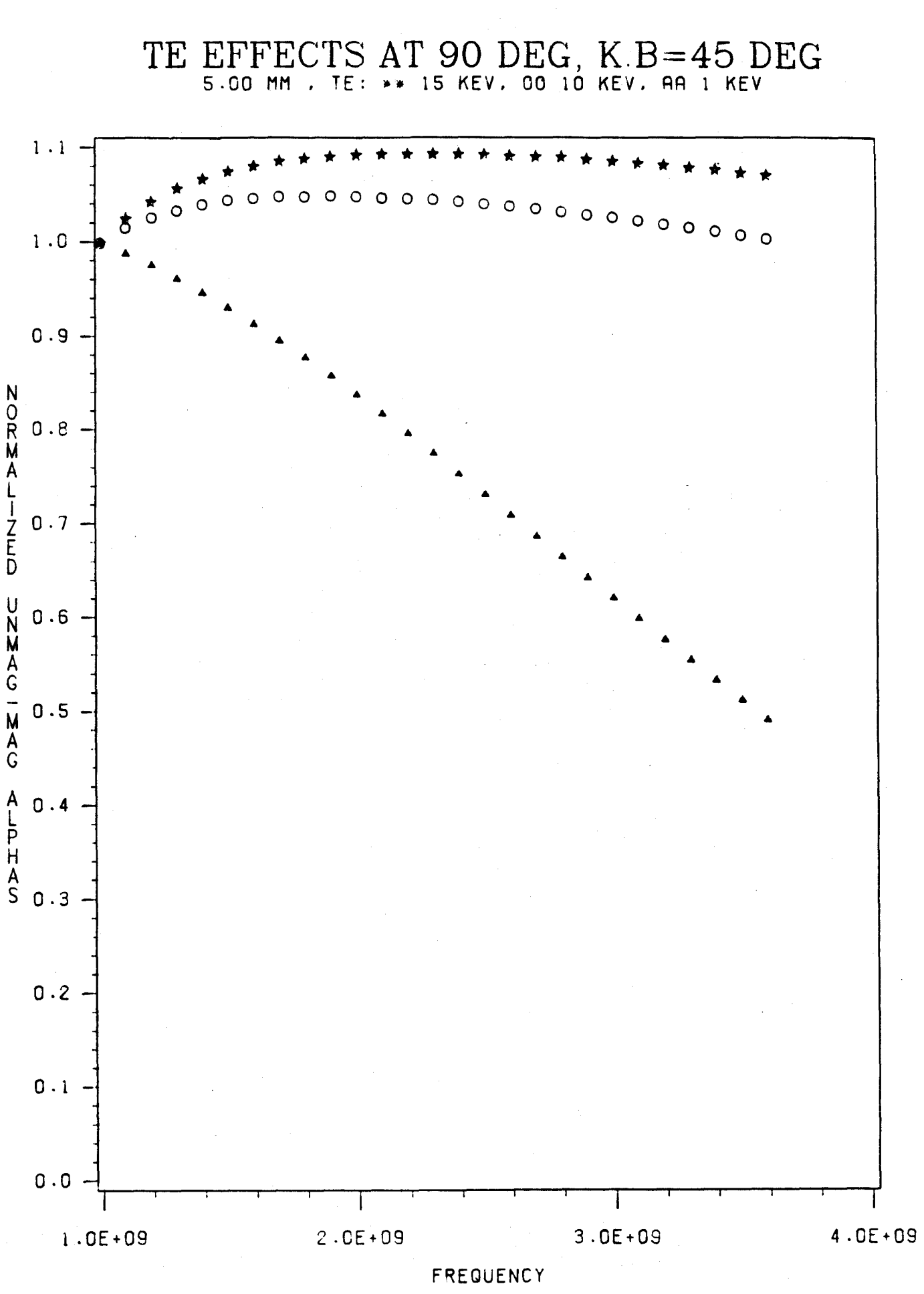
TE EFFECTS AT 90 DEG, K.B=45 DEG
5.00 MM , TE: ** 15 KEV, 00 10 KEV, AA 1 KEV
NORMALIZED UNMAG-MAG ALPHAS
1.1
1.0
0.9
0.8
0.7
0.6
0.5
0.4
0.3
0.2
0.1
0.0
1.0E+09
2.0E+09
3.0E+09
4.0E+09
FREQUENCY

Fig. 13g

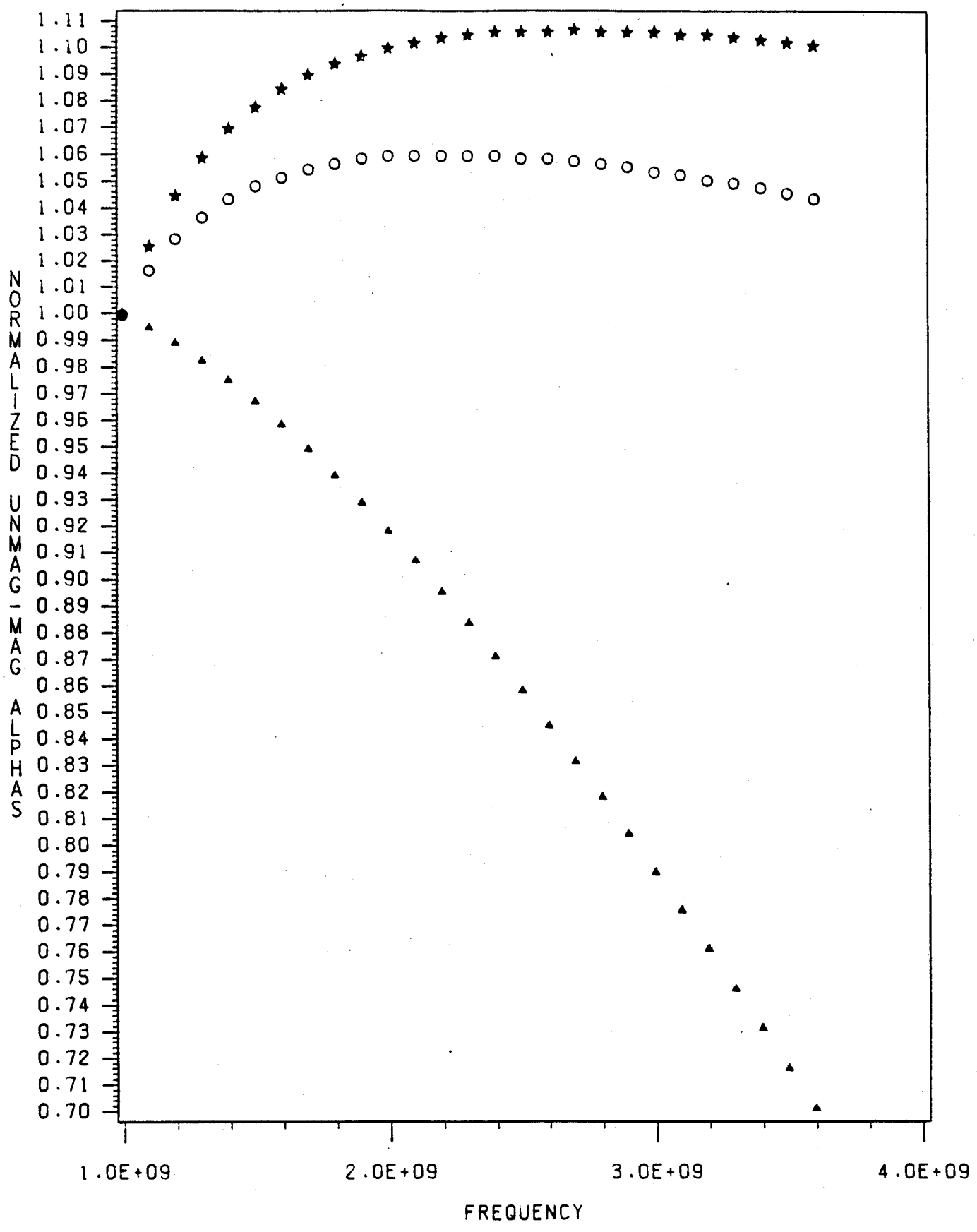
TE EFFECTS AT 90 DEG, K.B=0 DEG
5.00 MM , TE: ** 15 KEV, OO 10 KEV, AA 1 KEV
NORMALIZED UNMAG-MAG ALPHAS
1.11
1.10
1.09
1.08
1.07
1.06
1.05
1.04
1.03
1.02
1.01
1.00
0.99
0.98
0.97
0.96
0.95
0.94
0.93
0.92
0.91
0.90
0.89
0.88
0.87
0.86
0.85
0.84
0.83
0.82
0.81
0.80
0.79
0.78
0.77
0.76
0.75
0.74
0.73
0.72
0.71
0.70
1.0E+09
2.0E+09
3.0E+09
4.0E+09
FREQUENCY

Fig. 13h

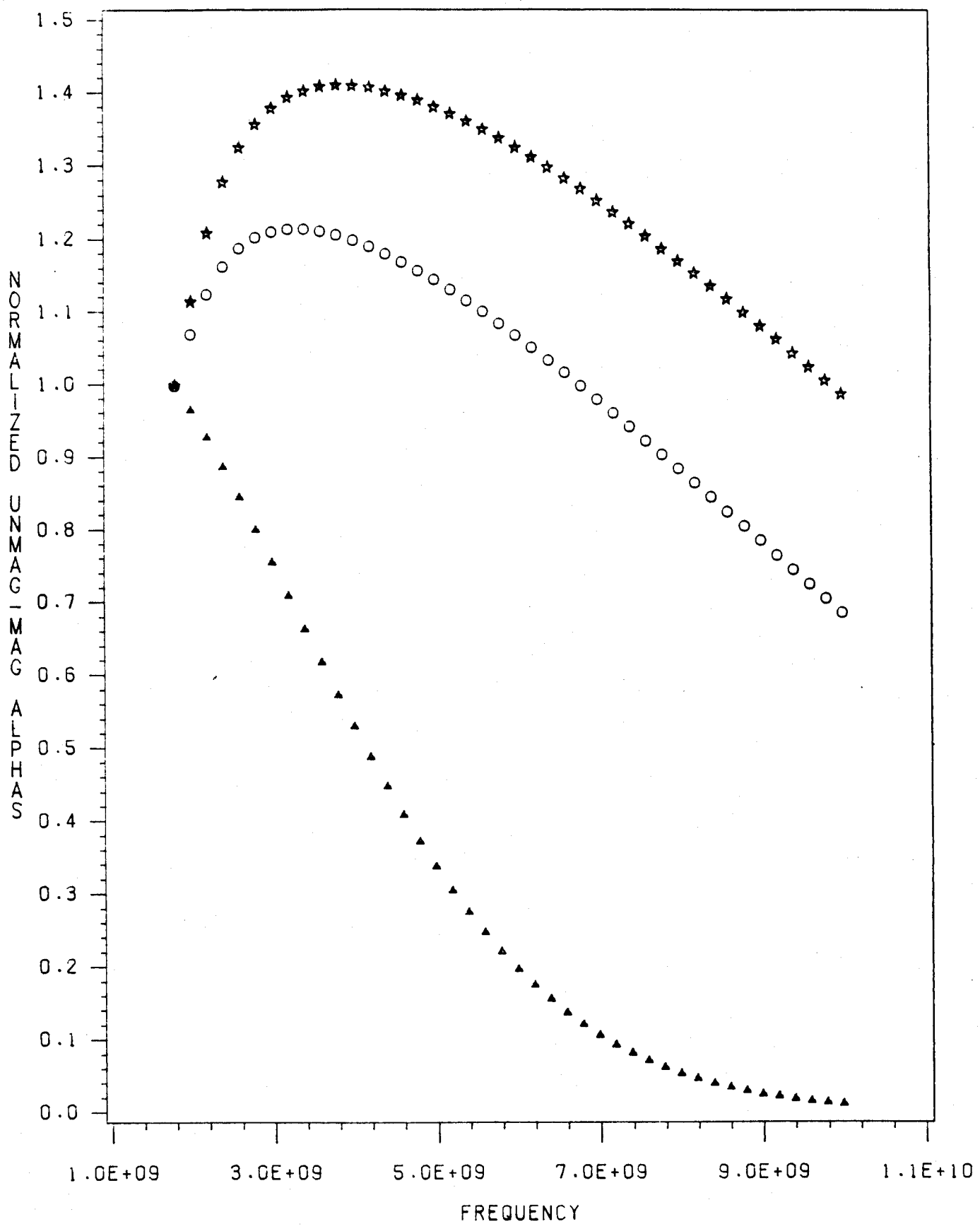
TE EFFECTS AT 135 DEG, K.B=75 DEG
2.14 MM , TE: ** 15 KEV, OO 10 KEV, AA 1 KEV
NORMALIZED UNMAG-MAG ALPHAS
1.5
1.4
1.3
1.2
1.1
1.0
0.9
0.8
0.7
0.6
0.5
0.4
0.3
0.2
0.1
0.0
1.0E+09
3.0E+09
5.0E+09
7.0E+09
9.0E+09
1.1E+10
FREQUENCY

Fig. 14a

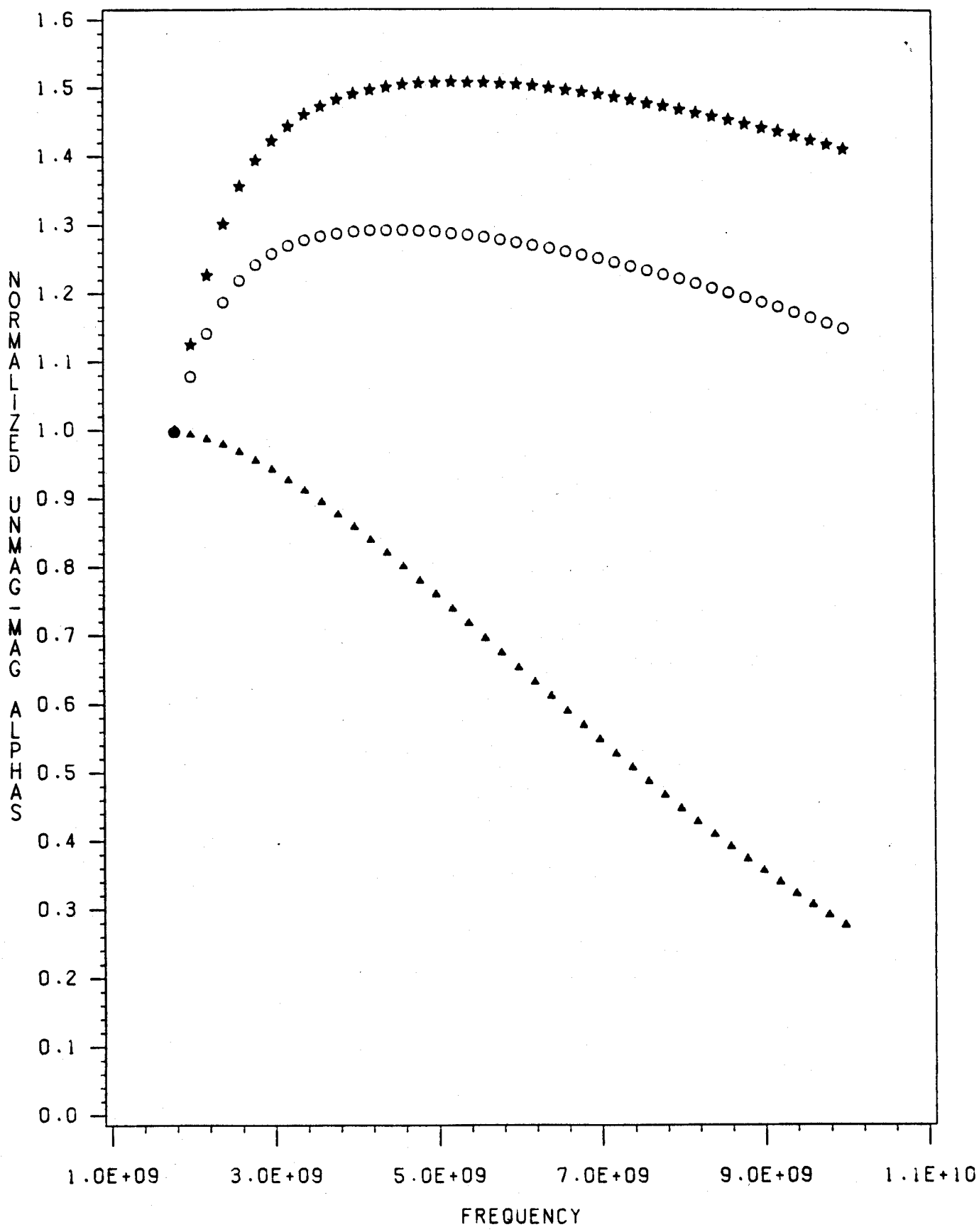
TE EFFECTS AT 135 DEG, K.B=60 DEG
2.14 MM , TE: ** 15 KEV, OO 10 KEV, AA 1 KEV
NORMALIZED UNMAG-MAG ALPHAS
1.6
1.5
1.4
1.3
1.2
1.1
1.0
0.9
0.8
0.7
0.6
0.5
0.4
0.3
0.2
0.1
0.0
1.0E+09
3.0E+09
5.0E+09
7.0E+09
9.0E+09
1.1E+10
FREQUENCY

Fig. 14b

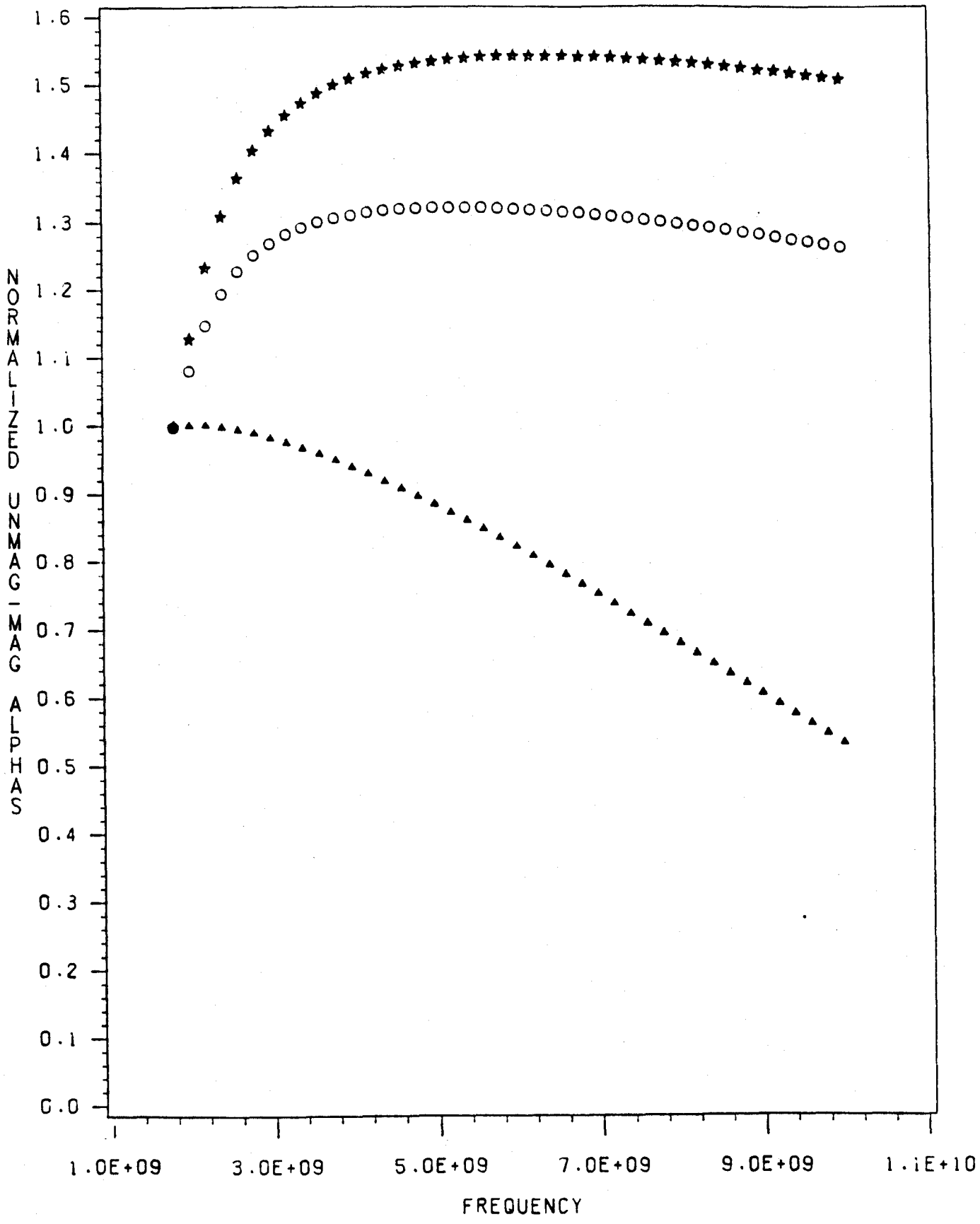
TE EFFECTS AT 135 DEG, K.B=45 DEG
2.14 MM , TE: ** 15 KEV, OO 10 KEV, AA 1 KEV
NORMALIZED UNMAG-MAG ALPHAS
1.6
1.5
1.4
1.3
1.2
1.1
1.0
0.9
0.8
0.7
0.6
0.5
0.4
0.3
0.2
0.1
0.0
1.0E+09
3.0E+09
5.0E+09
7.0E+09
9.0E+09
1.1E+10
FREQUENCY

Fig. 14c

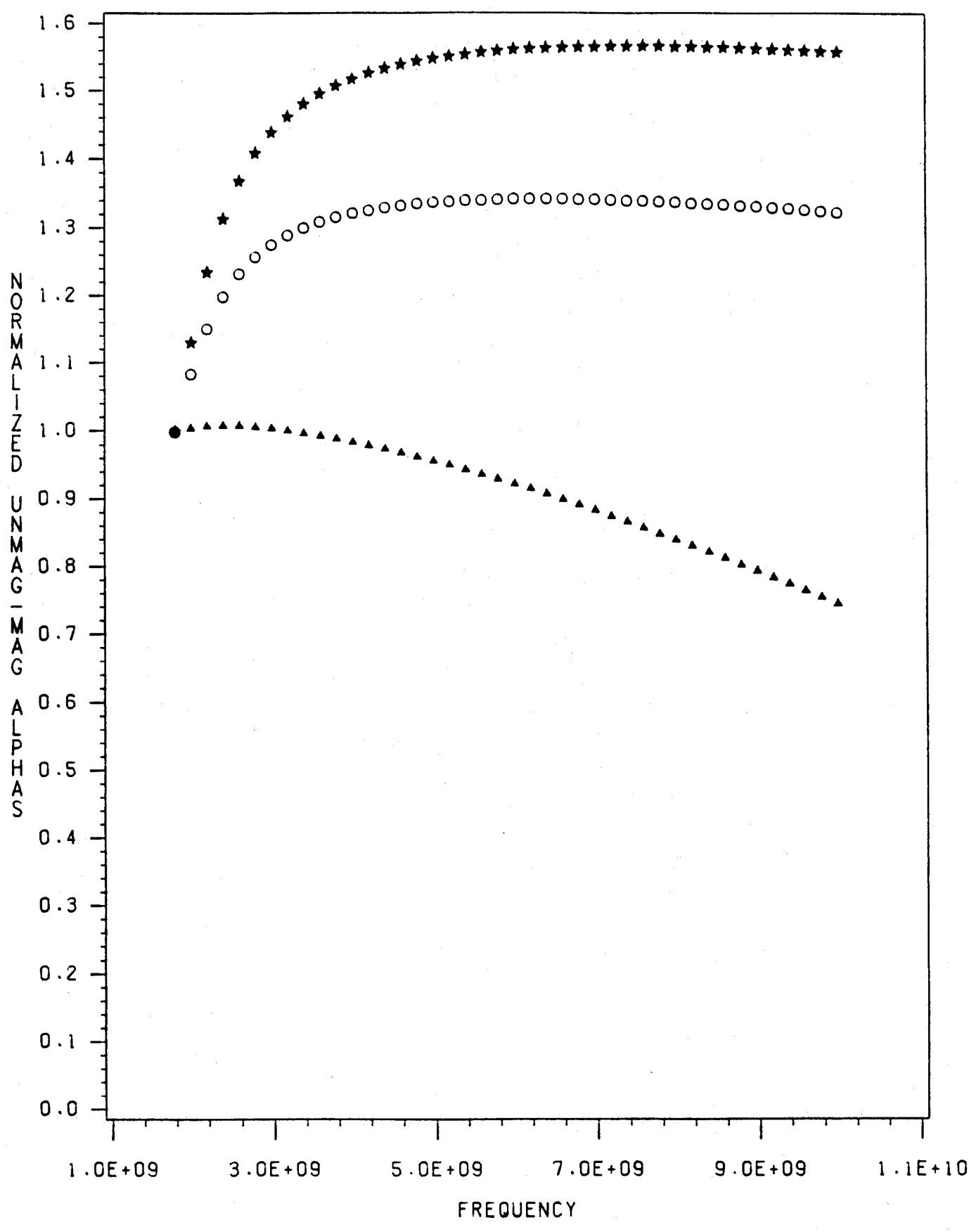
TE EFFECTS AT 135 DEG, K.B=0 DEG
2.14 MM , TE: ** 15 KEV, OO 10 KEV, AA 1 KEV
NORMALIZED UNMAG-MAG ALPHAS
1.6
1.5
1.4
1.3
1.2
1.1
1.0
0.9
0.8
0.7
0.6
0.5
0.4
0.3
0.2
0.1
0.0
1.0E+09
3.0E+09
5.0E+09
7.0E+09
9.0E+09
1.1E+10
FREQUENCY

Fig. 14d

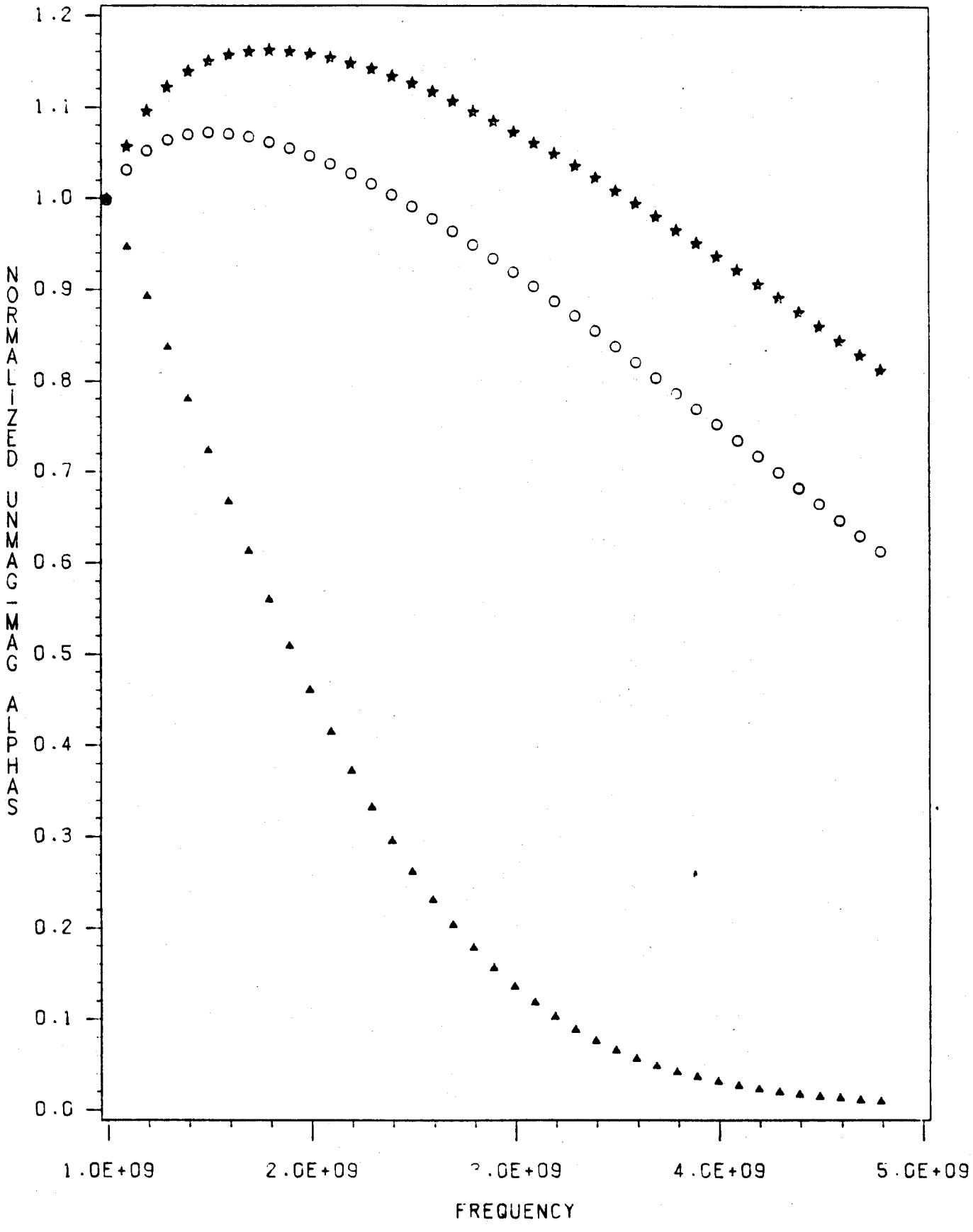
TE EFFECTS AT 135 DEG, K.B=75 DEG
5.00 MM , TE: ** 15 KEV, 00 10 KEV, AA 1 KEV
NORMALIZED UNMAG-MAG ALPHAS
1.2
1.1
1.0
0.9
0.8
0.7
0.6
0.5
0.4
0.3
0.2
0.1
0.0
1.0E+09
2.0E+09
4.0E+09
5.0E+09
FREQUENCY

Fig. 14e

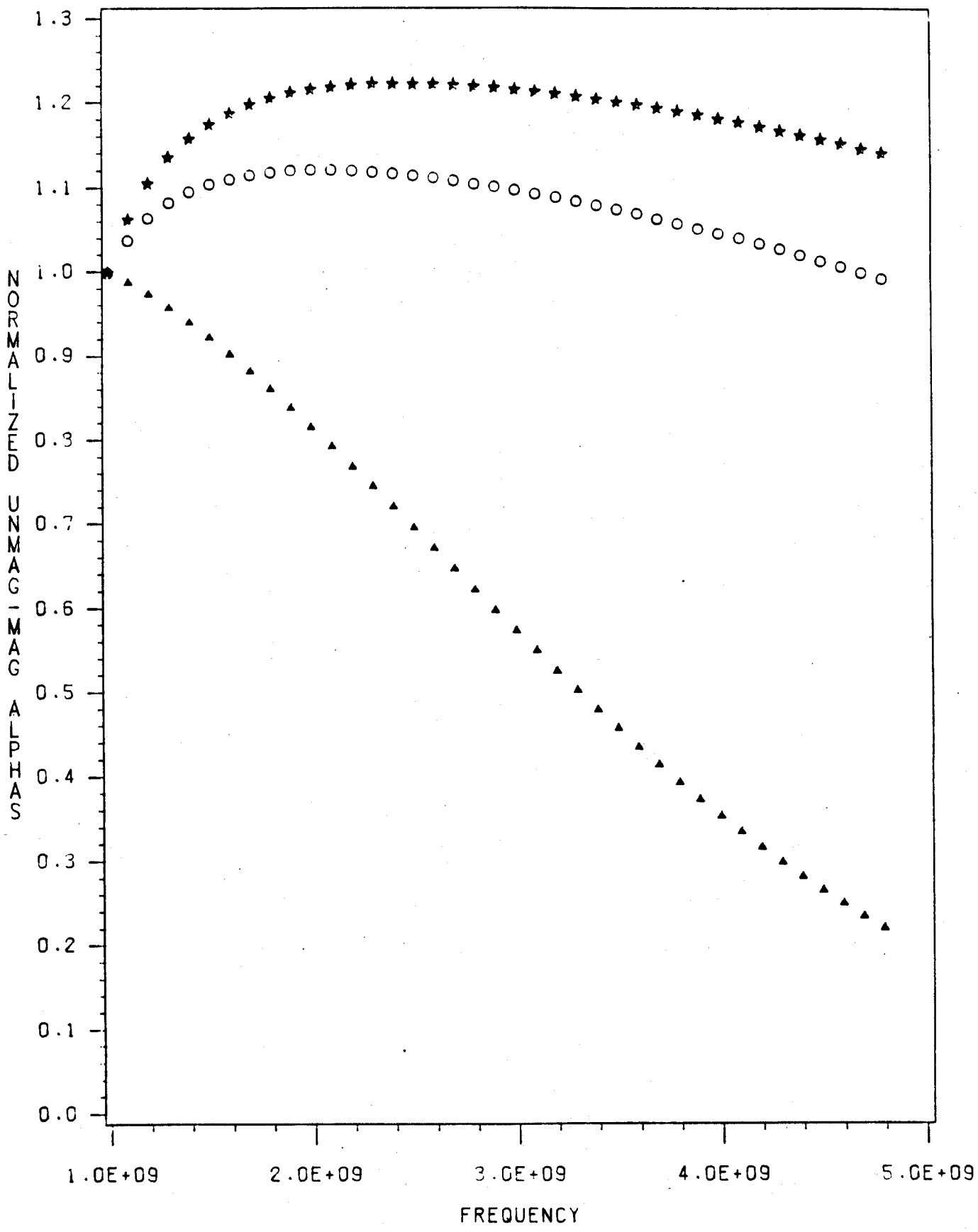
TE EFFECTS AT 135 DEG, K.B=60 DEG
5.00 MM , TE: ** 15 KEV, 00 10 KEV, AA 1 KEV
NORMALIZED UNMAG-MAG ALPHAS
1.3
1.2
1.1
1.0
0.9
0.8
0.7
0.6
0.5
0.4
0.3
0.2
0.1
0.0
1.0E+09
2.0E+09
3.0E+09
4.0E+09
5.0E+09
FREQUENCY

Fig. 14f

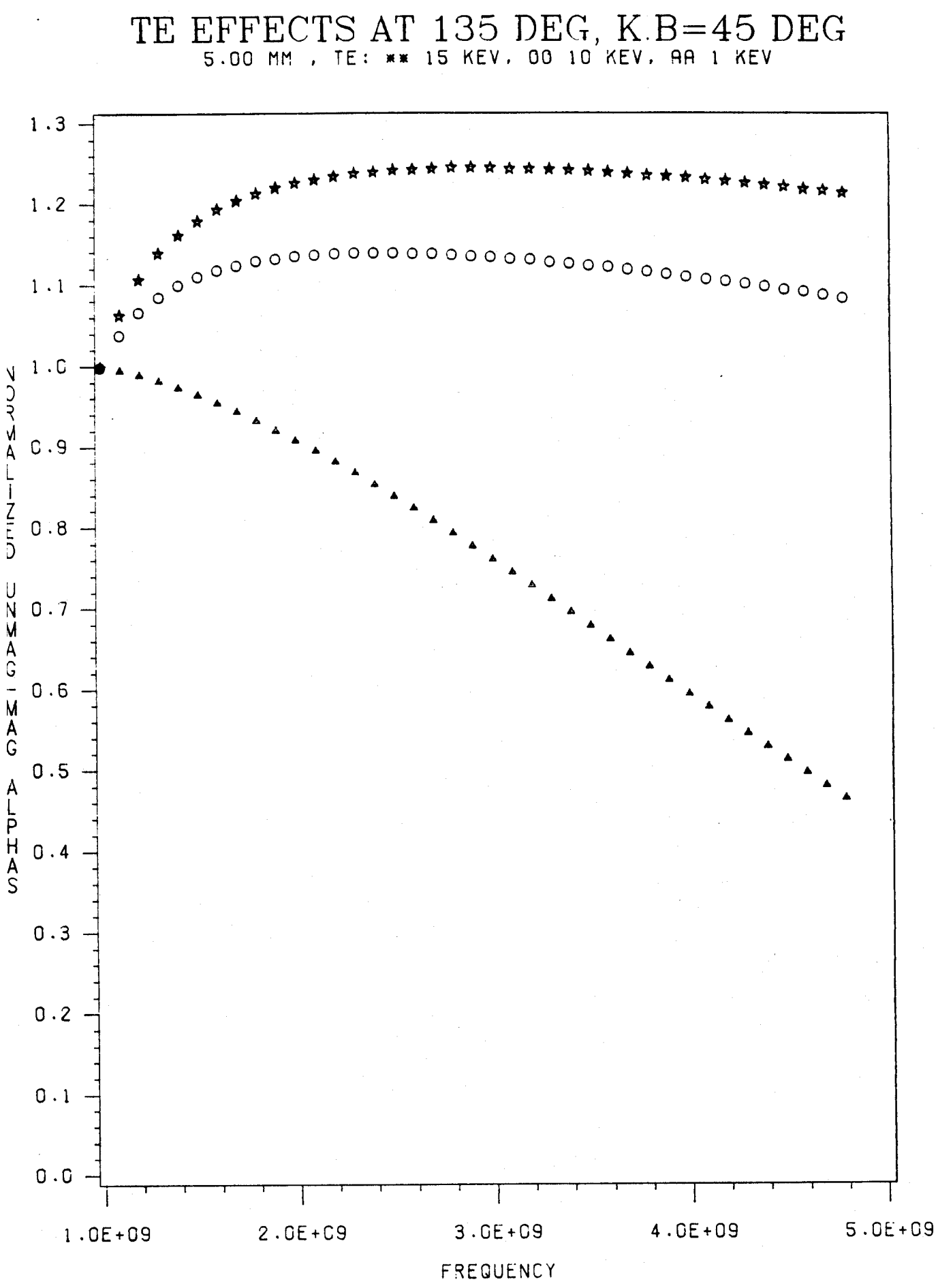
TE EFFECTS AT 135 DEG, K.B=45 DEG
5.00 MM , TE: ** 15 KEV, 00 10 KEV, AA 1 KEV
NORMALIZED UNMAG-MAG ALPHAS
1.3
1.2
1.1
1.0
0.9
0.8
0.7
0.6
0.5
0.4
0.3
0.2
0.1
0.0
1.0E+09
2.0E+09
3.0E+09
4.0E+09
5.0E+09
FREQUENCY

Fig. 14g

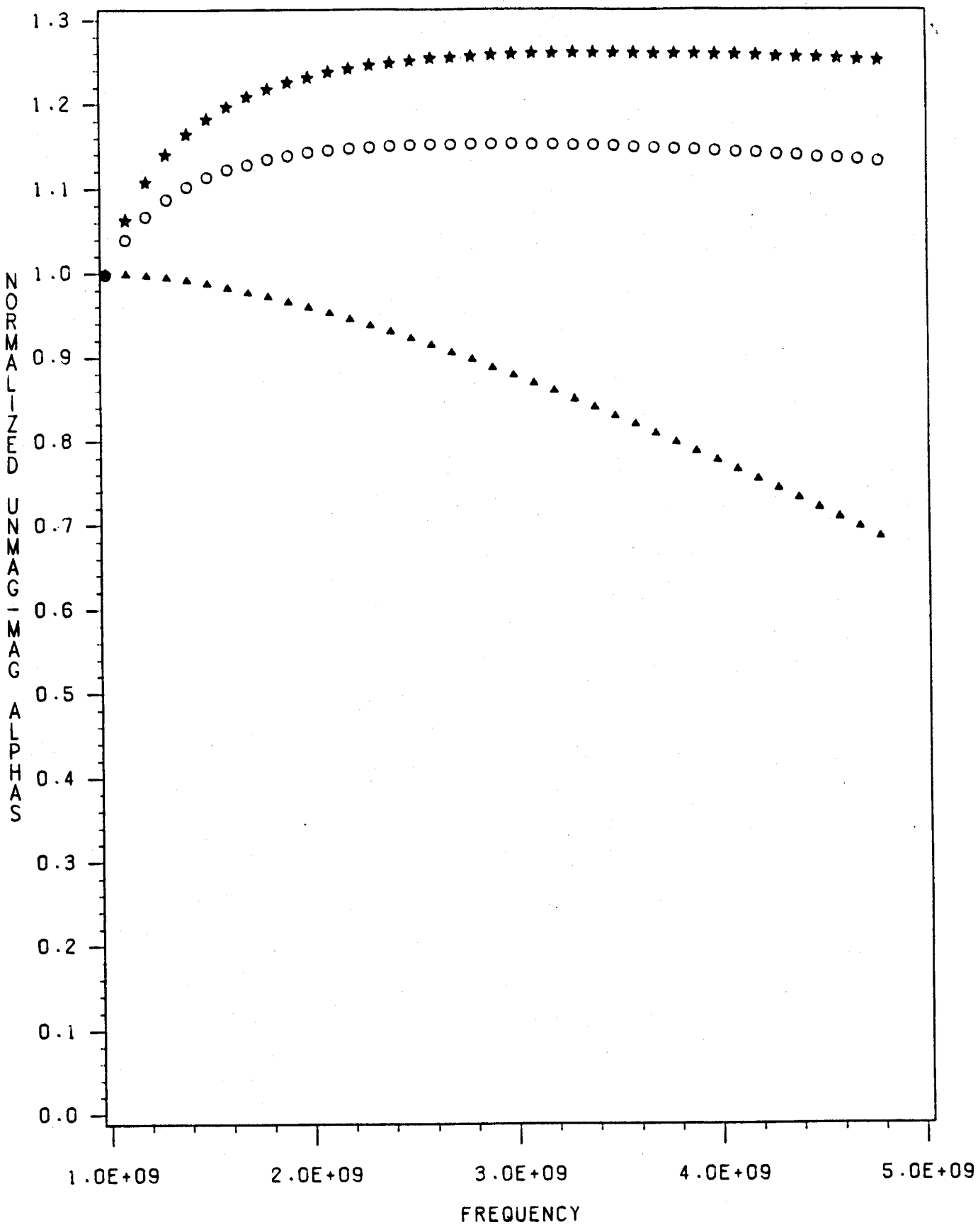
TE EFFECTS AT 135 DEG, K.B=0 DEG
5.00 MM , TE: ** 15 KEV, 00 10 KEV, AA 1 KEV
NORMALIZED UNMAG-MAG ALPHAS
1.3
1.2
1.1
1.0
0.9
0.8
0.7
0.6
0.5
0.4
0.3
0.2
0.1
0.0
1.0E+09
2.0E+09
3.0E+09
4.0E+09
5.0E+09
FREQUENCY

Fig. 14h